Studies of Interstellar Dust

A thesis

submitted for the degree of

Doctor of Philosophy

In

The Faculty of Science

University of Calicut, Calicut

by

Shalima P.

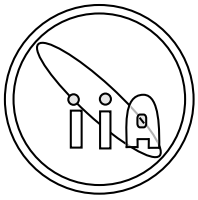

Indian Institute of Astrophysics

Bangalore 560 034, INDIA

August 2005

To my family...

DECLARATION

I hereby declare that the matter contained in this thesis is the result of the investigations carried out by me at the Indian Institute of Astrophysics, Bangalore, under the supervision of Prof. Jayant Murthy and Prof. K. Neelakandan. This thesis has not been submitted for the award of any degree, diploma, associateship, fellowship etc. of any university or institute.

Prof. Jayant Murthy	Prof. K. Neelakandan	Shalima P.
(Thesis Supervisor)	(Thesis Supervisor)	(Ph.D. Candidate)

Indian Institute of Astrophysics
Bangalore 560 034, INDIA
August, 2005

CERTIFICATE

This is to certify that the thesis entitled **"Studies of Interstellar Dust"** submitted to the University of Calicut by Ms. Shalima P. for the award of the degree of Doctor of Philosophy in the faculty of Science, is based on the results of the investigations carried out by her under my supervision and guidance, at the Indian Institute of Astrophysics, Bangalore. This thesis has not been submitted for the award of any degree, diploma, associateship, fellowship etc. of any university or institute.

Prof. Jayant Murthy
(Thesis Supervisor)

Indian Institute of Astrophysics
II Block, Koramangala
Karnataka
August, 2005

ACKNOWLEDGMENTS

First and foremost, I would like to express my sincere thanks to my guide Prof. Jayant Murthy for introducing me to this interesting area of study and giving me all the guidance and encouragement required throughout. I am also extremely thankful to my co-guide, Prof. Neelakandan for giving me all the help and support needed. My sincere thanks to Prof. B. R. S. Babu for all the help pertaining to the official matters at Calicut University which has played a significant role in the timely completion of my thesis.

I would like to take this opportunity to thank the Director of the Indian Institute of Astrophysics for giving me the opportunity to work at the institute and providing me with all the facilities required throughout the course of this work. I also thank the Board of Graduate studies for all the help and support provided throughout the course of my work. I sincerely thank Prof. Hassan, Prof. Vinod Krishan, Dr. Rangarajan and Dr. Anupama of the BGS for all the help given to me.

I thank the faculty of IIA, RRI, IISc and ISAC for all the guidance during the coursework. I sincerely thank Prof. Harish Bhatt who has guided me from the time I was a summer student at IIA and inspired me to take up research in this field. I am also extremely thankful to Dr. Chellathurai (IUCAA) for mentoring me regarding the path I should be taking in order to do research in Astrophysics and informing me about the opportunities for postgraduation at IIT. I sincerely thank Dr. Prajval Shastri, Prof. Sunethra Giridhar, Prof. Bhanu Das, Prof. Sivaram, and Dr. B. R. Prasad for all the help they have given me.

I especially thank Dr. N. V. Sujatha for helping me at various stages of my work, with all the useful discussions that have been very fruitful and interesting. I also thank Dr. Chiranjeeb Sur for providing all the useful information regarding the supercomputing facility and the various procedures involved. I am greatly thankful to all my seniors especially Sivarani, Sankar, Raji, Suresh, Preethi, Geetanjali, Ambika, Manoj, Maheshwar and all my juniors for all the motivation and help they have given me from time to time. I am also grateful to all my batchmates, Latha, Ravinder, Poonam, Vikram and Anand for all the fun during the coursework. Apart from that I would like to thank all my hostelmates for making the hostel life so memorable.

I also thank all the office staff of IIA including the Administrative Officer, Mr. Narasimha Raju, Mr. Mohan Kumar and Mr. Valsalan for all the help they have provided. I sincerely thank the office staff of Calicut University for whatever they have done from time to time. I thank Mr. Nathan and and Dr. Baba Verghese for helping me whenever there was any computer related problem. I also thank Mrs.

Jain, Mr. Shankar and Mr. Murali for their help and cooperation.

Last but not the least I express my heartfelt gratitude to my parents for encouraging me to do whatever I was interested in, right from my school days. I am also extremely grateful to my husband, Hansraj for supporting me and encouraging me at all times and being unconditionally tolerant with me. I would like to express my sincere gratitude to my friends, Patricia, Anusha, Aparna, Amritha, Vani, Manju and Jayanthi for having faith in me and giving me the courage to face any situation without which this would have been impossible.

LIST OF PUBLICATIONS

1. Modelling of dust scattering toward the Coalsack, P. Shalima & Jayant Murthy, 2004, MNRAS, 352, 1319

2. Modelling of dust scattering toward the Coalsack, Jayant Murthy & P. Shalima, 2003, in Astrophysics of Dust, Estes Park, Colorado, ed. Adolf N. Witt

3. Dust Properties in the FUV in Ophiuchus, Sujatha N. V., Shalima P., Jayant Murthy & R. C. Henry, 2005, ApJ, 633 (in press)

4. FUV Scattering Of Dust in Orion, P. Shalima, N. V. Sujatha, Jayant Murthy, R. C. Henry & David J. Sahnow (in preparation)

5. Modelling of dust properties in the FUV towards the Coalsack, N. V. Sujatha, P. Shalima & Jayant Murthy (in preparation)

Table of Contents

List of Tables **ix**

List of Figures **xiii**

Abstract **xiv**

1 INTRODUCTION **2**

1.1 The Interstellar medium 2

1.2 Dust Grains - Significance 4

1.2.1 Composition 5

1.2.2 Scattering 5

1.2.3 Absorption and infrared emission 7

1.2.4 Extinction 10

1.2.5 Polarization 16

1.3 Deriving Dust Properties from Observations 17

1.3.1 Column densities - Dust distribution 18

1.3.2 Extinction - Grain size, composition 20

1.3.3 Diffuse radiation - Optical constants 21

2 MODELS **25**

2.1 Introduction 25

2.2 Grain model 25

2.3 Interstellar radiation field 33

2.4 Scattering 34
2.5 Absorption 38

3 Dust Properties in the FUV in Ophiuchus 41
3.1 Introduction 41
3.2 Observations 43
3.3 Model 44
3.4 Results and Discussion 47
3.5 Conclusions 55

4 Modelling of dust properties in the FUV toward the Coalsack 58
4.1 Introduction 58
4.2 Observations 59
4.3 Model 62
4.4 Results and Discussion 64
4.5 Conclusions 72

5 FUV Scattering by Dust in Orion 76
5.1 Introduction 76
5.2 Observations 78
5.3 Model 79
5.4 Results and discussion 85
5.5 Summary 88

6 Conclusions 90
6.1 Future directions 95

A Sample calculation of scattered intensities in Orion 97

B Sample calculation of dust temperature 99

C 101

List of Tables

1.1 Extinction cross-sections 15

1.2 Symbols used and their meaning 24

2.1 Symbols used and their meaning 40

3.1 Details of observed locations in Ophiuchus 56

3.2 Properties of contributing stars 57

4.1 Details of observed locations in the Coalsack 61

4.2 Details of stars used in our model 63

5.1 FUSE observations 79

5.2 Properties of stars near target 81

C.1 Table corresponding to Figures 3.3 - 3.6 101

List of Figures

1.1 Schematic representation of scattering. 8
1.2 The average Galactic extinction curve (Whittet, 2003). 13
1.3 Theoretical extinction efficiency for graphite grain of size 0.25 μm (Draine, 2003a). 14
1.4 The transmission of the Earth's atmosphere for different wavelengths. 18

2.1 In this Monte Carlo model, photons are emitted by the star in a random direction and proceed until an interaction occurs. After each interaction, each photon is re-emitted in a new direction as determined by the scattering phase function. In order to save computational time, at each interaction, a fraction of the energy of the photon depending on its scattering angle is redirected to the observer. 36

3.1 IRAS 100 μm map of the region is shown with contours labelled in units of MJy sr^{-1}. The filled squares show the locations of the *Voyager* observations and the asterisks show the positions of the brightest UV stars in the region. 45
3.2 Best fit distances to the scattering layer for each of the locations as a function of galactic longitude in degrees. 48

3.3 Observed UV intensity at each location is plotted against the corresponding values of the total, N(H) (dotted line) and neutral, N(H I) (solid line) hydrogen column densities. There is clearly no correlation between the FUV intensity and either N(H) or N(H I). 49
3.4 Observed UV intensity at each location is plotted against the ISRF. The non-zero intercept is due to the absorption of the diffuse radiation in the intervening ISM. 50
3.5 Modeled FUV (1100 Å) intensities corresponding to $a = 0.40$ and $g = 0.6$ have been plotted against the observed values for each location. 52
3.6 Modeled IR intensities corresponding to an albedo of 0.40 and $g = 0.6$ have been plotted against the observed IRAS (100 μm) values for each location. 53
3.7 90% confidence contour for all 31 locations (solid contour) is shown. The contour corresponds to a limit of 0.40 ± 0.10 and 0.55 ± 0.25 on the albedo and g respectively. Also plotted is the intersection of the individual 90% confidence contours for each of the locations (dashed line). 54

4.1 The IRAS 100 μm (in units of MJy sr^{-1}) map of the region is plotted with the 34 observed locations superimposed on it. Filled squares represent FUSE locations while filled triangles represent the Voyager targets. The brightest UV stars in the region are also marked as asterisks. 60
4.2 90% and 68% confidence contours (a versus g) are plotted for 999Å. 65
4.3 90% and 68% confidence contours (a versus g) are plotted for 1056Å. 66
4.4 90% and 68% confidence contours (a versus g) are plotted for 1117Å. 67
4.5 90% and 68% confidence contours (a versus g) are plotted for 1159Å. 68
4.6 The variation of albedo with wavelength is plotted. The albedo, a varies from 0.3 to 0.35 with wavelength. 69

4.7 The variation of g as a function of wavelength is plotted. g remains a constant at 0.7 ± 0.15 with wavelength. 70
4.8 Relative contributions from two parts of the medium for the 4 *Voyager* locations. The solid line represents the contribution from the foreground medium for $g = 0.9$ and the dashed line denotes its contribution for $g = 0.0$. The contribution from the Coalsack for g =0.0 and $g = 0.9$ is represented by the asterisks and the filled diamonds, respectively. The albedo used is 0.4 for all the four locations. 71
4.9 The modelled FUV (1100 Å) intensities corresponding to an albedo of 0.3 and a g value of 0.7 have been plotted against the observed values for each location. There is a very good correlation between the two, implying the uniformity of the optical properties of grains in the region. 73
4.10 The model IR intensities corresponding to an albedo of 0.3 have been plotted against the observed IRAS (100 μm) values for each location. 74

5.1 DSS map of the region with the stars (asterisks) and the FUSE location (filled square) overplotted. 80
5.2 Observed diffuse spectrum from Murthy et al. (2005). The modelled continuum which is assumed to be the scattered intensity is plotted as the dark line. 83
5.3 Schematic representation of the distribution of dust at the location showing the path (arrow) taken by the observed photons from the Trapezium stars towards the observer. 84

5.4 Allowed values of a as a function of wavelength for dust cross-sections enhanced 1.6 times compared to the $R_v = 5.5$ model. The dotted line represents the theoretical values of Weingartner & Draine (2001) and the filled squares represent the values obtained by Mathis et al. (1981). 86

5.5 Modelled albedos for $R_v = 3.1$ with the corresponding theoretical values. Also plotted are the theoretical values of Weingartner & Draine (2001) (dotted line) and the derived values of Mathis et al. (1981) (filled squares). 87

abstract

ABSTRACT

The interstellar medium (ISM) is a very significant component of a galaxy that represents the material out of which stars are formed. It consists of several elements, the most abundant being hydrogen and helium as well as other heavy elements like carbon, calcium, sodium etc. in lesser quantities. In addition the ISM contains tiny submicron sized particles called dust grains that constitute as little as 1% of the total mass of the ISM. In spite of their lower abundance dust grains are important constituents of the ISM. They aid in the process of star formation due to their ability to absorb and radiate away the excess energy in molecular clouds. They also scatter a fraction of the incident radiation, the probability of which increases with decreasing wavelength. This results in high frequency radiation (e.g. ultraviolet), being scattered and absorbed much more than longer wavelength radiation like the infrared. Scattering can be observed in the form of the diffuse galactic light (DGL), reflection nebulae surrounding hot stars (in the visible and UV) and X-ray haloes around some stars, while absorption leads to subsequent thermal emission which can observed at longer wavelengths, mainly in the infrared. This work consists of analysing these phenomena and modelling them in order to extract useful information regarding the properties and distribution of the grains in our Galaxy.

This thesis contains the results of the research work done by me under the guidance of Prof. Jayant Murthy (Indian Institute of Astrophysics) and Prof. K. Neelakandan at the Indian Institute of Astrophysics, Bangalore.

The thesis has been organised as follows.
The first chapter consists of a basic introduction to the topic of interstellar dust and its properties with emphasis on the scattering and absorption by dust grains. The technique of modelling the scattering and absorption by dust have been discussed in detail in Chapter 2 along with other models like the grain model and the ISRF model which have been used.

The observed FUV emission in the Ophiuchus region has been modelled in Chapter 3 and the scattering properties of grains derived, while Chapter 4 deals with the analysis of the Coalsack region and the dust properties derived from the same. Chapter 5 consists of modelling FUSE observations near the Orion Nebula which is a hot reflection nebula heated by the young massive stars of the Trapezium cluster. Finally Chapter 6 contains the conclusions derived from the analysis of all the locations mentioned here and prospects for future work. The contents of each chapter have been described in detail below.

In Chapter 1 the different phases of the ISM have been discussed in terms of

their temperatures and densities with special emphasis on the properties of dust grains. The ISM consists of five phases namely, the Molecular clouds which are the densest regions of gas and dust in which stars form, the cold neutral medium, warm neutral medium, warm ionized medium and the hot ionized medium. Other than these gaseous phases the ISM also contains solid particles known as dust grains. They are a major component of the ISM and a knowledge of their properties is very important in understanding the way stars form and how radiation is processed in galaxies. Some of the ways in which we can gain information about dust grains is through observations of scattering, thermal emission and polarization by grains. Scattering consists of a change in the direction of the incident radiation. The amount of scattering depends on the albedo which is a function of the composition, size and shape of the grains. The directionality of scattering depends on the phase function asymmetry factor, g which is another function of the grain constitution, shape and size. The same parameters give information about the amount of radiation absorbed since scattering and absorption are two complementary processes. We can therefore derive these parameters by modelling the observed scattered radiation and the thermal emission of grains due to absorption. Another observational property of grains is the extinction which is the sum of scattering and absorption. A plot of extinction against the inverse of wavelength is called the extinction curve. Modelling the extinction curve has led to information regarding the composition and sizes of grains. Bohlin et al. (1978) has observed a correlation between the amount of gas and dust in the Galaxy. Using this correlation, the total amount of dust in front of a star can be derived from extinction measurements as well as from absorption line studies of elements like hydrogen, calcium, sodium etc. The extinction curve is known to vary depending on the environment which is due to variations in the size distributions of grains. We have modelled three different regions in the Galaxy namely, Ophiuchus, Coalsack and Orion in order to derive the dust properties in these regions and study variations in the scattering parameters with environment.

Chapter 2 consists of a description of the models used in deriving the dust properties. A model of scattering and absorption requires knowledge of the grain cross-sections (scattering or absorption) as well as the relative geometry of the stars and the dust grains. Weingartner & Draine (2001) has calculated the theoretical scattering cross-sections from the X-ray to the far-infrared regime by fitting the observed extinction curve of stars in the Galaxy by using a mixture of graphite and silicate grains. These cross-sections have been used for all the regions studied here. Another model which has been used is the interstellar radiation field model of Sujatha et al. (2004). This model calculates the total radiation field from all the stars in the Galaxy at any required distance from the Sun. Hipparcos distances have been used for the stars in this model. Using this model we have been able to pick out the main contributing stars for each location. Other than these two models, we have used a scattering as well as absorption model. A detailed Monte

Carlo scattering model has been developed as part of this work which is a very general model of multiple scattering since it is independent of the dust geometry. This method consists of tracking individual photons from a star as they travel through the ISM. A model for absorption and subsequent thermal emission has also been developed as part of the thesis. As in the case of scattering, depending on the optical depth either single scattering can be considered or else multiple scattering has to be used. Models corresponding to both the cases have been developed.

Chapter 3 consists of deriving the dust properties towards Ophiuchus. We have modelled 31 locations observed by Voyager towards the Ophiuchus region. We find that eight B-type stars contribute to the observed radiation at 1100Å and that it is the dust in the foreground of the molecular clouds that is responsible for scattering. An albedo of 0.4±0.1 and a g value of 0.55±0.25 is obtained at 1100 Å. These values are consistent with the theoretical predictions of Weingartner & Draine (2001) for average Milky Way dust with an R_v of 3.1. We have also calculated the 100 μm intensities for the best fit parameters and obtained a good correlation between the model and the observed IRAS (100 μm) intensities. We find that most of the infrared emission is seen to come from the foreground sheet itself.

Chapter 4 consists of deriving the optical constants of grains in the direction of the Coalsack molecular cloud. Using just five Voyager observations of the region we had constrained the albedo to 0.4±0.2 but these observations weren't sufficient to constrain g. Dust in the foreground sheet of the Coalsack molecular cloud was found to contribute to the observed emission rather than the denser molecular cloud. With the availability of additional 27 observations from the FUSE satellite we have been able to remove the degeneracy in g and constrain its value to 0.7 ± 0.2. We have also modelled the infrared intensities and obtained a good correlation between observations and the model for the best fit scattering parameters. We find that in this case both the foreground sheet as well as the molecular cloud contribute to the infrared emission equally unlike in the case of Ophiuchus where the foreground sheet itself was the major contributer.

Chapter 5 consists of deriving the properties of dust grains near the Orion Nebula. FUSE observations of a location which is 12′ from the Trapezium stars in the Orion Nebula are modelled. The observed intensities are as high as 2.9 × 10^5 photons cm^{-2} s^{-1} sr^{-1} $Å^{-1}$ at 1100Å. From the spectra, we derive a total hydrogen column density of 6.4 × 10^{20} cm^{-2} which causes the extinction from the star to the location and an N(HI) of 4.5 × 10^{19} cm^{-2} for the scattering medium from VLA 21 cm data. Since the region is known to have large grains with an R_v of 5.5 we have used the extinction cross-sections of Weingartner & Draine (2001) for $R_v = 5.5$. In order to account for the lower abundance of dust in Orion, we have increased the cross-sections by a factor of 1.6. We find that the albedos are larger than those derived for other regions in the Galaxy but reasonably consistent

with the theoretical albedos of Weingartner & Draine (2001). since the anomalous grains are found in the foreground sheet of the nebula, we conclude that scattering is also produced in this Veil. We obtain an albedo of 0.25 at 912 Å increasing to 0.4 at 1040 Å. We have restricted our analysis to 1040 Å due to the presence of fluorescent emission of molecular hydrogen at this location. We were unable to constrain g due to lack of sufficient data.

Chapter 6 contains the results derived by studying these different regions in the Galaxy and their implications. The results obtained show that the optical properties of grains are more or less constant in the FUV at the different locations considered here, except in the case of the Orion nebula which is also known to show a large variation in the extinction curve. This means that in regions of normal extinction the dust properties are also similar and agree with theoretical predictions for average Milky Way dust, whereas in other regions there are large differences in dust composition, size etc. Another important conclusion that we arrive at is that the grains need not be of a different composition to explain differences in the optical constants but instead variations in the size distribution are sufficient to cause these differences. From the analysis of the three regions namely Coalsack, Ophiuchus and Orion all of which lie within galactic latitude of 20 degrees we find that the diffuse emission in the FUV can be explained by scattering by dust grains alone. However for higher latitudes it may be necessary to consider other processes to explain the observed FUV emission. We will be analysing new observations at higher latitudes from the GALEX satellite in order to study the various processes that contribute to the observed diffuse FUV radiation.

The importance of these results lies in the fact that dust grains play a key role in determining the energy redistribution in galaxies, by absorbing ultraviolet radiation emitted by hot stars and re-emitting this energy at longer wavelengths. This process aids star formation as the excess energy released due to gravitational contraction of molecular cloud cores is radiated away paving the way for further gravitational collapse and eventual star formation. Therefore a detailed analysis of the properties of dust grains can help us understand the various processes in the Galaxy including star formation.

Studies of Interstellar Dust

Chapter 1

INTRODUCTION

1.1 The Interstellar medium

The interstellar medium (ISM) is a very important component of the Galaxy which represents the material that forms the stars by the process of gravitational collapse. It is enriched in heavy elements from time to time whenever a massive star explodes and throws out the heavy elements formed in the hot stellar core into the surrounding medium. The ISM consists of a mixture of several elements (mainly hydrogen (∼90%) and helium (∼10%)) in gaseous form and a small fraction of heavy elements in the form of tiny submicron sized particles known as dust grains. Other elements like Ca, K, Na, etc. too exist but in smaller quantities. The ISM can be divided into five phases depending on the temperature. The important phases are given below.

(a) Molecular Clouds

The coldest component is the molecular clouds which are composed mainly of molecular hydrogen (H_2). This component has a temperature of 10-20 K with densities ranging from 10^3 to 10^6 cm^{-3} (Scoville & Solomon, 1974). They are the sites of star formation, since most of them have dense cores which are gravitationally unstable. Even though $30 - 60\%$ of the mass of the ISM is in these clouds, they occupy less than 1% of the total volume. The molecular clouds are found mostly

in the Galactic plane.

(b) Cold Neutral Medium (CNM)

This component mainly consists of neutral hydrogen which is also known as HI gas. This component is in the form of sheets or filaments that are present almost everywhere in the Galaxy. They have higher temperatures of the order of 80 K (Spitzer, 1998), and densities ranging from $20 - 60$ cm^{-3} (Jura, 1975). They occupy about $1 - 4\%$ of the total ISM volume.

(c) Warm Neutral Medium (WNM)

The warm neutral medium consists mainly of HI gas which is located towards the boundaries of HII regions (regions of ionized hydrogen surrounding hot stars) and molecular clouds. It occupies $30 - 60\%$ of the ISM volume. The temperature is typically $\sim$ 6000 K (Davies & Cummings, 1975) and the density is ~ 0.2 cm^{-3} (Baker & Burton, 1975).

(d) Warm Ionized Medium (WIM)

It is comprised of diffuse gas with temperatures ranging from 6000 K $-$ 12000 K (Osterbrock, 1989) and densities of ~ 0.1 cm^{-3} (Spitzer, 1998). The medium is heated by massive O and B stars. Nearly 90% of the ionized hydrogen in the Galaxy resides in this phase while the rest lies in HII regions.

(e) Hot Ionized Medium (HIM)

This phase of the ISM comprises of very hot material ($T > 10^6$ K), at very low densities ($n < 0.01$ cm^{-3}), heated by supernova explosions. This hot gas emits

mainly in X-rays and can be studied using X-ray telescopes like the Chandra Space Telescope. The remaining volume of the ISM ($\sim 40\%$) is considered to be occupied by this medium and it merges with the hot X-ray corona of the Galaxy which is the spherical halo of hot gas surrounding the Galaxy.

1.2 Dust Grains - Significance

The ISM contains another important phase of matter known as dust grains. Dust grains are solid particles that are well mixed with the gas in the ISM and are known to exist in all the ISM phases except in the hot ionized medium. Bohlin et al. (1978) studied the correlation of dust with gas using ultraviolet absorption line spectroscopy and demonstrated that the two are well correlated. Their sizes can vary from a few microns to macromolecular sizes. Their composition is known mainly from the depletion of certain refractory elements in the ISM which indicate that a large fraction of heavy elements capable of condensing into solids, like carbon, silicates, and compounds of magnesium, iron etc. are present in dust grains. These dust grains constitute only 1% of the total mass in the gas phase (the observed average gas to dust ratio in our Galaxy is ~ 100). In spite of their lower abundance, they play a significant role in deciding the radiation field in galaxies. They contribute significantly at short wavelengths (optical and ultraviolet) by scattering a fraction of the incident radiation. The remaining fraction is absorbed and re-emitted at longer wavelengths (infrared, millimeter etc.). A large percentage of the total luminosity of the Galaxy in the infrared (IR) comes from dust grains. Therefore dust grains determine the energetics of the Galaxy and aid in star formation by radiating away excess energy in molecular clouds thereby making them collapse gravitationally to form stars. Apart from this they are also sites for the formation of molecular hydrogen in the ISM. Therefore a study of the properties of dust grains is very crucial in understanding the way radiation is processed in our Galaxy as well as in other galaxies and also in understanding the physics of star

formation. The composition and properties of dust grains are discussed in detail in the following sections.

1.2.1 Composition

Dust grains are thought to be composed of refractory materials like carbon, silicates etc. Many other elements like nitrogen, oxygen, sodium, magnesium, phosphorous, sulphur, chlorine, potassium and iron, which are stable also seem to be present in grains. Rather than being composed of one element, dust grains consist of a mixture of several elements and molecules. Silicates are mostly amorphous even though certain circumstellar disks show evidence of crystalline silicates. From observations, there are indications that silicate grains might have a Mg-rich mantle and an Fe-rich core (Spitzer & Fitzpatrick, 1993). Carbonaceous materials could be in the form of graphites, diamonds, amorphous carbon or polycyclic aromatic hydrocarbons (PAHs) and aliphatic hydrocarbons. SiC grains are also present in the ISM but in lesser quantities. Similarly calcite ($CaCO_3$) and dolomite ($CaMg(CO_3)_2$) are present in dusty disks of planetary nebulae which represent one of the final stages of a star like the Sun.

1.2.2 Scattering

Scattering involves a change in direction of incident electromagnetic radiation, which is dependent on the composition, size and shape of the scatterer (dust grain) as well as on the wavelength of the radiation. The parameter which decides the amount of radiation scattered is known as the albedo (a) which can be represented as:

$$a = \frac{Q_{sca}}{Q_{ext}}. \tag{1.1}$$

Here Q_{sca} is the scattering efficiency factor and Q_{ext} refers to the total extinction efficiency factor. The albedo can take values from 0 implying no reflection to 1 implying 100 % reflection of the incident radiation. In order to calculate the amount

of scattering in any direction, we should have some knowledge of the relative distribution of the sources (stars) and the scatterers (dust grains). Assuming that the scattering geometry is known, we can calculate the amount of radiation scattered into any angle θ as follows; The energy incident on a volume element of dust dV can be written as,

$$E_{inc} = \frac{L}{4\pi d^2} \times \sigma_{ext} \times ndV, \tag{1.2}$$

where, L represents the luminosity of the source at the wavelength under consideration, d is the distance between the star and the grain and n is the number density of dust grains. σ_{ext} is the extinction cross-section of the grains, which depends on the composition, size and shape of the grain. Out of the total incident radiation, the amount scattered in all directions is,

$$E_{sca} = a \times E_{inc}. \tag{1.3}$$

The amount scattered into unit solid angle about an angle θ can be written as,

$$E_{sca}(\theta) = a \times E_{inc} \times \phi(\theta), \tag{1.4}$$

where, $\phi(\theta)$ is known as the scattering phase function, which gives the amount of energy scattered into unit solid angle about a direction θ. The basic equation for $\phi(\theta)$ is given by,

$$\phi(\theta) = \frac{1}{\sigma_{sca}} \times \frac{d\sigma}{d\Omega}. \tag{1.5}$$

Here σ_{sca} is the total scattering cross-section integrated over all directions and $\mathrm{d}\sigma/\mathrm{d}\Omega$ is the differential scattering cross-section. The phase function depends on the composition, size and shape of the grains as well as on the incident wavelength.

The intensity observed at the detector (I_{det}) can be written as,

$$I_{det} = \frac{E_{sca}(\theta)\Omega_d}{\Omega_c A_d}. \tag{1.6}$$

Here Ω_d is the solid angle of the detector, Ω_c is the solid angle subtended by the cloud ($= \mathrm{A}_c/\mathrm{d}^2$) and A_d is the area of the detector.

Other than the albedo, an important scattering parameter of grains is the phase function asymmetry factor g which determines the direction of scattering and is given by,

$$g = \frac{\int cos\theta\phi(\theta)d\omega}{\int \phi(\theta)d\omega}. \tag{1.7}$$

g can range from -1 through 0 to +1 each corresponding to different types of scattering. g = 0.0 corresponds to isotropic scattering where the incident radiation is scattered equally in all directions. g = -1.0 corresponds to complete back scattering where the scattered beam undergoes a reflection of 180° and g = 1.0 corresponds to strong forward scattering where the scattered radiation continues in the same direction as the incident beam. Fig. 1.1 shows the different types of scattering corresponding to different values of g.

1.2.3 Absorption and infrared emission

Absorption is the complementary process to scattering where the incident radiation that is not scattered is absorbed resulting in an increase in the internal energy of the grain. The basic principle behind calculating the temperature of the dust grains is the equilibrium between absorption and emission of radiation. This depends on the optical properties of dust grains, like the cross-section and the albedo besides the distance between the stars and the grains. With knowledge of these parameters, the temperature of the grain can be derived as follows.

Let L be the total luminosity of the star and d be the distance between the star and the grains. Therefore the amount of radiation incident on volume element dV of the medium which has a density n of grains is given by the equation,

$$E_{inc} = \frac{L}{4\pi d^2} \times \sigma_{ext} \times ndV. \tag{1.8}$$

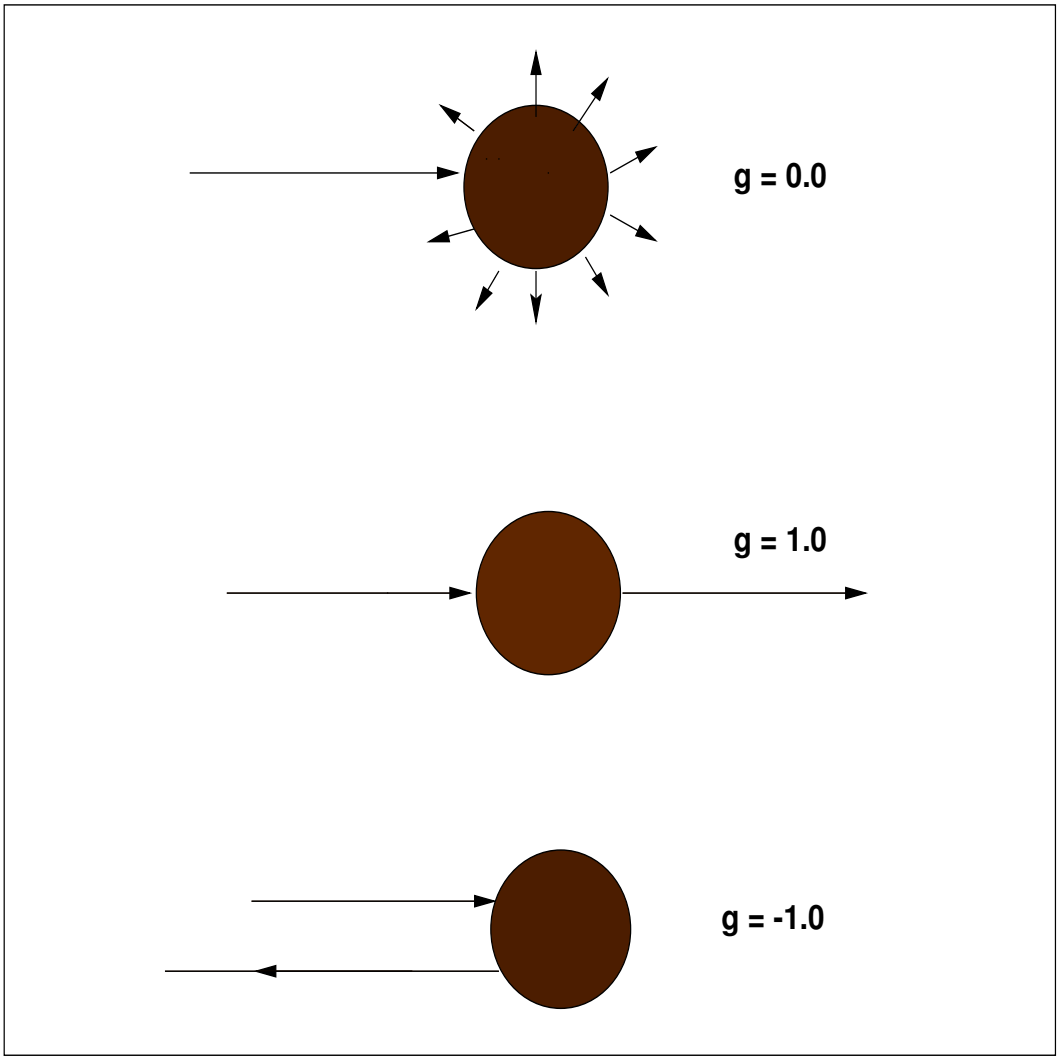

Figure 1.1: Schematic representation of scattering.

A part of this radiation is absorbed by the volume element, which is dependent on the albedo of the grains. If a is the albedo of the dust grains, the energy absorbed is given by,

$$E_{abs} = (1 - a) \times E_{inc}. \tag{1.9}$$

This energy is radiated at longer wavelengths, given by

$$E_{rad} = 4\pi \times ndV \times \sigma_B T_d^4 \tag{1.10}$$

where, T_d is the equilibrium temperature and σ_B is the Stephan-Boltzman constant. By assuming the grains to follow Kirchoff's law for a perfect blackbody which states that the emissivity of a blackbody is equal to its absorptivity, their equilibrium temperature can be obtained by equating the energy absorbed and radiated.

$$E_{abs} = E_{rad} \tag{1.11}$$

The equilibrium temperature is given by,

$$T_d = \left[\frac{L(1-a)\sigma_{ext}}{16\pi^2 d^2 \sigma_B}\right]^{1/4}. \tag{1.12}$$

In the case of more stars heating the grains with luminosities L_1, L_2, L_3,..etc. at distances of d_1, d_2, d_3,.. etc. from the grains, the equation becomes,

$$T_d = \left[\frac{\left[\frac{L_1}{d_1^2} + \frac{L_2}{d_2^2} + ..\right] \times (1-a)\sigma_{ext}}{16\pi^2 \sigma_B}\right]^{1/4}. \tag{1.13}$$

Therefore energy radiated at a wavelength λ can be written as,

$$E_{rad}(\lambda) = 4\pi \times ndV \times B_\lambda(T_d) \times \sigma_{abs}. \tag{1.14}$$

Here σ_{abs} is the absorption cross-section of dust and $B_\lambda(T_d)$ is the planck function which can be written as

$$B_\lambda(T_d) = \frac{2hc^2}{\lambda^4} \frac{1}{exp(\frac{hc}{\lambda k T_d} - 1)}, \tag{1.15}$$

where h is the planck's constant and c is the velocity of light in vacuum. The energy reaching the detector of area A_d at the earth at a distance r from the volume element dV is given by,

$$E_{det}(\lambda) = \frac{E_{rad}(\lambda) \times A_d}{4\pi r^2}. \tag{1.16}$$

The flux at the detector is therefore,

$$F_{det}(\lambda) = \frac{E_{rad}(\lambda)}{4\pi r^2}. \tag{1.17}$$

From a diffuse source we can detect the radiation per unit solid angle of source or the intensity. Therefore the intensity at the detector is given by,

$$I_{det} = \frac{F_{det}(\lambda)}{\Omega_c} \tag{1.18}$$

where, Ω_c is the solid angle subtended by area A_c of the cloud at the detector. The final expression for intensity at the detector can be written as,

$$I_{det} = ndz \times B_\lambda(T_d) \times \sigma_{abs}. \tag{1.19}$$

When represented in units of MJy sr^{-1} the expression becomes,

$$I_{det} = \frac{ndz \times B_\lambda(T_d)\lambda^2 \times \sigma_{abs} \times 10^5}{3.0}. \tag{1.20}$$

1.2.4 Extinction

The sum of scattering and absorption is known as extinction since both processes remove radiation from our line of sight. Extinction causes the observed magnitudes of stars to increase or the flux to decrease (since higher magnitudes imply lower observed fluxes). This can be measured in stars of known spectral type using the pair method. Consider two stars of the same spectral type, one without extinction and the other which is behind some cloud and hence radiation from it suffers

extinction. Let m_1 be the magnitude of the star without extinction and m_2 be the magnitude of the one with extinction. Therefore,

$$m_{1\lambda} = -2.5 \times log(f_{1\lambda}) + C. \tag{1.21}$$

$$m_{2\lambda} = -2.5 \times log(f_{2\lambda}) + C + A_\lambda. \tag{1.22}$$

Here f_1 and f_2 are the observed fluxes of the two stars, and C is a constant for stars of similar spectral type. The additional term A_λ is the extinction in magnitudes at a particular wavelength λ which can be derived using the two equations given above and is given by,

$$A_\lambda = 2.5 \times log\frac{f_{2\lambda}}{f_{1\lambda}} + \Delta m\lambda. \tag{1.23}$$

Here $\Delta m\lambda$ is the difference in magnitudes. The difference in extinction at two wavelengths is known as the colour excess represented by,

$$A_B - A_V = E(B-V) = (B-V) - (B-V)_o. \tag{1.24}$$

Here (B−V) is the observed difference in B and V magnitudes (B corresponds to 4400 Å and V corresponds to 5500 Å in the Johnson UBV system), and $(B\text{-}V)_o$ is the intrinsic difference in colour. A plot of E(λ-V) against wavelength is called the extinction curve. The ratio of total to selective extinction in the optical (A_v/E(B-V)) is known as R_v and is a measure of the slope of the extinction curve. For very large grains, $Rv \rightarrow \infty$, and small particles would have an $R_v \approx 1.2$. The typical value of R_v for most regions in the Milky Way galaxy is 3.1.

A sample extinction curve is shown in Fig. 1.2. Some of the important features of the curve include,

(a) linear dependence in the optical and IR,

(b) 2175 Å bump,

(c) far-UV rise and

(d) diffuse interstellar bands (visible only at higher resolution).

The extinction curve is almost linear in the visible and infrared and such a dependence can only be produced by particles having sizes of the order of the wavelength. This is clear from Table 1.1 which shows the cross-sections for various sizes of the scatterers. Fig. 1.3 shows the variation of the theoretical cross-section of a graphite grain of size 0.25μm with wavelength (Draine, 2003a). From the two figures it is clear that the linear dependence of the theoretical extinction curve is similar to the variation in the observed extinction curve. Therefore by comparing the observations with the theoretical values, Whittet (2003) concluded that it is possible to explain the linear portion of the extinction curve with graphite grains of size 0.2 μm having refractive index $m = 1.5 - 0.05i$.

The broad bump at 4.4 μm^{-1} (2175 Å), is the strongest feature in the extinction curve. Since this feature is common to almost all sightlines in the Galaxy, the carrier has to be extremely stable. Graphite which is the most stable form of carbon having a sheet like structure where the atoms all lie in a plane is considered to be the most suitable candidate to explain this feature. Apart from being stable, small graphite grains (0.003 μm) have an extinction peak at 2175 Å, and an abundance (b_c) of 6.3×10^{-5} atoms per hydrogen which agrees with the values derived from the equivalent width of this feature which is, $b_c \geq 10^{-5}$ atoms per hydrogen (Draine, 1989). An important property of this feature is that even though the width of the feature varies from one sightline to another, the central wavelength is a constant.

Almost all lines of sight show an increase in extinction in the far ultraviolet (FUV) which is known as the FUV rise. From the similarity of the shape of the

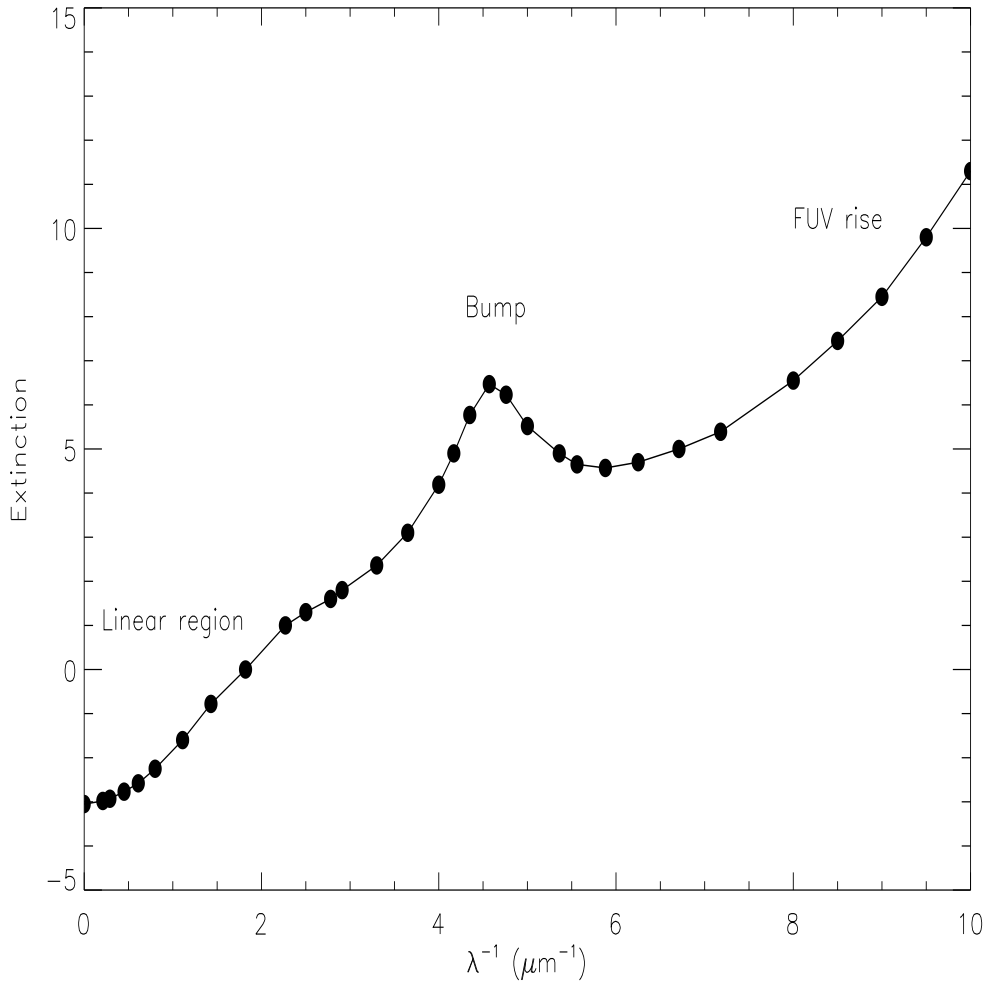

Figure 1.2: The average Galactic extinction curve (Whittet, 2003).

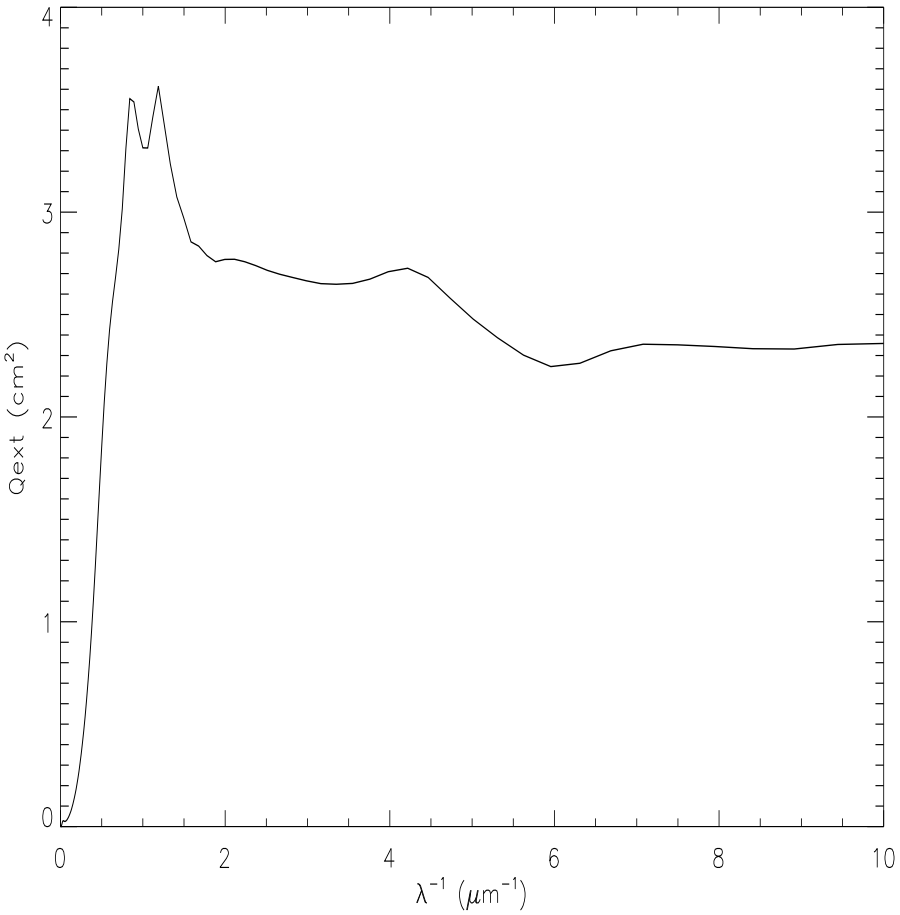

Figure 1.3: Theoretical extinction efficiency for graphite grain of size 0.25 μm (Draine, 2003a).

Table 1.1: Extinction cross-sections

Ingredient	Extinction law	Cross-section
Free electrons	λ^0	σ_T
Molecules	λ^{-4}	$\sim \pi$ a^2
Small (a $<<$ λ) particles	λ^{-4}	$<< \pi$ a^2
Large (a $>>$ λ) particles	λ^0	π a^2
Particles with a $\sim \lambda$	λ^{-1}	$Q_{ext}\pi$ a^2

FUV rise regardless of environment, Fitzpatrick & Massa (1988) attributed it to an independent grain population rather than changes in the size distribution where the variation in the amplitude is caused by variations in abundance of the carriers. Small grains, either PAHs (Désert et al., 1990) or small silicate grains (Mathis, 1996; Li & Draine, 2001) are required to explain the FUV rise. Studies of reflection nebulae (Gordon, 2004) show that this increase in extinction is mainly due to an increase in absorption at these wavelengths rather than scattering.

Another feature of a typical extinction curve is the presence of diffuse interstellar bands or DIBs. The DIBs are weaker features present in the extinction curve. Even though several studies have been devoted to these features none have been able to positively identify the materials responsible for them (Draine, 2003b). Apart from these features the extinction curve also contains silicate features at 9.7 μm and 18 μm.

The basic features of the extinction curve are common to almost any line of sight in the Galaxy as well as in most of the neighbouring galaxies like the Large Magellanic Cloud (LMC) and M31, which is indicative of the similarity of the carriers in space. However another neighbouring galaxy, the Small Magellanic Cloud (SMC) lacks the 2175 Å feature which is probably due to the absence of carbonaceous grains.

Depending on the environment, dust grains show different characteristics. For example, dust grains inside molecular clouds tend to be larger than those in the diffuse ISM, because they are shielded from the radiation of stars. On the other hand, dust grains close to star-forming regions, are destroyed by the intense ra-

diation field (photodissociation). They tend to be smaller and hence are better isotropic scatterers. Volatile components of dust grains evaporate due to the incident radiation, resulting in porous grains at these locations. These variations are reflected in changes in the extinction curve for different parts of the Galaxy. For example stars embedded within or behind diffuse clouds tend to have relatively strong bumps with average width while stars associated with HII regions have narrow, weak bumps (Whittet, 2003). This shows that the abundance of the carrier is affected by the environment.

1.2.5 Polarization

In addition to absorption and scattering, dust grains are also capable of polarizing incident radiation. Due to the observation of this phenomenon, dust grains are considered to be elongated and globally aligned (probably due to the Galactic magnetic filed). Polarization is due to linear dichroism, resulting from a variation in the values of the extinction efficiency factor, Q_{ext} ($= \pi \times a^2 / \sigma$), perpendicular and parallel to the long axis of the grain. For example electromagnetic waves with electric vector $\vec{E}$, parallel to the long axis of the grain will see a higher effective Q_{ext} (and suffer more extinction), than waves with the electric vector perpendicular to the long axis. Therefore these waves will not only suffer extinction but will also therefore appear polarized. Polarization (P) can be quantified in terms of the extinction efficiency factor as,

$$P = n_d \times 0.5\pi a^2 (Q_{max} - Q_{min}) \tag{1.25}$$

where Q_{max} and Q_{min} correspond to the maximum and minimum extinction efficiencies respectively. The number density of the grains is denoted by n_d and a is the grain radius. The observed polarization also shows a dependence on wavelength and can be described by an empirical relation known as the Serkowski

law (Serkowski, 1968). This relation can be written as,

$$P_\lambda = P_{max} e^{-K(ln(\frac{\lambda}{\lambda_{max}}))^2} \tag{1.26}$$

where λ_{max} is the wavelength of maximum polarization P_{max} and K is a constant (=1.15). The maximum value of polarization occurs at 5500 Å, which is in the visible region and decreases on either side. This is very different from extinction and can be attributed to different types of grains contributing to the two processes. For starlight scattered by circumstellar dust, the radiation will be linearly polarized as a result of orthogonal scattering by spherical grains or elongated grains with no net alignment. This is known as scattering polarization. Polarization can also be observed in the far-infrared (FIR) when the IR radiation deep within molecular clouds is polarized by the time it reaches the outer regions of the cloud. This is known as FIR emission polarization.

1.3 Deriving Dust Properties from Observations

Observations at different wavelengths give information about the different phases of the ISM. Of the various difficulties encountered in making the observations, the Earth's atmosphere presents the biggest problem. The molecules in the Earth's atmosphere absorb certain wavelengths and scatter some of them, and allow certain wavelengths to pass through. As a result, at wavelengths like the optical and the radio, ground based observations can provide some information, whereas for the ultraviolet (UV) and the IR, we have to depend on space based observations. However even in the optical, the ground based observations are affected by atmospheric turbulence and so space based observations using satellites like the Hubble Space Telescope (HST) are much more reliable.

Fig. 1.4 shows the transmission of the Earth's atmosphere with the windows where electromagnetic radiation can reach the earth. Therefore using a combination of ground-based and space-based observations, it is possible to understand a

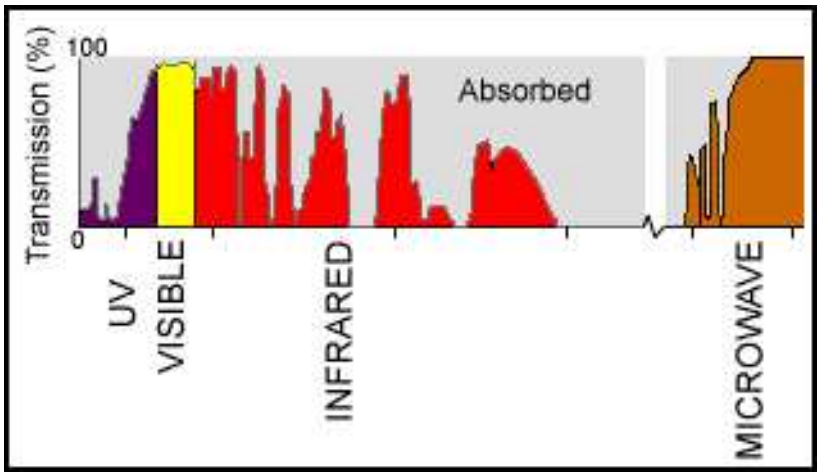

Figure 1.4: The transmission of the Earth's atmosphere for different wavelengths.

great deal about the ISM and particularly about dust grains. The following sections deal with the methods used to derive the different properties of dust grains.

1.3.1 Column densities - Dust distribution

The dust distribution is one of the most important requirements in modelling the interaction of electromagnetic radiation with grains. Several methods are employed in order to get a handle on the dust density and distribution in any given direction. Since the dust seems to follow the gas almost anywhere in the Galaxy, the gas to dust ratio is a constant. Therefore it is sufficient to get the density and distribution of the hydrogen (the most abundant), or any other gaseous element in the ISM, in order to obtain information about the distribution of dust grains.

Neutral hydrogen gas radiates line radiation at 21 cm due to hyperfine transitions in the ground electronic state. Since cold HI clouds make up the bulk of the mass in the ISM, observations at these wavelengths help to map the ISM not only in the Galaxy but also in other galaxies. Another major advantage is that these wavelengths suffer negligible extinction compared to shorter wavelengths. Dickey & Lockman (1990) have done an HI survey of the Galaxy revealing the distribution of HI clouds in the Milky Way. Molecules like CH, NH_3, $C^{18}O$ and CS also

emit radiation in the radio regime and can similarly be traced with the help of observations.

Molecules like CO, CN and HCN emit at millimetre (mm) wavelengths. CO observations are very important in the understanding of cold dense molecular clouds. This is because, molecular hydrogen (H_2), which is the most abundant constituent of these clouds, is very difficult to detect since it doesn't have a permanent electric dipole moment and hence no strong transitions that we can observe. Therefore it is elusive at almost all wavelengths. However the CO molecule acts as a tracer of H_2, since the J=1$\rightarrow$0 rotational transition of CO is a collisionally excited transition and is due to collisions with the H_2 molecule (being the most abundant). The CO survey by Dame et al. (2001) has helped to map the molecular clouds in the Milky Way. From the N(H_2) to W_{CO} ratio (2.8×10^{20} cm^{-2}) of Bloemen et al. (1986), where W_{CO} is the velocity integrated CO intensity, the value of N(H_2) can be derived.

It was the emergence of infrared (IR) astronomy that revealed the importance of dust grains as a major constituent of the Universe. Dust grains can be directly observed in the IR because they emit thermally at these wavelengths. The Infrared Astronomical Satellite (IRAS) (1983) mapped the sky at four wavelengths, i.e. at 12, 25, 60 and 100 μm. Other than that, the ISO (1996-1998), KAO, COBE and WMAP satellites have mapped the entire sky from near to far-infrared and produced excellent images of the ISM. From these observations, it became evident that most of the dust lies in the Galactic plane with the density decreasing at higher latitudes. Boulanger & Perault (1988) showed that the IR intensities are correlated with the total amount of hydrogen in any direction. They calculated the ratio of the IR intensities of the 12μm, 25μm, 60μm and 100μm IRAS bands to the total hydrogen column density for different locations. For the IRAS (100 μm) intensities, the ratio can be written as,

$$\frac{I_\nu(100)}{N(H)} = 1.3 \pm 0.1 \ MJy \ sr^{-1} \ cm^{-2} \tag{1.27}$$

for the Orion region and is as high as 2.4 ± 0.5 for the Lupus clouds.

Apart from this, there is a linear relationship between E(B-V) and the total hydrogen column density in any line of sight (Bohlin et al., 1978), which is given by

$$\frac{N(H)}{E(B-V)} = 5.8 \times 10^{21} cm^{-2} mag^{-1}. \tag{1.28}$$

Here the total hydrogen column density was determined by using the absorption lines of hydrogen Lyman - α and the absorption lines of H_2.

If E(B-V) is known, we can use this equation and calculate the dust density by assuming the average gas to dust ratio in the Galaxy. Accurate distances of stars from the Hipparcos (Perryman et al., 1997) catalogue, when used in conjunction with the extinction measurements can be used to get the exact distribution of dust at any location. Corradi et al. (2004) have used the Strømgren E(b-y) measurements in order to derive the dust distribution towards the Coalsack and Chameleon-Musca clouds.

The analysis of interstellar absorption lines in the UV like Lyα (1215.67 Å), Ly β (1025.72 Å) and Ly γ (972.54 Å) help to measure the hydrogen column density along any line of sight. Probes like HST STIS, ORFEUS-SPAS I & II and FUSE have observed UV absorption lines in several directions. Even the hot ionized medium can be traced due to absorption of light from hot stars by highly ionized species (e.g. OIV, NV and CIV) in the FUV.

1.3.2 Extinction - Grain size, composition

From the extinction curve, which is a plot of E(λ-V) v/s wavelength, it is seen that the extinction is inversely proportional to the wavelength in the visible part of the spectrum, i.e. the absorption and scattering are larger for shorter wavelengths. This gives an estimate of the size of the grains, which have to be of the order of

the wavelength in order to give this dependence. Therefore the radius (a) of the grain is,

$$a = \frac{\lambda}{2\pi}. \tag{1.29}$$

From this observation, and from the presence of various features in the extinction curve, like the 2175 Å bump and the far-UV rise, (see Fig. 1.2) the grains have been estimated to be sub-micron sized and composed mainly of graphite, silicates and very small molecules known as PAHs.

Absorption measurements of elements in space led to the conclusion that the heavy elements are depleted compared to the solar abundances. From these measurements, it was possible to get a handle on the elements which are tied up in grains. It was found that heavier elements like C, N, O, Na, Mg, Si, Cl, K and Fe are the major constituents of grains.

1.3.3 Diffuse radiation - Optical constants

Diffuse radiation has been observed throughout the spectra ranging from the radio to the γ-ray regime. Different processes are responsible for this radiation depending on the wavelength.

In the radio, it is due to synchrotron radiation from cosmic-ray electrons that traverse the Galactic magnetic field. At 21cm, neutral hydrogen contributes due to the hyperfine transition between two spin states. The cosmic microwave background radiation discovered by Penzias & Wilson (1966) with a temperature of 2.736 ± 0.017 K has a cosmological origin due to the expansion of the Universe after the Big Bang.

At near and far-infrared (NIR and FIR) wavelengths, the diffuse emission is due to thermal radiation of small and large dust grains heated by absorption of star-light. There is also a contribution from hot dust in the solar system in addition to the integrated emission from redshifted galaxies.

In the visible, the main contribution is from the scattering of solar photons by the interplanetary medium known as zodiacal light. In the ultraviolet, X-ray and also in the optical, scattering of starlight by interstellar dust grains contribute to the diffuse background. Maximum scattering and absorption occurs at shorter wavelengths due to the λ^{-1} property of extinction. Since this work aims at deriving the interstellar dust properties, we shall restrict our studies to wavelengths at which the dust grains contribute. However out of the different possible wavelengths, we will consider only the far-ultraviolet (FUV) regime, i.e., from 912 Å − 1200 Å. The main advantage of deriving dust properties in the FUV is that there is little contribution from zodiacal emission, which is a major contributor at longer wavelengths. Also there being few sources emitting in the FUV, the sky is extremely dark and well suited for the study of faint diffuse sources. Another advantage of FUV observations over long wavelength observations is that there is negligible contamination due to atomic continuum. Therefore whatever is observed will be purely dust scattered light due to which, there is no need to model and subtract the continuum.

Diffuse radiation has been observed in the FUV from different regions in the Galaxy like the Coalsack molecular cloud, Ophiuchus and Orion. These observations are different from observations of extinction, polarization etc. because they help to separate the scattering and absorption properties of grains. Satellites like FUSE, Coppernicus, GALEX and Voyager have observed a number of sources in the FUV, and obtained intensities ranging from a few tens to more than 3×10^5 photons cm^{-2} s^{-1} sr^{-1} Å^{-1}. The International Ultraviolet Explorer (IUE) has obtained UV spectra in the range 1150 Å − 3000 Å while FUSE observed the wavelength range between 900Å and 1200Å.

The two important optical constants of dust grains which have been derived from observations of dust scattered radiation are the albedo (a) and the phase function asymmetry factor (g). Since these values are related to the composition, size and shape of the grains, knowing these quantities is of utmost importance in

interstellar dust studies.

Although a potentially useful test of models of interstellar dust grains, measurements of these optical constants have been too uncertain to have been of much utility (for a recent review see Draine, 2003b). There are two methods to investigate the scattering properties of grains and both of them have been problematic: reflection nebulae because an uncertain geometry can heavily influence the derived parameters (Mathis et al., 2002); and the diffuse background because of its faintness and because there is often a tradeoff between a and g which allows neither to be tightly constrained (Draine, 2003b).

From the spectra of the observed FUV radiation Henry (2002) has suggested that, a significant fraction of the background radiation at high and moderate latitudes might be due to red shifted radiation from the hot intergalactic medium. However for most of the sources near the galactic plane, the diffuse spectra resembles spectra of early O or B type stars indicating that it is produced as a result of scattering of light of these stars.

This thesis aims to constrain the optical constants of grains in the FUV by modelling FUV observations at different locations in the Galaxy. Owing to the differences in the environment from one region to the other, each region has been modelled separately. Locations near Coalsack, Ophiuchus and Orion have been modelled as part of this thesis and the optical constants of dust grains derived. It is of significance that these locations lie within 20° galactic latitude and their spectra are characteristic of the stars near them. Since absorption is complementary to scattering, i.e. energy absorbed in the UV is reradiated in the infrared, IR modelling also has been done to further constrain these optical constants.

Table 1.2: Symbols used and their meaning

Symbol	meaning
a	albedo
g	phase function asymmetry factor
Q_{sca}	scattering efficiency factor
Q_{ext}	extinction efficiency factor
σ_{ext}	extinction cross-section of grain
σ_{abs}	absorption cross-section of grain
σ_T	Thomson cross-section
σ_B	Stefan-Boltzman constant
ϕ	scattering phase function
θ	scattering angle
E_{inc}	energy incident on grain
E_{sca}	energy scattered
E_{det}	energy reaching detector
F_{det}	flux at detector
I_{det}	intensity at detector
I_ν	intensity of radiation at frequency ν
L	stellar luminosity
d	distance between star and grain
a	radius of grain
n	number density of grains
dV	volume element, dAdz
Ω_d	detector solid angle
Ω_c	solid angle of cloud
A_d	area of detector
E_{rad}	energy radiated by grain
T_d	temperature of dust grain
h	Planck's constant
c	velocity of light in vacuum
r	distance from Sun to cloud
B_λ	planck function
A_B	extinction in Johnson B filter (4400Å)
A_V	extinction in Johnson V filter (5500Å)
E(B-V)	colour excess
R_v	ratio of total to selective extinction, A_V/E(B-V)
N(H)	total hydrogen column density

Chapter 2

MODELS

2.1 Introduction

In order to derive the properties of dust grains, several models have to be incorporated into the main scattering and absorption models. These include models of the dust grain composition, sizes etc. and a model of the total stellar radiation field at the location of the grain. This chapter deals with these different models as well as the main models of scattering and absorption by dust.

2.2 Grain model

Mathis, Rumpl, & Nordsieck (1977) fitted the observed extinction curve for lines of sight passing through diffuse clouds by using a grain model consisting of graphite and silicate ($MgFeSO_4$) grains. Graphite is the most stable form of carbon and has a sheet like structure where the atoms all lie in a plane. They derived a grain-size distribution given by,

$$dn = Cn_H \mathrm{a}^{-3.5} d\mathrm{a},\ \mathrm{a}_{min} < \mathrm{a} < \mathrm{a}_{max}, \tag{2.1}$$

where $\mathrm{a}_{min} = 50$ Å and $\mathrm{a}_{max} = 0.25$ μm, n_H is the number density of hydrogen and C is the proportionality constant. They assumed spherical grains and computed the cross-sections using Mie theory, which was formulated by Mie (1909) and independently by Debye (1909). This involves assuming a complex refractive index

for the grain material and solving the Maxwell's equations with the appropriate boundary conditions at the grain surface.

Draine & Lee (1984) extended the calculations to the mid and far infrared wavelengths and Laor & Draine (1993) calculated the cross-sections for the X-ray regime. Due to the variation of extinction from one location to the other, there were revisions to the model. Cardelli et al. (1989a) found that this variation can be characterized effectively with a parameter R_v where,

$$R_v = \frac{A_v}{E(B-V)} \tag{2.2}$$

takes a value of $R_v = 3.1$ for diffuse dust in the Galaxy increasing with density of the cloud. In order to explain the observed extinction in the IR and microwave region, Weingartner & Draine (2001) extended the model to include very small carbonaceous grains (including PAHs). For the observed extinction they adopted the parametrization of Fitzpatrick (1999) where the normalized extinction curve (normalized with respect to the Cousins I band (0.802 μm) extinction A_I) could be approximated by a function (f) of seven parameters given by,

$$A_\lambda / A_I = f(\lambda; R_v, C_1, C_2, C_3, C_4, \lambda_\circ, \gamma). \tag{2.3}$$

Here C_1, C_2 and C_4 provide the slope and curvature of the extinction curve in the NUV and FUV, C_3 provides the strength of the 2175Å bump, $\lambda_\circ$ represents the central wavelength of the bump and γ provides its width.

The size distribution of Weingartner & Draine (2001) allows for a smooth cutoff size for grain radius greater than some value, a_t and also allows for a change in the slope for radius less than a_t. The form of the size distribution for graphite grains is given by,

$$\frac{1}{n_H}\frac{dn_{gr}}{da} = D(a) + \frac{C_g}{a}\left(\frac{a}{a_{t,g}}\right)^{\alpha_g} F(a; \beta_g, a_{t,g}) \times \begin{cases} 1, 3.5\text{Å} < a < a_{t,g} \\ exp\{-[(a-a_{t,g})/a_{c,g}]^3\}, a > a_{t,g} \end{cases} \tag{2.4}$$

and for silicate grains by,

$$\frac{1}{n_H}\frac{dn_s}{da} = \frac{C_s}{a}(\frac{a}{a_{t,s}})^{\alpha_s} F(a;\beta_s, a_{t,s}) \times \begin{cases} 1, 3.5\text{Å} < a < a_{t,s} \\ exp\{-[(a-a_{t,s})/a_{c,s}]^3\}, a > a_{t,s} \end{cases} \quad (2.5)$$

Here the term D(a) is the sum of two log-normal size distributions and F(a;β,a_t) is given by

$$F(a;\beta, a_t = \begin{cases} 1+\beta a/a_t, \beta \geq 0 \\ 1-\beta a/a_t{}^{-1}, \beta < 0 \end{cases} \quad (2.6)$$

There are a total of 6 adjustable parameters (b_c, C_g, $a_{t,g}$, $a_{c,g}$, α_g, β_g) for graphite and an additional 5 parameters (C_s, $a_{t,s}$, $a_{c,s}$, α_s, β_s) for silicate. Here b_c represents the abundance of carbon with respect to hydrogen.

The theoretical extinction at any wavelength λ is given by :

$$A(\lambda) = 2.5\pi log_e \int dln\, a \frac{dN(a)}{da} a^3 Q_{ext}(a,\lambda). \quad (2.7)$$

Here N(a) is the column density of the material of radius a and Q_{ext} is the extinction efficiency factor which is calculated from Mie theory. The basic principle for calculating Q_{ext} is outlined below.

The Maxwell's equations are:

$$\nabla \times \mathbf{H} = \frac{4\pi\sigma\mathbf{E}}{c} + \frac{\epsilon}{c}\frac{d\mathbf{E}}{dt} = ik\mathbf{E}m^2, \quad (2.8)$$

$$\nabla \times \mathbf{E} = -\frac{1}{c}\frac{d\mathbf{H}}{dt}, \quad (2.9)$$

$$\nabla \cdot \mathbf{H} = 0 and \quad (2.10)$$

$$\nabla \cdot \mathbf{E} = \frac{4\pi\rho}{\epsilon}, \quad (2.11)$$

where $\mathbf{H}$ is the magnetic field strength, $\mathbf{E}$ is the electric field, ω is the circular frequency, c is the velocity of light, ρ is the charge density and m is the refractive index given by,

$$m^2 = \epsilon - \frac{4\pi i\sigma}{\omega}. \quad (2.12)$$

Here σ represents the conductivity and ϵ is the dielectric constant of the medium.

For a homogeneous medium, any rectangular component of **E** or **H** satisfies the scalar wave equation,

$$\Delta\psi = -k^2 m^2 \psi, \tag{2.13}$$

where k is the propagation constant given by $2\pi/\lambda$. The solution of the wave equation is given by,

$$\psi = e^{ikmz+i\omega t}. \tag{2.14}$$

The wave is damped if m has a negative imaginary part and is undamped if m is real.

In the spherical polar co-ordinate system, the scalar wave equation is separable and has solutions of the form:

$$\psi_{ln} = \begin{matrix} cosl\phi \\ sinl\phi \end{matrix} \} \; P_n^l cos(\theta) z_n(mkr) \tag{2.15}$$

Here n and l are integers, $P^l{}_n$ is an associated Legendre polynomial and z_n is a spherical Bessel function. The linear combination of such elementary solutions will give the general solution of the wave equation.

The vectors **E** and **H** satisfy the vector wave equation in a homogeneous medium given by,

$$\Delta\mathbf{A} + k^2 m^2 \mathbf{A} = 0. \tag{2.16}$$

The solution of this equation can be written in terms of two vectors $\mathbf{M}_\psi$ and $\mathbf{N}_\psi$ (that satisfy the vector wave equation) given by,

$$\mathbf{M}_\psi = curl(r\psi) \tag{2.17}$$

$$mk\mathbf{N}_\psi = curl(M_\psi) \tag{2.18}$$

Here ψ satisfies the scalar wave equation.

The two vectors are related by the equation,

$$mk\mathbf{M}_\psi = curl(N_\psi) \tag{2.19}$$

If u and v are two solutions of the scalar wave equation the field vectors can be written as,

$$\mathbf{E} = M_v + iN_u, \tag{2.20}$$

$$\mathbf{H} = m(-M_u + iN_v) \tag{2.21}$$

In order to solve the equation of scattering of a plane wave by a homgeneous sphere of refractive index m, the method of applying the boundary conditions is used. The outside medium is considered to be vacuum (m_2 =1). The incident field (which is assumed to be linearly polarized) is given by,

$$\mathbf{E} = \mathbf{a_x} e^{-ikz+i\omega t} \tag{2.22}$$

$$\mathbf{H} = \mathbf{a_y} e^{-ikz+i\omega t}. \tag{2.23}$$

The direction of propagation is the z-axis and the x-axis is in the plane of the electric vibration of the incident wave.

The incident wave can be written as,

$$u = e^{i\omega t} cos\phi \sum_{n=1}^{\infty} (-i)^n \frac{2n+1}{n(n+1)} P_n^1 cos(\theta) j_n(kr), \tag{2.24}$$

$$v = e^{i\omega t} sin\phi \sum_{n=1}^{\infty} (-i)^n \frac{2n+1}{n(n+1)} P_n^1 cos(\theta) j_n(kr). \tag{2.25}$$

Here j_n is the spherical Bessel function. The total field outside the sphere contains the incident as well as the scattered waves. The scattered wave can be written as,

$$u = e^{i\omega t} cos\phi \sum_{n=1}^{\infty} -a_n (-i)^n \frac{2n+1}{n(n+1)} P_n^1 cos(\theta) h_n^{(2)}(kr), \tag{2.26}$$

$$v = e^{i\omega t} sin\phi \sum_{n=1}^{\infty} -b_n (-i)^n \frac{2n+1}{n(n+1)} P_n^1 cos(\theta) h_n^{(2)}(kr). \tag{2.27}$$

a_n and b_n are the coefficients to be determined. $h_n^{(2)}$ is a spherical Bessel function and has asymptotic behaviour, which when combined with the factor exp(iωt) represents the scattered spherical wave.

$$h_n^{(2)}(kr) \sim \frac{i^{n+1}}{kr} e^{-ikr} \tag{2.28}$$

The field inside the sphere can be described by,

$$u = e^{i\omega t} cos\phi \sum_{n=1}^{\infty} m c_n (-i)^n \frac{2n+1}{n(n+1)} P_n^1 cos(\theta) j_n(mkr), \tag{2.29}$$

$$v = e^{i\omega t} cos\phi \sum_{n=1}^{\infty} m d_n (-i)^n \frac{2n+1}{n(n+1)} P_n^1 cos(\theta) j_n(mkr). \tag{2.30}$$

Now the boundary conditions have to be applied to get the coefficients. The only factors which are different for waves inside and outside the sphere are, v and $\frac{1}{m}\ \frac{\partial(ru)}{\partial r}$ in E_θ and E_ϕ and mu and $\frac{\partial(rv)}{\partial r}$ in H_θ and H_ϕ.

These expressions need to be equal at the boundary between the sphere and the medium i.e. at $r =$ a, where a is the radius of the sphere. The equations can be further simplified by using the following functions:

$$\psi_n(z) = z j_n(z) = S_n(z), \tag{2.31}$$

$$\chi_n(z) = -z n_n(z) = C_n(z), \tag{2.32}$$

$$\zeta_n(z) = z h_n^2(z) = C_n(z). \tag{2.33}$$

Therefore the equations representing the continuity of the waves can be written as:

$$[mu] : \psi_n(x) - a_n \zeta_n(x) = m c_n \psi_n(y), \tag{2.34}$$

$$\left[\frac{1}{m}\frac{\partial(ru)}{\partial r}\right] : \psi_n'(x) - a_n \zeta_n'(x) = c_n \psi_n'(y), \tag{2.35}$$

$$[v] : \psi_n(x) - b_n \zeta_n(x) = d_n \psi_n(y), \tag{2.36}$$

$$\left[\frac{\partial(rv)}{\partial r}\right] : \psi_n'(x) - b_n \zeta_n'(x) = m d_n \psi_n'(y). \tag{2.37}$$

Here $x = \frac{2\pi \mathrm{a}}{\lambda}$ and $y = mk\mathrm{a}$. These equations give the following solutions:

$$a_n = \frac{\psi_n'(y)\psi_n(x) - m\psi_n(y)\psi_n'(x)}{\psi_n'(y)\zeta_n(x) - m\psi_n(y)\zeta_n'(x)}, \tag{2.38}$$

$$b_n = \frac{m\psi_n'(y)\psi_n(x) - \psi_n(y)\psi_n'(x)}{m\psi_n'(y)\zeta_n(x) - \psi_n(y)\zeta_n'(x)}. \tag{2.39}$$

Similarly c_n and d_n can also be derived.

Knowing the co-efficients, and substituting for $h_n^{(2)}$, the scattered wave components can be written as,

$$u = -\frac{i}{kr}e^{-ikr+i\omega t}cos\phi \sum_{n=1}^{\infty} a_n \frac{2n+1}{n(n+1)} P_n^1(cos\theta), \tag{2.40}$$

$$v = -\frac{i}{kr}e^{-ikr+i\omega t}sin\phi \sum_{n=1}^{\infty} b_n \frac{2n+1}{n(n+1)} P_n^1(cos\theta). \tag{2.41}$$

The tangential field components of the scattered wave can be derived by using the vector fields **M** and **N** and written as,

$$E_\theta = H_\phi = -\frac{i}{kr}e^{-ikr+i\omega t}cos\phi S_2(\theta) \tag{2.42}$$

$$-E_\phi = H_\theta = -\frac{i}{kr}e^{-ikr+i\omega t}sin\phi S_1(\theta) \tag{2.43}$$

Here S_1 and S_2 are known as the amplitude functions given by,

$$S_1(\theta) = \sum_{n=1}^{\infty} \frac{2n+1}{n(n+1)} \{a_n \pi_n(cos\theta) + b_n \tau_n(cos\theta)\}, \tag{2.44}$$

$$S_2(\theta) = \sum_{n=1}^{\infty} \frac{2n+1}{n(n+1)} \{b_n \pi_n(cos\theta) + a_n \tau_n(cos\theta)\}, \tag{2.45}$$

where $\pi_n(cos\theta)$ and $\tau_n(cos\theta)$ are,

$$\pi_n(cos\theta) = \frac{1}{sin\theta} P_n^1(cos\theta), \tag{2.46}$$

$$\tau_n(cos\theta) = \frac{d}{d\theta} P_n^1(cos\theta). \tag{2.47}$$

The efficiency factor can be calculated from the amplitude function for $\theta = 0$.

$$S(0) = \frac{1}{2}\sum_{n=1}^{\infty}(2n+1)(a_n + b_n) \tag{2.48}$$

The expression for the extinction efficiency factor is,

$$Q_{ext} = \frac{2}{x^2}\sum_{n=1}^{\infty}(2n+1)Re(a_n + b_n) \tag{2.49}$$

The scattering efficiency factor can be written as,

$$Q_{sca} = \frac{1}{x^2}\int_0^{\pi}\{i_1(\theta) + i_2(\theta)\}sin\theta d\theta, \tag{2.50}$$

where, $i_1(\theta) = \|S_1(\theta)\|^2$ and $i_2(\theta) = \|S_2(\theta)\|^2$ are the intensities.

Knowing Q_{ext} and Q_{sca}, the absorption efficiency factor can be calculated from the relation,

$$Q_{abs} = Q_{ext} - Q_{sca} \tag{2.51}$$

In the grain model of Weingartner & Draine (2001), silicate dielectric functions were based on the astronomical silicate functions of Draine & Lee (1984) and Laor & Draine (1993) for all wavelengths except in the UV. The dielectric function $\epsilon = \epsilon_1 + i\epsilon_2$ of Draine & Lee (1984) is based on laboratory measurements of crystalline silicates in the UV, which contains a feature at 6.5 μm^{-1} not present in the observed interstellar extinction. Therefore in this model, this feature was excised from ϵ_2 and the oscillator strength redistributed between 8 and 10 μm^{-1}. Then ϵ_1 was recalculated using the Kramers-Kronig relation which is the relation between ϵ_1 and ϵ_2.

For carbonaceous grains, this model follows Li & Draine (2002) where the smallest grains are PAH molecules, the largest grains consist of graphite and intermediate size grains have properties between PAHs and graphite. Carbon grains are considered to be 50% neutral and 50% ionized. Graphite dielectric functions were taken from Draine & Lee (1984) and Laor & Draine (1993).

The 1/3 – 2/3 approximation was used according to which the extinction efficiency is the sum of the efficiencies due to the parallel and perpendicular components of the dielectric tensor in the ratio 1:2 given by,

$$Q_{ext} = [Q_{ext}(\epsilon_{||}) + 2Q_{ext}(\epsilon_{\perp})]/3. \quad (2.52)$$

Here $\epsilon_{||}$ and $\epsilon_{\perp}$ are the components of the dielectric tensor for electric field vector parallel and perpendicular to the c-axis of the crystal which is the axis normal to the atomic planes in graphite. This value of Q_{ext} is input into equation 2.7 and the theoretical extinction curve is derived by changing the dust distribution to get the best fit. The cross-section ($= \pi$ a^2 Q) for a mixture of grains consisting of different species is calculated by summing over all the grain sizes and species (Draine, 2003a).

2.3 Interstellar radiation field

The radiation field at any location is very important in modelling the scattering and absorption of dust grains. Mathis et al. (1983) has developed a model of the interstellar radiation field (ISRF), which is a global representation but doesn't predict the ISRF at any specific location. We have used the ISRF model of Sujatha et al. (2004), which can predict the ISRF at any point in space within a few hundred parsecs of the Sun for the Ophiuchus and Coalsack regions. The major contributors to the ISRF in the UV are hot early type stars, which emit mainly in the ultraviolet (912 Å– 3000 Å). The model of Sujatha et al. (2004) has made use of the Hipparcos catalogue which has the most accurate stellar distances available. It contains 107,514 stars of spectral type earlier than R, out of which only 10% – 15% contribute in the UV. The intrinsic luminosity of each star has been computed with the help of a Kurucz (Kurucz, 1992) model, which was scaled to the observed visual magnitude of each star using the following equation.

Let V be the visual magnitude of the star and the distance be d. The observed flux F_v of the star can be written as,

$$F_v = \frac{\gamma K(5500\text{Å})e^{-\tau}}{4\pi d^2} \quad (2.53)$$

Here γ is a scaling factor, K is the Kurucz flux at 5500 Å, d is the distance to the star and τ is the optical depth to the star given by,

$$\tau = \frac{A_v}{1.0863}. \tag{2.54}$$

The visual magnitude V can be written in terms of the flux as,

$$V = -2.5log(F_v) + c. \tag{2.55}$$

Since the observed flux of Vega is 3.64×10^{-9} ergs cm^{-2} s^{-1} Å^{-1} at 5500Å and the visual magnitude is zero we can compare the magnitudes of the two stars as follows,

$$V - 0.0 = -2.5log(\frac{F_v}{3.64 \times 10^{-9}}). \tag{2.56}$$

Therefore we can write F_v in terms of the Vega flux as,

$$F_v = 3.64 \times 10^{-9} \times 10^{-V/2.5}. \tag{2.57}$$

If we expand the equation for F_v we get,

$$\frac{\gamma K(5500\text{Å})e^{-\tau}}{4\pi d^2} = 3.64 \times 10^{-9} \times 10^{-V/2.5}. \tag{2.58}$$

Hence we get the scaling factor between the Kurucz flux and observed flux for all the stars which is used to obtain the stellar luminosities in the FUV. The total optical depth to the star was calculated by assuming the theoretical cross-sections of Weingartner & Draine (2001), together with the observed column densities upto the distance of the star. This model of the ISRF has been able to match accurately the observations of the Belgian/UK UV sky survey telescope (S2/68) on the ESRO TD-1 satellite in the NUV and FUV.

2.4 Scattering

Any scattering model depends on the following;

(a) position, density and properties of scatterers (grains) and

(b) position and fluxes of sources (stars).

Once these quantities are known, the scattered radiation can be modelled depending on the density of the dust grains. In general the photons undergo multiple scattering, i.e. the photons get scattered several times before reaching the detector. In order to model this process we make use of a method known as the Monte Carlo method, since using the equations of radiative transfer is cumbersome and geometry dependent. In this method single photons are tracked as they get scattered and absorbed by grains in the ISM as opposed to a bunch of photons used in the radiative transfer equations.

As part of this thesis, a generalized Monte Carlo model has been developed to simulate the scattered emission from a star in an arbitrary scattering geometry. A schematic of the model is shown in Fig. 2.1. In this model each photon from the star is emitted in a random direction and continues in that direction until an interaction occurs. In order to track the photon, it is essential to know the distance travelled between consecutive scatterings and the scattering angle. Both the quantities can be obtained by sampling from their respective probability distributions. The probability of interaction depends on the local dust density at the point of interaction, and the cross-section of the grain. If the photon travels an element of length dl, the probability that it interacts with a grain is given by,

$$P_{int} = n\sigma dl. \tag{2.59}$$

Here σ is the cross-section of the grain (absorption or scattering), and n is the number density of the grains. Therefore, the probability of travelling without interaction is $1 - \mathrm{P}_{int}$.

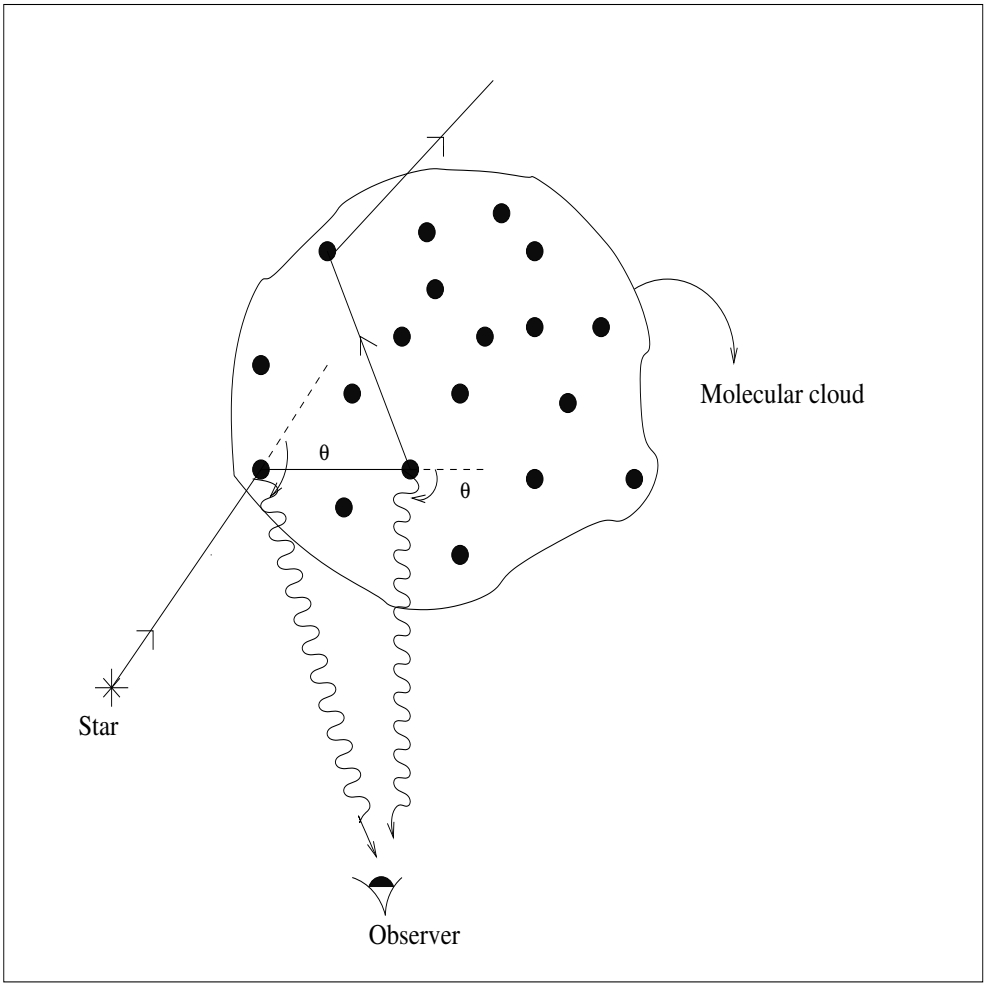

Figure 2.1: In this Monte Carlo model, photons are emitted by the star in a random direction and proceed until an interaction occurs. After each interaction, each photon is re-emitted in a new direction as determined by the scattering phase function. In order to save computational time, at each interaction, a fraction of the energy of the photon depending on its scattering angle is redirected to the observer.

For a distance L given by,

$$L = Ndl \tag{2.60}$$

where N is the number of length elements required to cover a distance of L, the probability of travelling a distance L without interaction can be written as,

$$P_L = (1 - n\sigma L/N)^N = e^{-\tau} = \upsilon. \tag{2.61}$$

Here υ is a number between 0 and 1 and τ is the optical depth ($\tau = \int$n σ dl = n σ L). A set of random numbers is generated which corresponds to this probability. By reversing Eqn. 2.61, τ and the distance L can be calculated.

The probability distribution for the scattering angle is the phase function. At the location of scattering, the angle is sampled from the phase function, (in this case the Henyey-Greenstein (Henyey & Greenstein, 1941) function). The Henyey-Greenstein phase function is an empirical form of the actual phase function which depends only on the parameter g and the scattering angle.

$$\phi(\theta) = \frac{(1 - g^2)}{4\pi(1 + g^2 - 2gcos(\theta))^{3/2}} \tag{2.62}$$

In Eqn. 2.62, g is the phase function asymmetry factor (defined as $\langle cos(\theta) \rangle$) and θ is the angle of scattering. If g is close to zero, the scattering is nearly isotropic while a value of g near 1 implies strongly forward scattering grains.

The concept of weighted photons is used here since the actual number of photons from a star can be as high as 10^{45} s^{-1} and cannot be tracked even with the fastest computers. One weighted photon is equivalent to **N** stellar photons thereby reducing the number of photons tracked. At each interaction the photon's weight is reduced by a factor a, the grain albedo. To save computational time, a part of the energy of every photon is redirected to the observer at each interaction. This fraction depends on the phase function corresponding to the direction towards the observer. The photon is similarly followed through a sequence of interactions until it either leaves the area considered or its intensity drops to a negligible value. The

model converges to a solution in a few million iterations, after which the results are scaled to the stellar output.

This model has a 3-dimensional dust density array as the input which can be modified according to the location under study, thereby making it a very general model for scattering calculations. Similarly it can accommodate many stars and calculate the total contribution from all of them.

However if the density of the grains is considerably low ($\tau < 1$), it is sufficient to make the approximation of single scattering, where the photon gets scattered only once before reaching the detector. In this case we can use the radiative transfer equations given in Chapter 1.

2.5 Absorption

During the interaction of a grain with the incident radiation, a fraction of the energy is absorbed by the grain. The scattering model described in the previous section has been modified to include this absorption also. In this model, at the location of the grain, the effective weight of the photon that is absorbed is $1 - a$ times the incident photon's weight. The remaining weighted photon gets scattered several times, during which a fractional photon gets absorbed at each interaction. Whenever the next photon is absorbed, its weight is added to the previous value at the location. After all the photons have been considered, the total value at each location is converted to a flux and stored in an array and the next wavelength is considered. This is repeated for all wavelengths and the total energy absorbed in each bin of the 3-dimensional density array is computed.

This value is then equated to a modified planck function as given in Eqn. 1.12 from which the temperature is obtained. Knowing the temperature and the density, the intensity of thermal emission at the desired wavelength can be calculated.

The procedure is repeated for all combinations of a and g before comparing

the results with observations. As in the case of scattering there may be several bright stars contributing in the region, in which case the total absorbed energy has to be calculated for each star separately and then summed up. The additional summation over wavelengths is extremely time consuming and therefore we have to resort to parallel processing. This can be done in two ways. The simplest method is to do the computation for each star in different computers at the same time and then add up the intensity arrays. Another program then adds these arrays and computes the thermal emission intensities. Otherwise, the program can be modified to use parallelising methods such as MPI (Message Passing Interface) or OpenMP, where in a single program, the wavelengths or photons or both get distributed among the different processors of a supercomputer. The Monte Carlo program used as part of this work has been modified so as to do both types of processing. If the number of contributing stars in a location is less (< 5), the former method is sufficient. Otherwise we have to go for the latter procedure.

As in the case of scattering, if the optical depth τ is less than 1, we can opt for a single scattering model where the photon is assumed to get scattered only once before reaching the detector. Hence we can use equation 1.12 to calculate the temperature of the grains and the corresponding thermal intensities.

Table 2.1: Symbols used and their meaning

Symbol	meaning
n_H	number density of hydrogen
A_I	extinction in Cousins I band (8020 Å)
a	grain radius
$\lambda_\circ$	central wavelength of 2175Åbump
C_1, C_2, C_3, C_4, γ	extinction curve parameters of Fitzpatrick (1999)
D(a)	grain size distribution which is sum of two log-normal distributions
C_g, α, β	dust distribution parameters
b_c	abundance of carbon grains relative to hydrogen
H	magnetic field strength,
E	electric field,
m	refractive index
ω	circular frequency
c	velocity of light in vacuum
ρ	charge density
σ	conductivity
ϵ	dielectric constant
k	propagation constant
${P^l}_n$	associated Legendre polynomial
z_n, j_n	spherical bessel functions
r	spherical polar coordinate
A	vector wave function
${h_n}^{(2)}$	spherical bessel function
$S(\theta)$	amplitude functions of wave
$K(\lambda)$	Kurucz flux
d	distance to the star
τ	optical depth
P_{int}	interaction probability of a photon with a grain

Chapter 3

Dust Properties in the FUV in Ophiuchus

3.1 Introduction

The Ophiuchus molecular cloud is one of a large complex of clouds at a distance of about 160 pc from the Sun (Chen et al., 1997). It is believed to be the remnant of a Giant Molecular cloud (GMC), from which the stars of the Scorpio-Centaurus OB association were formed. HI studies by Cappa de Nicolau & Pöppel (1986) have indicated the presence of a loop like structure at certain velocities, surrounding the early-type stars in the Upper Scorpius. The Ophiuchus complex of clouds lies within this HI loop. Even the high-latitude clouds of Magnani et al. (1985) are probably associated with these clouds (de Geus et al., 1990). The region has been extensively studied in CO (de Geus et al., 1990; Dame et al., 2001) as well as with four-colour photometry (Corradi et al., 2004) allowing us to determine the three-dimensional distribution of the matter in this direction. There is an under abundance of CO in this region, most likely due to the photodissociation of the molecular clouds by the bright stars in the nearby OB association. The conversion factor between W_{CO} and $N(H_2)$ is a factor of five times smaller than that found by Bloemen et al. (1986), due to the higher temperatures there (de Geus et al., 1990). The region has also been observed in the near and far infrared by the IRAS satellite. However, Ophiuchus being in the ecliptic plane all the infrared bands

have zodiacal contamination.

Our interest in this region is that one of the first observations of diffuse emission in the far ultraviolet (FUV – 912 - 1216 Å) was made here by Holberg et al. (1991) who identified the emission as starlight from the nearby Scorpius-Centaurus OB association scattered by dust in the Ophiuchus molecular cloud.

Because of the technical difficulties inherent in diffuse observations in the FUV, largely due to scattering from the intense geocoronal Lyα line, there have been very few observations of the background radiation in this spectral region (see Bowyer, 1991; Henry, 1991, for reviews of the diffuse radiation in both the near and far ultraviolet). By far the largest and most reliable data set has come from the ultraviolet spectrographs (UVS) aboard the two Voyager spacecraft which made observations of various astrophysical targets during the interplanetary phase of their mission, between their hugely successful planetary encounters. Many of these targets were of objects with no intrinsic FUV flux and Murthy et al. (1999) used them for a comprehensive study of the diffuse FUV radiation field. Because of the sensitivity of the Voyager UVS to diffuse radiation and the distance of the spacecraft far from the Earth where emission from interplanetary H I is minimized, these remain the definitive observations of the diffuse radiation field in the FUV.

Except for a small extragalactic component at high latitudes (Henry, 1991), the diffuse UV radiation is largely due to starlight scattered by interstellar dust and as such can be used to derive the scattering properties of the interstellar dust grains. Unfortunately there has been considerable controversy about both the level of the diffuse radiation and the modeling used to extract the optical constants (see Draine, 2003b; Mathis et al., 2002, for a discussion of the difficulties) and there have been only loose observational constraints on the albedo (a) and phase function asymmetry factor (g) of the dust grains.

As mentioned above, Holberg et al. (1991) discovered intense diffuse emission from Ophiuchus using the Voyager UVS and interpreted this emission as starlight back-scattered by the Ophiuchus molecular cloud. We have re-examined these

observations along with others from the Voyager archives (Murthy et al., 1999) in the light of a more sophisticated model and an improved understanding of the dust distribution in the direction of Ophiuchus (Corradi et al., 2004) and have found that the emission is actually due to the forward scattering of the light from a much lower density sheet of material in front of the Ophiuchus molecular cloud. There were many observations spread throughout the entire region and so we have been able, for the first time, to remove the degeneracy between the albedo (a) and the phase function asymmetry parameter (g) which have plagued studies of the diffuse radiation (Draine, 2003b). We have constrained a to 0.40 ± 0.10 and g to 0.55 ± 0.25, in good agreement with the theoretical prediction of Weingartner & Draine (2001) for a mixture of graphite and silicate grains.

3.2 Observations

The two Voyager spacecraft include identical Wadsworth-mounted objective grating ultraviolet spectrographs (UVS) covering the wavelength region between 500 and 1700 Å, with their greatest sensitivity at wavelengths below 1200 Å. The field of view of the spectrographs is $0.1^\circ \times 0.87^\circ$ with a spectral resolution of 38 Å for diffuse sources. The spacecraft were launched within two weeks of each other — Voyager 2 in 1977 August and Voyager 1 in 1977 September — and obtained a wealth of information on all four of the giant planets. The two spacecraft are still continuing operation at the edge of the solar system with more than 10,000 days of operation each. A full description of the UVS spectrographs and further information about the interstellar mission of the Voyager spacecraft is given by Holberg & Watkins (1992).

While the spacecraft were between planetary encounters, they observed many astronomical targets. Amongst these targets were a series of scans in the vicinity of Ophiuchus with the Voyager 2 spacecraft in 1982 (Holberg et al., 1991). We have supplemented these with further observations from the Voyager archives taken at

various times between 1982 and 1994 (Murthy et al., 1999). There were a total of 31 such locations and these are plotted on an IRAS 100 μm map in Fig. 3.1 and tabulated in Table 3.1 with the total hydrogen column density (Schlegel et al., 1998) and the IRAS 100 μm flux (Wheelock et al., 1994). There was a limit cycle motion of a few tenths of a degree in the Voyager pointing and the position reported in the table is an average of the actual pointing of the instrument.

The data reduction is described in detail in Murthy et al. (1999) and Holberg (1986) and consists of fitting three components to the observed signal: dark noise from the spacecraft's radioisotope thermoelectric generator (RTG); emission lines from interplanetary H I; and emission from cosmic sources. The dark noise was subtracted using the continuum below the Lyman limit (912 Å) and the astronomical and heliospheric emission were then simultaneously fit using templates for the emission. This reduction procedure was shown to be consistent and reproducible over observations separated widely in time and between the two spacecraft and yielded 1σ limits as low as 30 photons cm^{-2} s^{-1} sr^{-1} Å^{-1} over a large part of the sky. For the bright sources reported on here, the diffuse emission dominated the raw data and there was little uncertainty in the derived levels.

3.3 Model

The diffuse emission in Ophiuchus is the result of light from the nearby stars scattering from interstellar dust in the line of sight and were modeled in a similar manner to Shalima & Murthy (2004) in the Coalsack. The stellar radiation field was calculated at the location of the scattering dust using the model of Sujatha et al. (2004), in which the distance and spectral type of each star was taken from Hipparcos data (Perryman et al., 1997) and the flux calculated using Kurucz models (Kurucz, 1992) with the latest modifications from his web page (http://kurucz.harvard.edu). Eight stars (see Fig. 3.1) contribute ∼90% of the total ISRF in this region. The properties of the stars are given in Table 3.2.

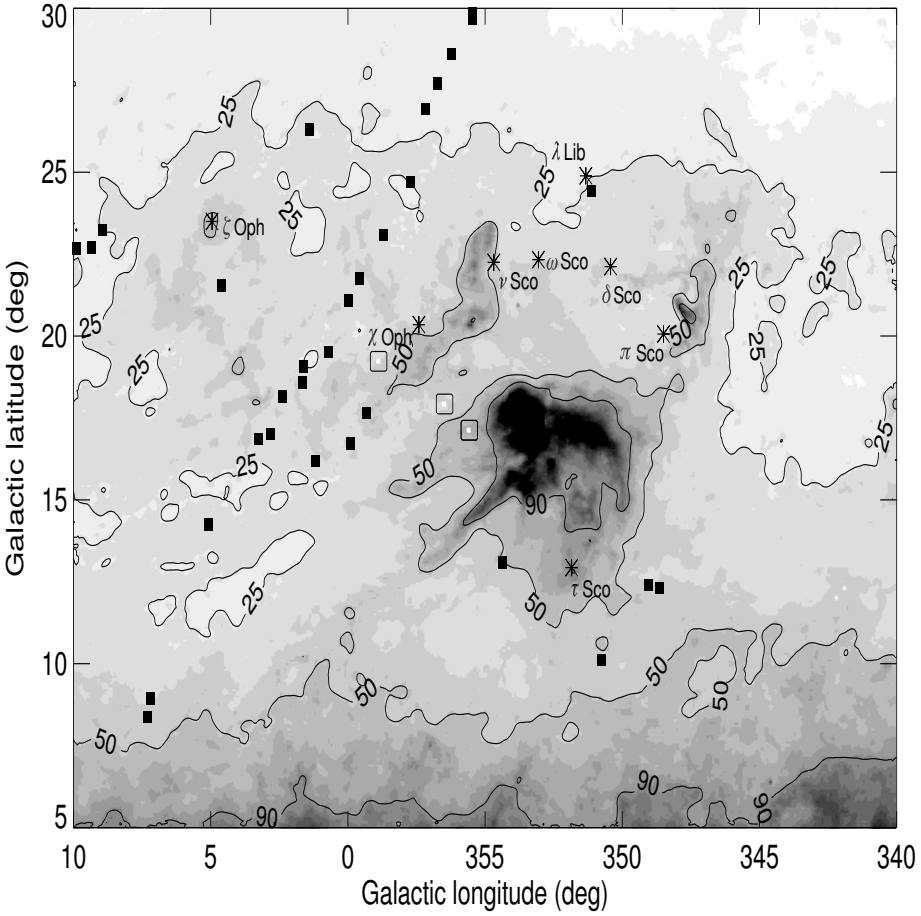

Figure 3.1: IRAS 100 μm map of the region is shown with contours labelled in units of MJy sr^{-1}. The filled squares show the locations of the *Voyager* observations and the asterisks show the positions of the brightest UV stars in the region.

The amount of radiation scattered to the observer is dependent on the scattering function of the grains and we have used the Henyey-Greenstein scattering phase function, $\phi(\theta)$ (Henyey & Greenstein, 1941).

$$\phi(\theta) = \frac{a}{4\pi} \frac{(1-g^2)}{(1+g^2-2gcos(\theta))^{1.5}} \tag{3.1}$$

Here a is the albedo — which can range from 0 for dark grains to 1 for fully reflecting grains — and g is the phase function asymmetry factor with $g = 0$ indicating isotropic scattering and higher values indicating forward scattering grains.

Draine (2003a) has suggested that the Henyey-Greenstein function underestimates the scattered radiation for highly forward scattering grains ($g > 0.7$) in the FUV. We have found, empirically, that using the theoretical scattering function of Weingartner & Draine (2001) for a mixture of graphite and silicate grains makes no more than a 10% difference in the derivation of the optical constants for $g = 0.65$ and so, for consistency with the literature, we only cite the results using the Henyey-Greenstein function. The primary uncertainty in our procedure is in the location of the scattering dust and we discuss this below.

The interstellar medium in the direction of Ophiuchus is dominated by the huge molecular complexes in Ophiuchus (Fig. 3.1) at a distance of $\sim$ 160 pc (Chen et al., 1997). Because of the thickness of the cloud, only foreground stars will contribute to the diffuse radiation observed at the Earth. Back-scattering from the molecular cloud is an order of magnitude too small to account for the observed UV intensity and hence we conclude that the scattering must be from two extended sheet-like structures which Corradi et al. (2004) have shown to cover the entire region between the galactic longitudes of 290° − 10° and latitudes of -25° − +25°. The nearer of the two sheets is at a distance of d $\leq$ 60 pc from the Sun and the other, from which most of our observed scattering comes, lies between 100 and 150 pc from the Sun, depending on the direction. The latter sheet is likely part of the neutral ring surrounding the complex of molecular clouds in Ophiuchus discovered by Egger & Aschenbach (1995) in the ROSAT all-sky survey. Corradi et al. (2004) has found

a column density of 3.2×10^{19} cm^{-2} in the nearer cloud and a much larger column density of $3.7 - 27 \times 10^{20}$ cm^{-2} in the further cloud. Other than these two clouds and the Ophiuchus molecular cloud, there is very little material out to a distance of at least 200 pc from the Sun (Frisch, 2002a).

In our model, we have divided the total H I from Dickey & Lockman (1990) in any line of sight into the two foreground clouds, with a constant value of 3.2×10^{19} cm^{-2} in the nearer cloud and the rest in the further cloud. For the Ophiuchus molecular clouds, we have subtracted the H I column density from the total hydrogen column density of Schlegel et al. (1998) and distributed this excess material at the location of the molecular cloud. We converted the H I column density to a dust scattering cross-section using the theoretical values of Weingartner & Draine (2001), implicit in which is the dust to gas ratio of Bohlin et al. (1978). In practice, the observed UV emission is almost entirely from the more distant of the two sheets and so is most sensitive to the exact distance of that sheet, or rather to the distance between the sheet and the stars dominating the ISRF in this region, and the amount of dust in that cloud. Because this distance is uncertain, we have used a 3 parameter model in which we allow the distance to the dust to vary but fix a and g to a common value over all 31 positions. We then use a single scattering model to calculate the scattered flux in the UV and independently calculate the thermal emission at 100 μm for the best fit parameters. The best fit distances are plotted in Fig. 3.2 and show a variation of 100 - 125 pc in this region, consistent with the values found by Corradi et al. (2004).

3.4 Results and Discussion

It is interesting to note that the level of the diffuse emission is not at all correlated with the amount of material in the line of sight (Fig. 3.3). Instead there is a tight correlation between the level of the ISRF and the scattered radiation (Fig. 3.4). This has important implications for the study of the diffuse radiation field.

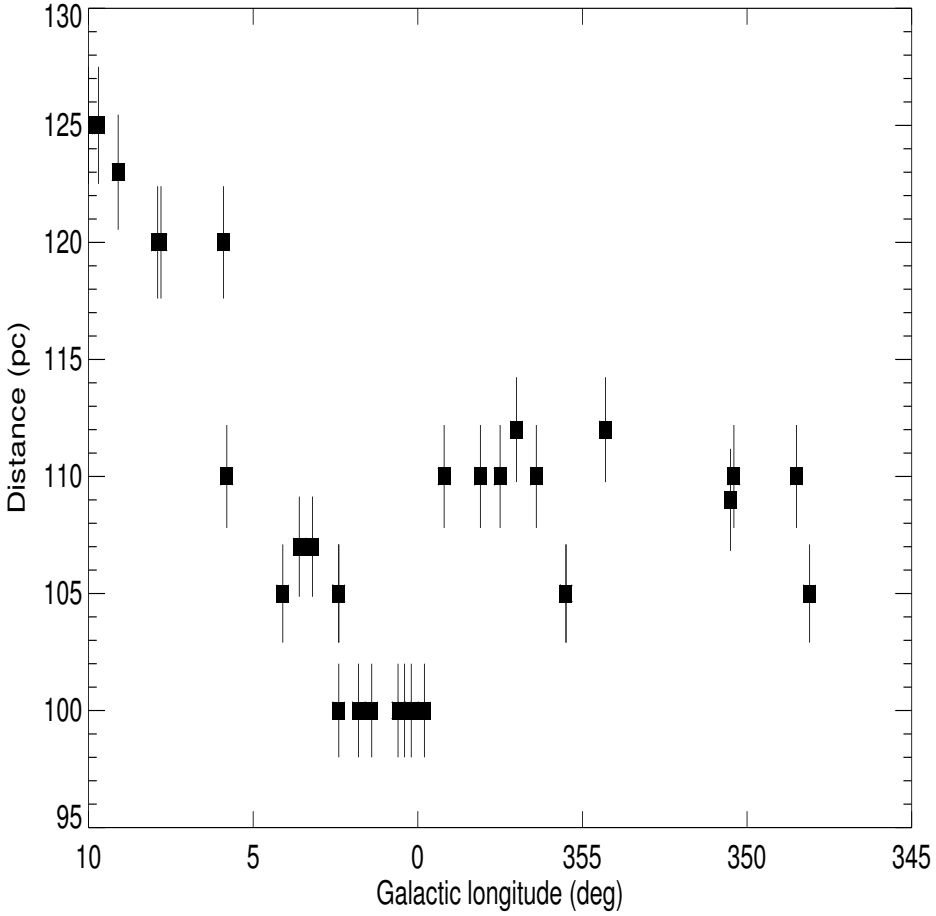

Figure 3.2: Best fit distances to the scattering layer for each of the locations as a function of galactic longitude in degrees.

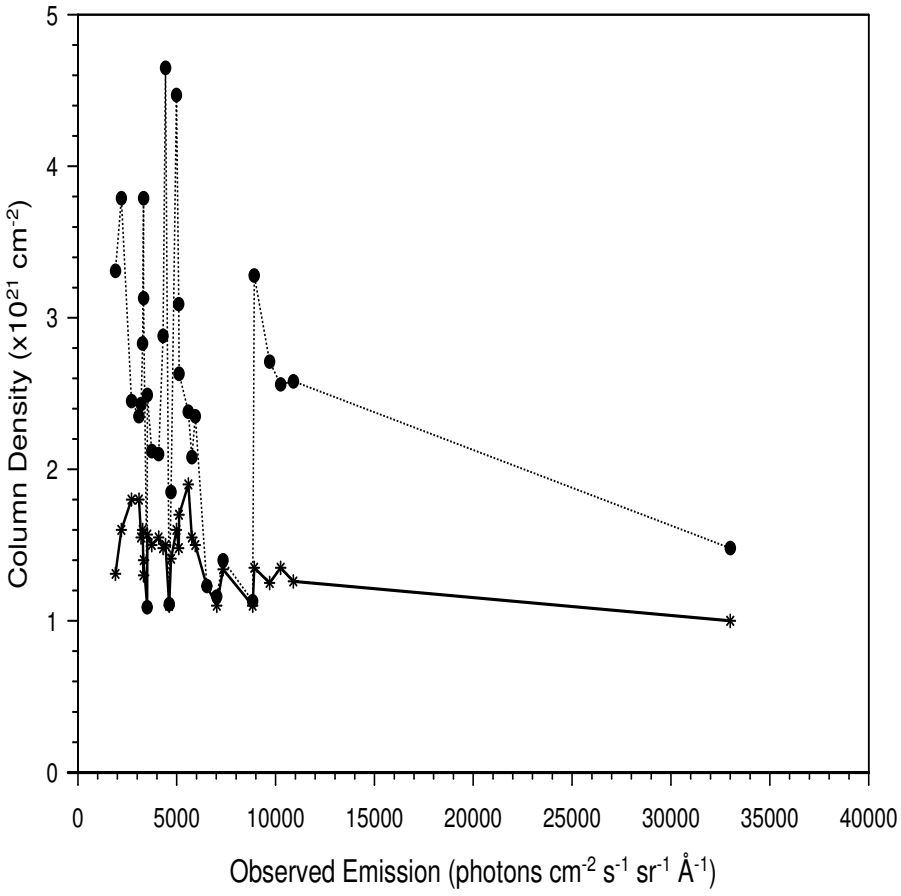

Figure 3.3: Observed UV intensity at each location is plotted against the corresponding values of the total, N(H) (dotted line) and neutral, N(H I) (solid line) hydrogen column densities. There is clearly no correlation between the FUV intensity and either N(H) or N(H I).

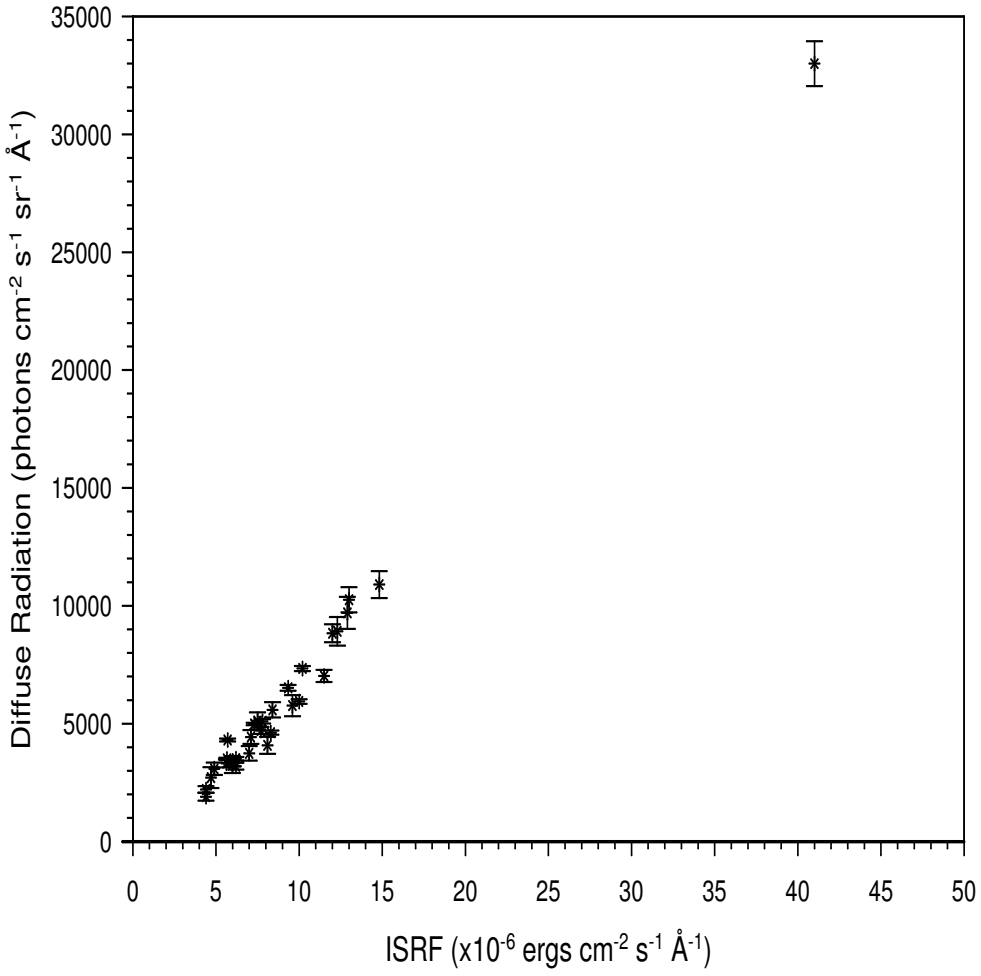

Figure 3.4: Observed UV intensity at each location is plotted against the ISRF. The non-zero intercept is due to the absorption of the diffuse radiation in the intervening ISM.

It is often claimed that the diffuse radiation is correlated with the H I column density (e.g. Bowyer, 1991; Schiminovich et al., 2001); however, it is becoming increasingly evident that the diffuse radiation is dominated by local effects, particularly near bright stars (c.f. Murthy & Sahnow, 2004).

Our model predictions match the observations extremely well both in UV scattering (Fig. 3.5) and in 100 μm infrared emission (Fig. 3.6). We have derived a 90% confidence contour (as per Lampton, Margon, & S.Bowyer, 1976) for a and g and this is shown in Fig. 3.7. Our 90% confidence limits on a and g are 0.40 ± 0.10 and 0.55 ± 0.25 respectively and are consistent with the theoretical predictions of Weingartner & Draine (2001) for average Milky Way dust with R_V=3.1 ($a = 0.365$, $g = 0.6$).

There are very few determinations of the optical parameters of interstellar grains at wavelengths shorter than 1200 Å (Draine, 2003b; Gordon, 2004) and most of these have come from observations of reflection nebulae. Witt et al. (1993) found an albedo of 0.42 ± 0.04 from *Voyager* 2 observations of NGC 7023 and Burgh et al. (2002) found an albedo of 0.30 ± 0.10 from rocket observations of NGC 2023. Both groups claimed that the grains were highly forward scattering with $g \sim 0.8$. Shalima & Murthy (2004) found a similar value of 0.40 ± 0.20 through *Voyager* observations of the Coalsack Nebula but were not able to constrain g.

Although our derived albedo (0.40 ± 0.10) is consistent with the earlier determinations, we find a slightly lower value for g (0.55 ± 0.25). It is possible that conditions are different in reflection nebulae as opposed to the diffuse ISM we observe or it may be that, as Draine (2003a) suggests, the scattering function is poorly represented by the Henyey-Greenstein function in the FUV leading to differences between determinations in different geometries, particularly for highly forward scattering grains.

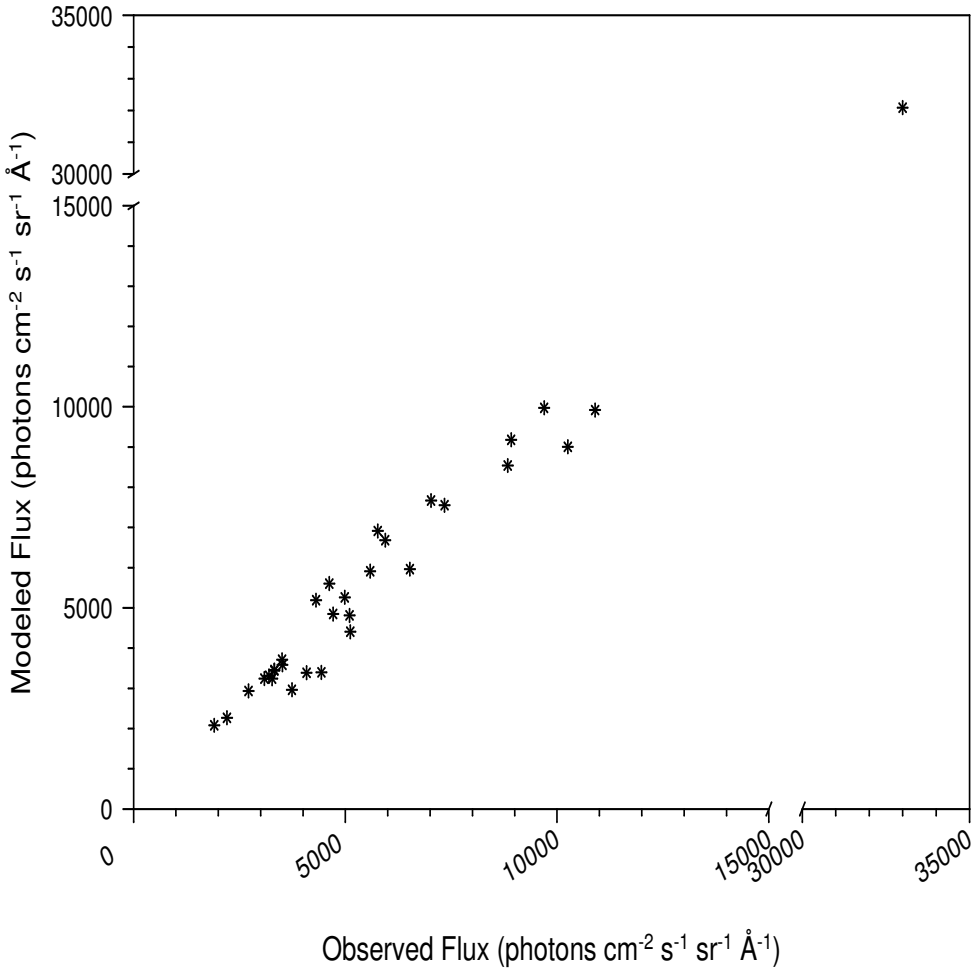

Figure 3.5: Modeled FUV (1100 Å) intensities corresponding to $a = 0.40$ and $g = 0.6$ have been plotted against the observed values for each location.

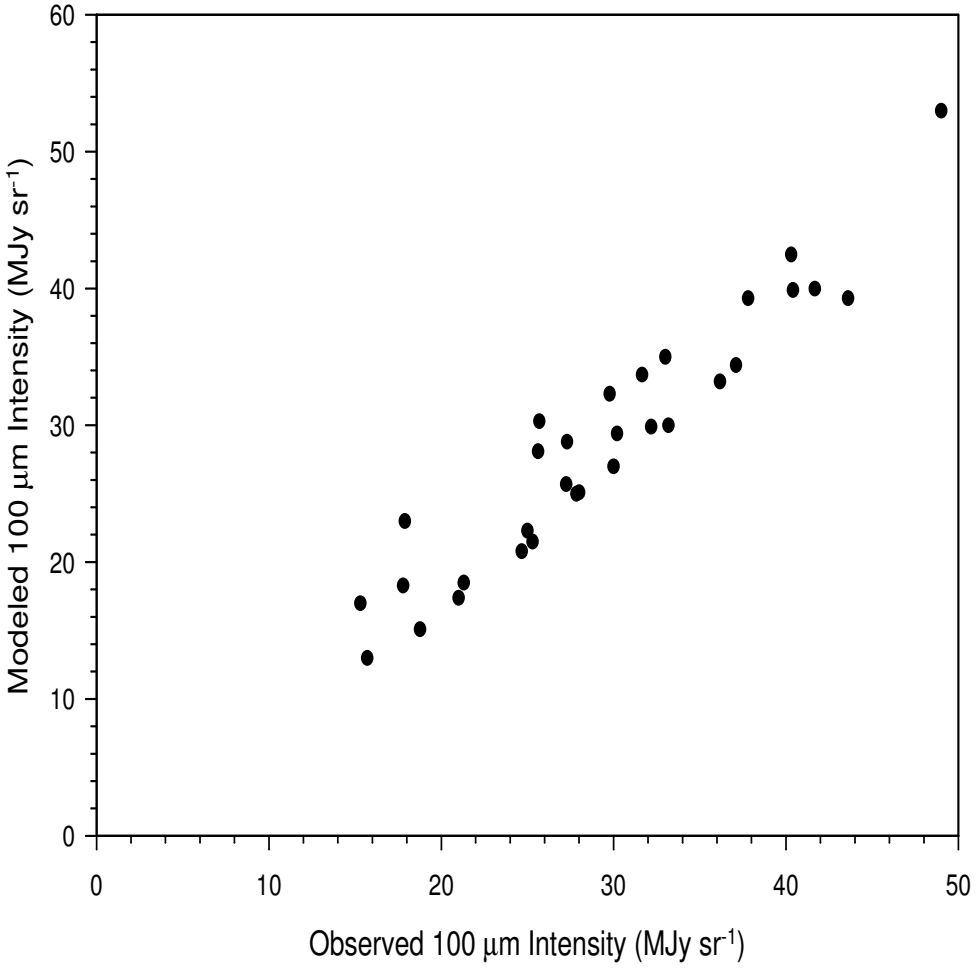

Figure 3.6: Modeled IR intensities corresponding to an albedo of 0.40 and $g = 0.6$ have been plotted against the observed IRAS (100 μm) values for each location.

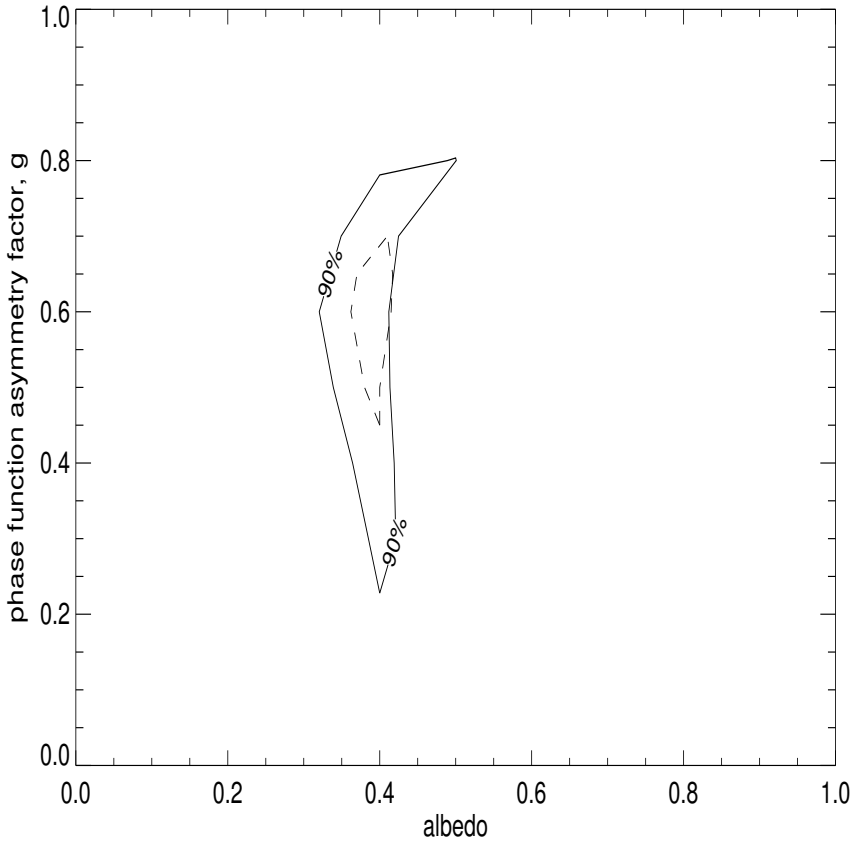

Figure 3.7: 90% confidence contour for all 31 locations (solid contour) is shown. The contour corresponds to a limit of 0.40 ± 0.10 and 0.55 ± 0.25 on the albedo and g respectively. Also plotted is the intersection of the individual 90% confidence contours for each of the locations (dashed line).

3.5 Conclusions

We have used *Voyager* observations of the diffuse FUV radiation in the region of Ophiuchus to investigate the optical constants of the interstellar dust grains. We have found that the intense emission in this region arises not in the dense molecular cloud which contains most of the matter in this direction but rather in a much thinner neutral sheet in front of the cloud. In fact, there is no correlation between either the 100 μm IRAS emission or N(H) and the scattered FUV light. Instead the FUV emission is tightly correlated with the strength of the local ISRF. Thus unlike thermal dust emission in the IR, where the dust is optically thin and the material along the entire line of sight contributes to the total, scattering in the FUV requires much thinner clouds and nearby bright stars.

In general, one should not expect correlations on global scales between the UV and IR or UV and N(H). This is borne out by Murthy & Sahnow (2004) who find only a mild dependence on the 100 μm for the FUV flux but not by Schiminovich et al. (2001) who claim a correlation between the UV (at 1500 Å) and N(H) using data from the NUVIEWS rocket flight. We are pursuing further investigations with data from the Galaxy Evolution Explorer (GALEX) to test these correlations.

We find that the interstellar dust grains are highly forward scattering with a g ($= \langle cos\theta \rangle$) of 0.55 ± 0.25 and an albedo of 0.40 ± 0.10. These results are in general agreement both with the theoretical predictions of Weingartner & Draine (2001) and previous observations of reflection nebulae. As a test of our model, we have independently calculated the 100 μm intensities for each of the locations for our best fit a and g values and found them to match the IRAS (100 μm) observations.

Table 3.1: Details of observed locations in Ophiuchus

Location	l (deg)	b (deg)	Observed Flux±Error (ph cm^{-2} s^{-1} sr^{-1} Å^{-1})	IRAS(100 μm)[a] (MJy sr^{-1})	N(H)[b] ($\times$ 10^{21} cm^{-2})
1	359.8	17.8	1900±170	43	3.3
2	0.2	22.1	2200±140	38	3.8
3	7.9	7.8	2710±440	21	2.5
4	7.8	8.4	3090±260	17	2.4
5	0.6	21.4	3200±140	36	2.4
6	1.4	19.7	3270±360	30	2.8
7	0.4	16.8	3320±140	37	3.8
8	1.8	16.2	3320±180	32	3.1
9	355.5	31	3510±50	19	1.1
10	5.8	21.6	3510±75	33	2.5
11	2.4	19.2	3740±310	26	2.1
12	348.1	12.1	4080±360	40	2.1
13	2.4	18.7	4310±65	32	2.8
14	4.1	16.8	4430±295	30	4.7
15	355.5	30.3	4620±90	16	1.1
16	2.4	26.7	4710±150	27	1.8
17	3.6	17	4990±50	28	4.5
18	3.2	18.2	5100±90	30	3.1
19	5.9	14	5120±360	28	2.6
20	350.4	9.8	5580±325	42	2.4
21	348.5	12.2	5760±445	40	2.0
22	359.2	23.5	5940±95	33	2.4
23	357.5	27.5	6520±125	18	1.2
24	356.4	29.2	7020±260	15	1.2
25	358.1	25.2	7340±110	26	1.4
26	357	28.3	8840±380	18	1.1
27	10.2	22.4	8920±610	25	3.3
28	9.1	23.1	9700±680	27	2.7
29	9.7	22.5	10250±540	25	2.6
30	354.3	13	10900±570	49	2.6
31	350.5	24.9	33000±955	25	1.4

[a] Wheelock et al. (1994).

[b] Column densities from Schlegel et al. (1998).

Table 3.2: Properties of contributing stars

Star	l (deg)	b (deg)	Spectral Type	Temperature (K)	log (g)	log (z)
ζ Oph	6.28	23.59	O9V	35000	3.94	0
χ Oph	357.93	20.68	B2Vne	22000	3.94	0
ν Sco A	354.61	22.70	B2IV	22000	3.94	0
ω Sco	352.75	22.77	B1V	25600	3.94	0
δ Sco	350.10	22.49	B0.2IV	30000	3.94	0
π Sco	347.22	20.23	B1V	25600	3.94	0
τ Sco	351.54	12.81	B0V	30000	3.94	0
λ Lib	350.72	25.38	B3V	19000	3.94	0

Chapter 4

Modelling of dust properties in the FUV toward the Coalsack

4.1 Introduction

The Southern Coalsack extends over $5^\circ \times 6^\circ$ in the sky and is located in the galactic plane ($b = 0.0^\circ$) at a longitude of 303°. It is highly irregular and inhomogeneous and made up of several large and small clouds. It is one of the few massive clouds (3500 $M_\odot$), where there is no star formation. The extinction here is as high as 2.4 magnitudes at 4400 Å. CO observations (Nyman et al., 1989) have shown that it has a very complex structure with clumps and filaments and several velocity components. At least 27 globules have been found to be associated with the Coalsack (Bok et al., 1977) with no evidence for star-formation. Andersson et al. (2004) have observed X-ray emission at the perimeter of the Coalsack molecular cloud using the Roentgen satellite (ROSAT) which they attributed to the interaction zone between the Sco-Cen superbubble and the molecular cloud. This has been observed in the high energy bands but not in the lower energy bands due to foreground extinction. In addition the authors also observed OVI absorption in the FUV for stars behind the Coalsack molecular cloud due to which they established that the emission was associated with the molecular cloud. It represents an excellent direction for the determination of the scattering properties of dust grains particularly in the UV and was found to be one of the brightest sources of diffuse

UV emission in the sky by Murthy et al. (1994). Without detailed modeling, they were unable to provide useful constraints on the optical constants of the grains but suggested that most of the observed emission was due to forward scattering of photons from three of the brightest UV stars in the sky by foreground dust, rather than back-scattering from dust in the molecular cloud. Mattila (1970) has also observed scattering in the visible from this region which was however considered to be scattering from the Coalsack. In view of our results, we suggest that scattering by the foreground medium may be the major source of the visible emission also.

In Shalima & Murthy (2004) (here after referred to as paper I), we have constrained the far ultraviolet (FUV) dust properties of the region using five Voyager observations of four locations in the Coalsack and a detailed Monte Carlo scattering model. We found that the FUV albedo in the region is 0.4±0.2 at 1100 Å but couldn't constrain the phase function asymmetry factor g because of the lack of sufficient data. Now with additional data from the Far Ultraviolet Spectroscopic Explorer (FUSE) we have observations at 28 locations in this region for five different wavelengths in the FUV (Fig. 4.1) using which we can constrain both a and g.

4.2 Observations

There are a total of 118 observations in the region from Voyager and FUSE spacecraft covering five different wavelengths in the FUV (Table 4.1). These have been described in detail in Murthy et al. (1999) and Murthy & Sahnow (2004) respectively. Five of the observations were taken by the spectrographs aboard the two Voyager spacecrafts (Voyager 1 & 2). The FUSE observations are part of the S405/505 program where regions of nominally blank sky were observed for several thousand seconds. Out of these observations Murthy & Sahnow (2004) found diffuse signal in several locations including the Coalsack. The intensities toward the

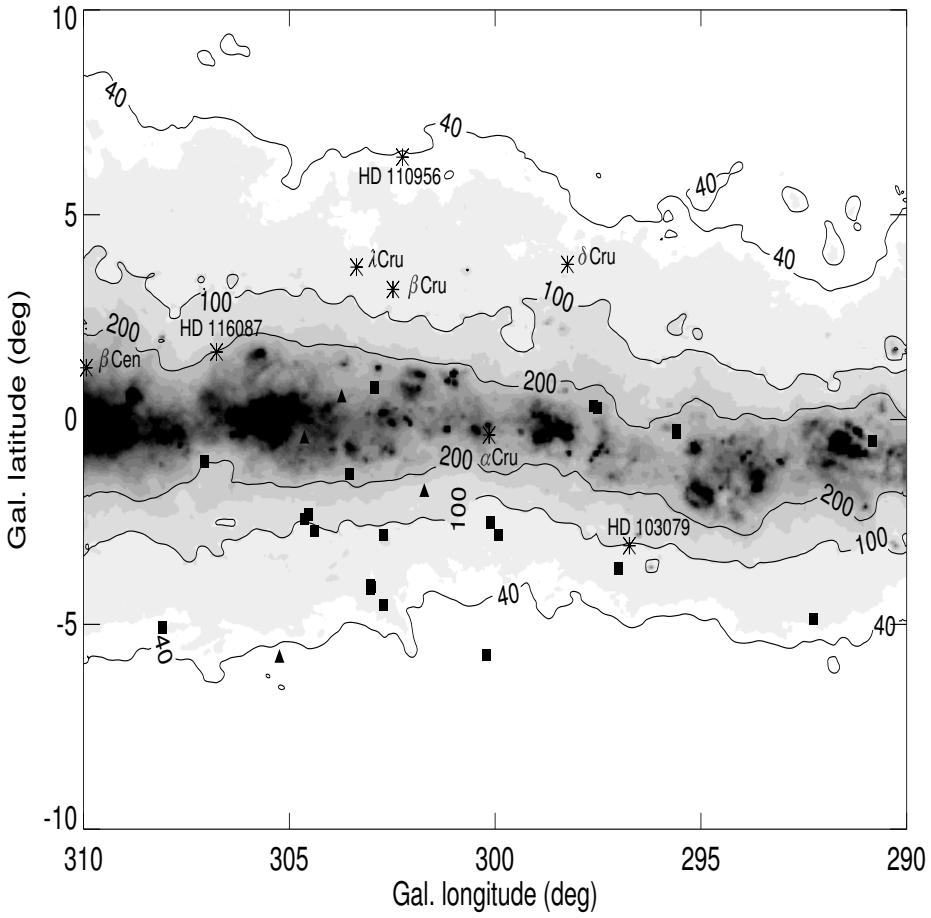

Figure 4.1: The IRAS 100 μm (in units of MJy sr^{-1}) map of the region is plotted with the 34 observed locations superimposed on it. Filled squares represent FUSE locations while filled triangles represent the Voyager targets. The brightest UV stars in the region are also marked as asterisks.

Table 4.1: Details of observed locations in the Coalsack

No.	l	b	Observed UV Intensity[a]					IRAS (100μm)	Ref.
	(deg)	(deg)	999 Å	1056 Å	1100 Å	1157 Å	1159 Å	(MJy sr^{-1})	
1	290.9	-0.5	750±750	1360±780	3360±940	370±370	3090±950	270	1
2	290.9	-0.5			5980±800			270	1
3	292.3	-4.8	4510±1950	4630± 970	7500±1410		4340±1180	50	1
4	295.6	-0.24			6690±1180			270	1
5	297.5	0.3	13130±2360	15830±1500	13440±890	12730±1400	17600±2680	260	1
6	297.5	0.3	22840±6850	10040±1810	9965±1020	9330±1040	10570±1160	260	1
7	297.5	0.3	18360±3480	12450±1000	14600±1860	15960±2800	16090±2380	260	1
8	295.6	-0.3	3700±1810	5150±600	3350±1050	3150±1500	5070±1260	240	1
9	297.0	-3.6	6920±2010	5120±1220	6650±1340	7370±2200	4630±1790	60	1
10	303.5	-1.3	10295±3200	12320±1600	9520±3450	14140±2870	10750±2390	235	1
11	297.6	0.34			12420±1300			270	1
12	297.6	0.34			12450±1300			270	1
13	299.9	-2.8	9620±5400	12150±3590	10160±3730	4670±4670		70	1
14	300.1	-2.5	15850±3520	17040±1860	14400±2070	17120±2290	15720±2570	70	1
15	300.2	-5.7	1170±1170	3280± 870	3030±770	460±460	3200±1020	25	1
16	301.7	-1.7			18860±380			120	2
17	302.7	-2.8	4010±3200	7560±2970	8190±2890	6930±1700	10920±5400	80	1
18	302.7	-4.5	8190±2890	10160±2060	9040±1870	8580±2620	11030±2360	60	1
19	302.7	-4.5	8240±4290	6870±2480	5370±3590	5470±3570	3520±2400	60	1
20	302.9	0.8			29000±15000			290	1
21	302.98	-4.05			14000±7000			50	1
22	302.7	-2.78			16000±5000			80	1
23	303.0	-4.0	4430±3660	5460±2040	8270 ±3670	5020±3500		50	1
24	303.0	-4.1	6810±6290	5580±3270	5590±5020	3460±3460	4600± 4600	50	1
25	303.7	0.6			13800±2400			340	2
26	303.7	0.6			14000±2300			340	2
27	304.36	-2.68			14000±7000			90	1
28	304.5	-2.3	1635±1635	1330±1330	3740±3740	3360±3360	6380±5900	120	1
29	304.6	-2.4	7840±5530	6090±3410	3980±3010	5150±4510	7060±3220	110	1
30	304.6	-0.4			11900±2400			400	2
31	305.2	-5.7			8000±2000			30	2
32	307.0	-1.0	4340±3300	4140±2180	4630±2300	3120±3120	3791±3570	200	1
33	308.0	-5.0	3360±2740	2850±1770	4830±1640	4780±2230	4380±1340	40	1
34	304.6	-2.4	2060±2060	4480±3140	3230±3230	4170±4170	15240±9730	110	1

[a] photons cm^{-2} s^{-1} sr^{-1} Å^{-1}.
[1] Murthy & Sahnow (2004)
[2] Murthy et al. (1999)

Coalsack range from 3000 - 29000 photons cm^{-2} s^{-1} sr^{-1} $Å^{-1}$ at 1100 Å.

4.3 Model

We have made use of a generalized Monte Carlo model to predict the scattered radiation at each of the locations. Here individual weighted photons from the star get scattered several times before reaching the detector. A detailed description of this method is given in chapter 2. Here we make use of the Henyey-Greenstein (Henyey & Greenstein, 1941) scattering phase function and the dust cross-sections from Weingartner & Draine (2001) which correspond to a mixture of graphite and silicate grains with $R_v = 3.1$. The dust distribution, as usual, is more difficult to characterize and is the main source of uncertainty in our model. One of the major advantages of this direction is that the density and distribution of the medium in this region has been well studied. The molecular cloud comprising the Coalsack is clearly delimited by the CO contours of Dame et al. (2001) which we have converted into a total hydrogen column density using the N_{H_2}/W_{CO} ratio of 2.8×10^{20} mol cm^{-2} K^{-1} km^{-1} s (Bloemen et al., 1986). The dark nebula is at a distance of 190 $\pm$ 10 pc from the Sun (Franco, 1989), behind the hot stars listed in Table 4.2. As will be shown below, the contribution from the Coalsack is negligible compared to that from the foreground diffuse medium.

There is virtually no interstellar matter in this direction up to a distance of about 40 pc from the Sun, except for the Local Cloud, which has a column density of only about 5×10^{18} cm^{-2} (see Frisch, 2002b). The medium beyond 40 pc has been found to be in two extended sheet-like features (Corradi et al., 1997, 2004), one at a distance of about 60 pc and the other at 120 - 150 pc from the Sun. Using the Na I column densities obtained by Corradi et al. and the N_{NaI}/N_{HI} ratio of Ferlet et al. (1985), we have obtained a neutral hydrogen column density of about 3×10^{19} cm^{-2} for the 60 pc feature and $3.7 \times 10^{20} - 2.6 \times 10^{21}$ cm^{-2} for the 120 - 150 pc feature. We have used a column density of 10^{21} cm^{-2} and a distance of

Table 4.2: Details of stars used in our model

Name	l (deg)	b (deg)	Sp. Type	distance (pc)	Luminosity at 1100 Å (photons s^{-1} $Å^{-1}$)
β Cen	311.77	1.25	B1III	161.3	2.10×10^{46}
α Cru	300.13	-0.36	B1	98.3	7.35×10^{45}
β Cru	302.46	3.18	B0.5IV	108.1	6.03×10^{45}
δ Cru	298.23	3.79	B2IV	111.61	1.36×10^{45}
HD 116087	306.71	1.65	B3V	108.686	8.69×10^{43}
λ Cru	303.34	3.72	B4Vne	110.6	6.49×10^{43}
HD 110956	302.23	6.38	B3V	121.36	6.11×10^{43}
HD 103079	296.73	-3.05	B4V	103.734	4.87×10^{43}

130 pc for the denser sheet.

The current model differs from Paper I in the addition of more number of stars that contribute nearly 40% of the radiation field at the distance of the foreground sheet (130 pc) for the central locations and as much as 70% towards the edges. The radiation field was calculated using the model of Sujatha et al. (2004).

We have used data from the Hipparcos catalogue (Perryman et al., 1997) to specify the stellar spectral types, locations, and distances. The flux from each star was calculated using a Kurucz (1992) model. Owing to the large fraction of stars (> 500) contributing to the observed radiation, we have done the detailed Monte Carlo modelling only for the brightest stars given in Table 4.2. These stars contribute $\sim 60\%$ of the total radiation towards the centre of the Coalsack. In order to include the contribution from other stars we ran a single scattering model by considering all the remaining stars in the Hipparcos catalogue. This method will result in an error of only 10% in the derived optical constants compared to a Monte Carlo model using all the stars.

Fig. 4.1 shows the IRAS 100 μm map of the region (in units of MJy sr^{-1}) with the brightest stars (asterisks) and the observed locations (filled squares, triangles) over plotted. The figure also contains the 100 μm contours at 40, 100 and 200 MJy sr^{-1}. We have run our model for various combinations of a and g at five different wavelengths and obtained the intensity over the entire $28^\circ \times 28^\circ$ field for each

combination. By comparing the model intensities with the observations, we were able to constrain the values of both the optical parameters at these wavelengths.

4.4 Results and Discussion

We have modelled the Voyager and FUSE observations in the direction of the Coalsack and constrained a and g in the FUV. The individual 90% confidence levels for both the parameters for different wavelengths are shown in Figs. 4.2 – 4.5. It is significant that with the inclusion of more number of observations and stars we have been able to remove the degeneracy in g. Figs. 4.6 and 4.7 show the variation of these parameters as a function of wavelength. The theoretical predictions of Weingartner & Draine (2001) for $R_v = 3.1$ are also overplotted (dotted line). We find that there is only a slight increase in the albedo from 0.3 to 0.35 while g remains constant at 0.7 ± 0.15 for the assumed dust distribution. This is consistent with the predictions of Weingartner & Draine (2001) for average Milky Way dust.

We find that the dust grains in the foreground HI sheet produce the observed scattered radiation. This can be understood from Fig. 4.8 where we can see that for $g = 0.0$, the Coalsack as well as the foreground medium contribute equally, whereas in the case of forward scattering all the contribution is made by the medium in front of the Coalsack. Since in this case the scattering is forward we can consider the latter to be true. Further evidence for this foreground material being responsible for scattering in the FUV comes from the absence of OVI emission in the spectra which is characteristic of the stars behind the Coalsack molecular cloud (Andersson et al., 2004). This shows that the scattering dust in the neutral sheet has the same properties as the general diffuse interstellar medium. There is a decrease of 0.1 in the albedo at 1100 Å compared to Paper I (0.4 ± 0.2) due to the contribution from the additional stars in the model. In Fig. 4.9, we have plotted the observed UV intensities against the corresponding model values for an albedo of 0.3 and a

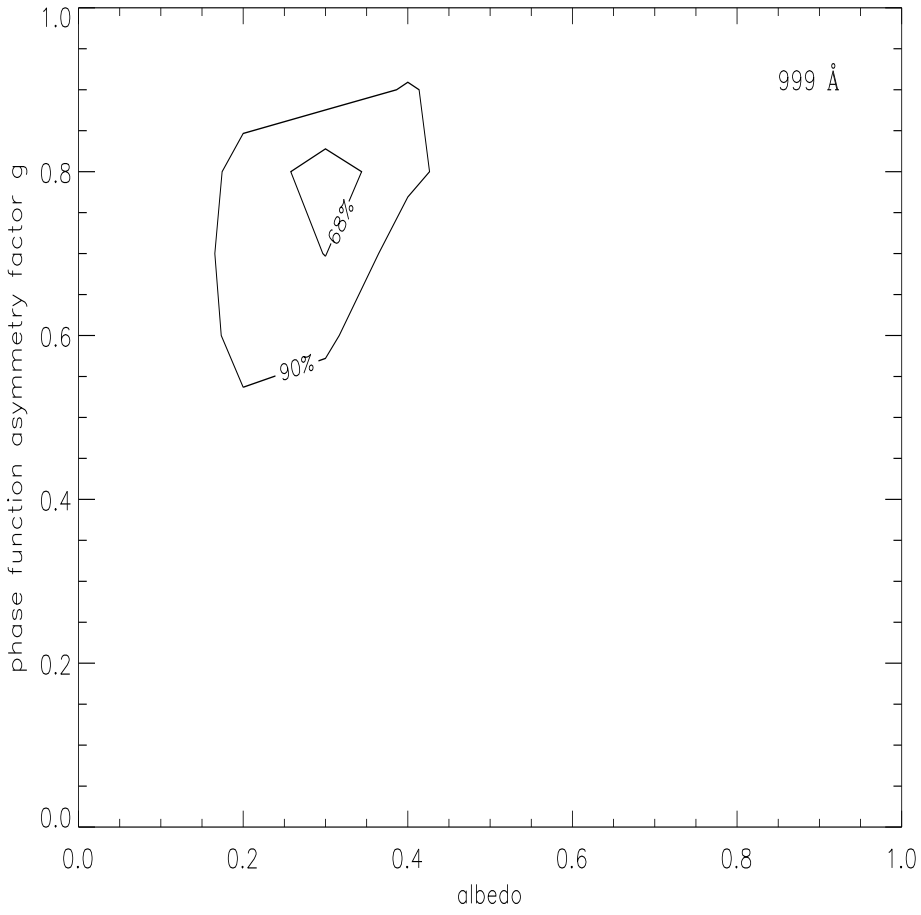

Figure 4.2: 90% and 68% confidence contours (a versus g) are plotted for 999Å.

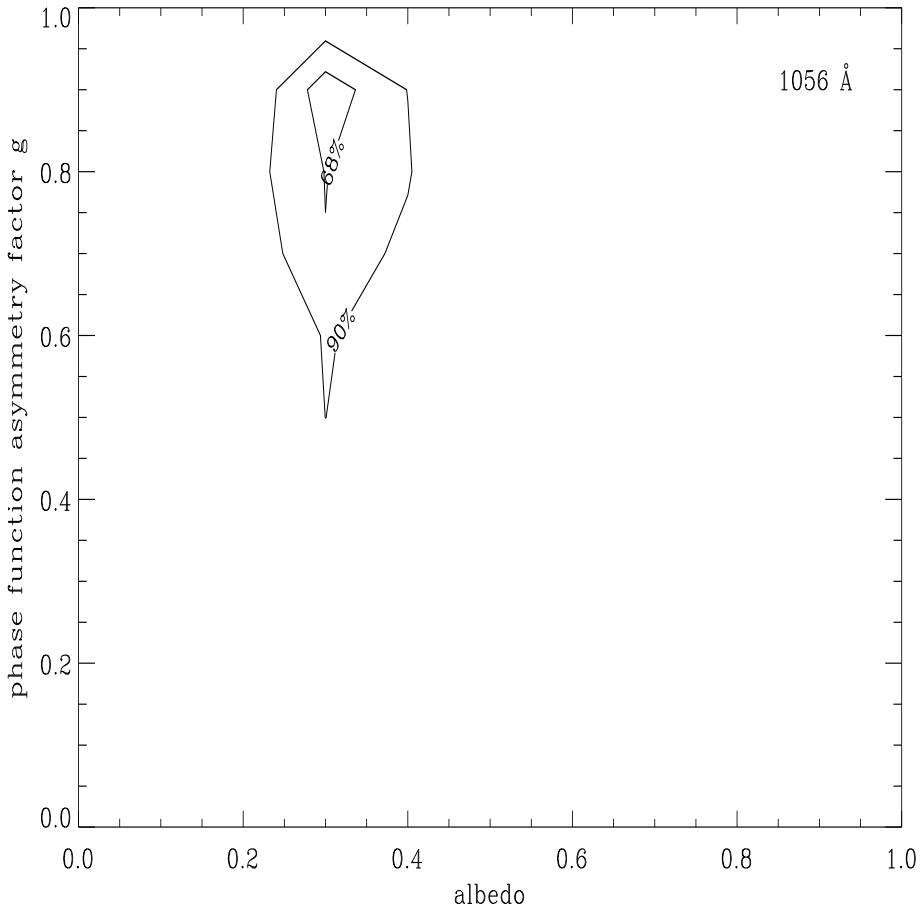

Figure 4.3: 90% and 68% confidence contours (a versus g) are plotted for 1056Å.

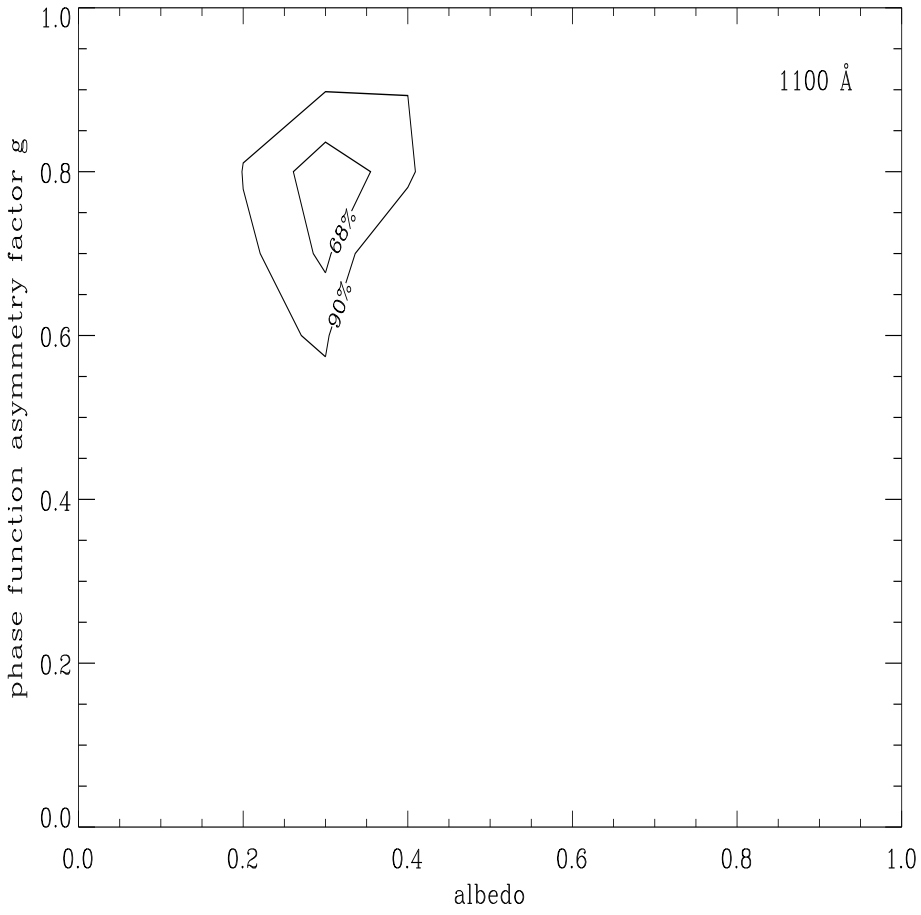

Figure 4.4: 90% and 68% confidence contours (a versus g) are plotted for 1117Å.

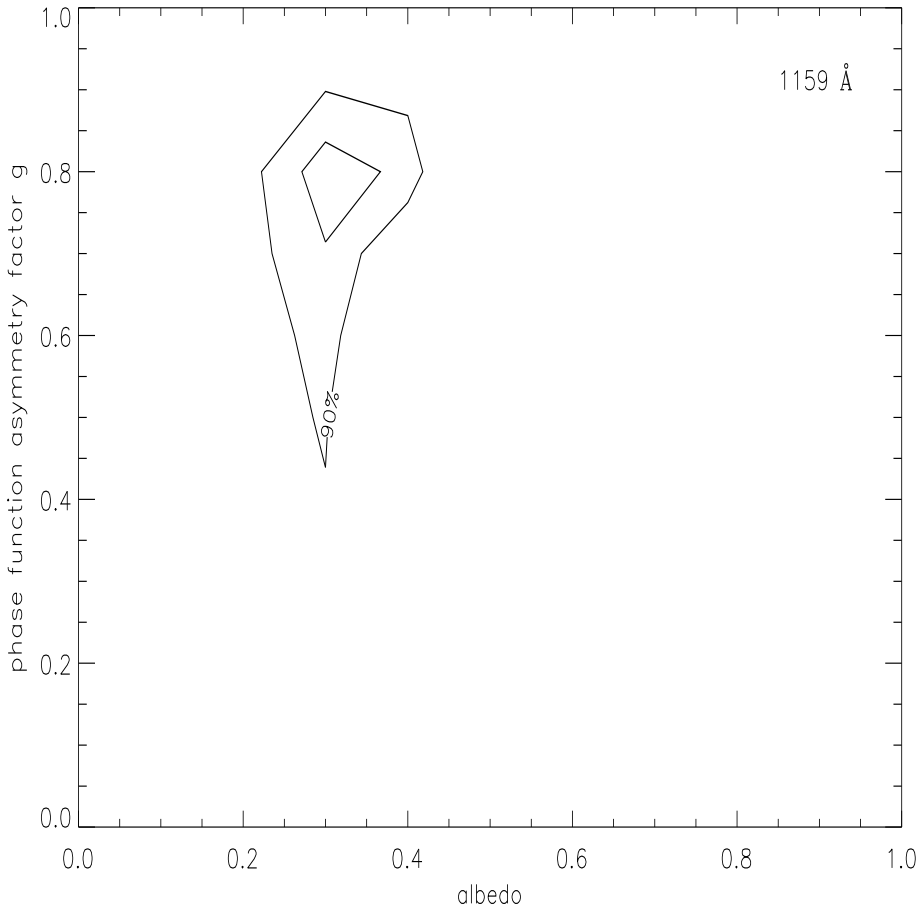

Figure 4.5: 90% and 68% confidence contours (a versus g) are plotted for 1159Å.

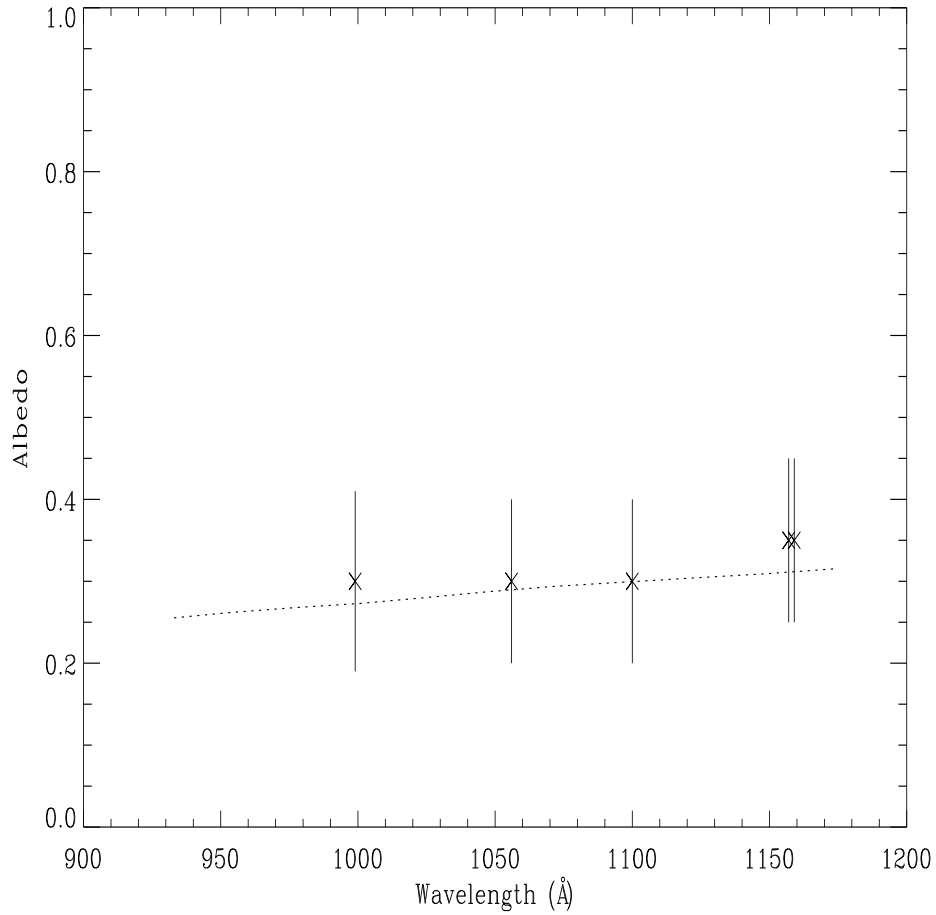

Figure 4.6: The variation of albedo with wavelength is plotted. The albedo, a varies from 0.3 to 0.35 with wavelength.

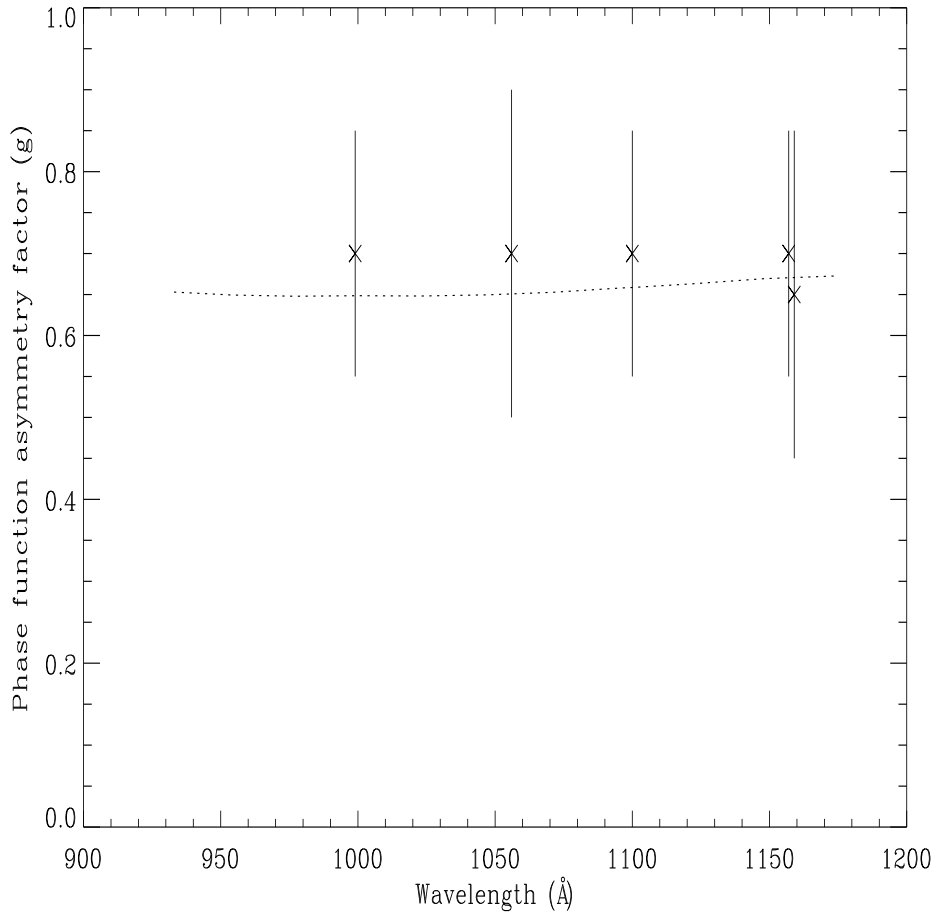

Figure 4.7: The variation of g as a function of wavelength is plotted. g remains a constant at 0.7 ± 0.15 with wavelength.

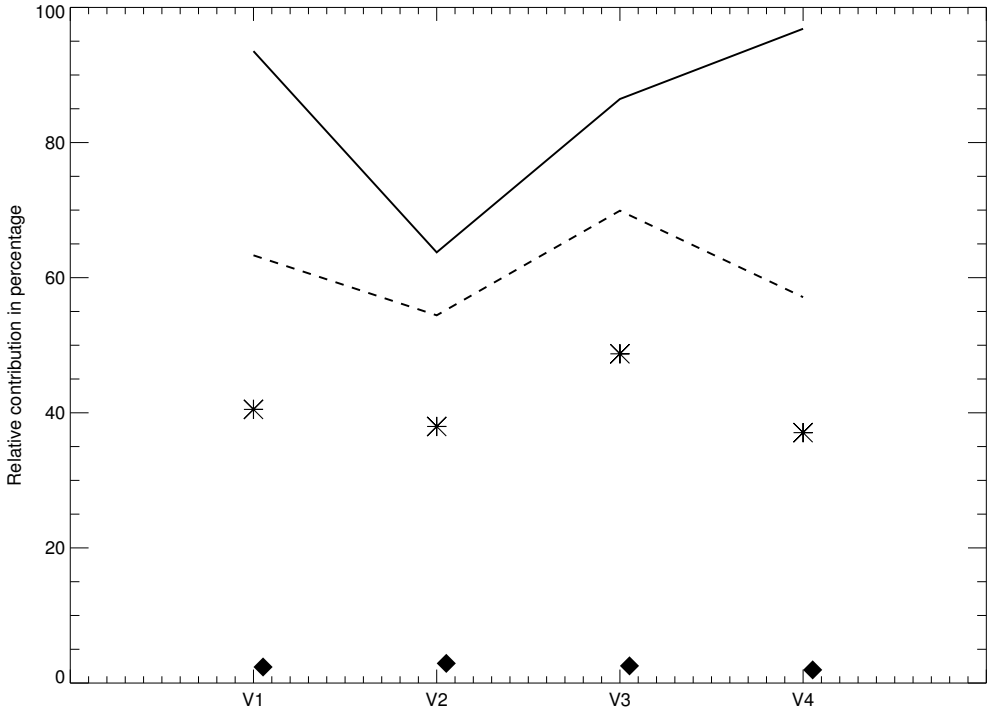

Figure 4.8: Relative contributions from two parts of the medium for the 4 *Voyager* locations. The solid line represents the contribution from the foreground medium for g = 0.9 and the dashed line denotes its contribution for $g = 0.0$. The contribution from the Coalsack for g =0.0 and $g = 0.9$ is represented by the asterisks and the filled diamonds, respectively. The albedo used is 0.4 for all the four locations.

g value of 0.7 which are the best fit values for these parameters at 1100 Å. There is good correlation between the two implying the constancy of grain properties in the foreground cloud in the FUV.

We have also calculated the infrared (IR) 100 μm intensities for all the locations using the condition of thermal equilibrium for the best fit parameters and compared with the IRAS 100 μm data (given in Table 4.1). The difference in intensities between the IRAS data and the modified values of Schlegel et al. (1998) are plotted as error bars in Fig. 4.10. There is a reasonably good correlation between the observed and model values. Note that for locations with lower intensities (< 100 MJy sr^{-1}), the correlation is much better than for the high intensity values. This is because in the former case the same HI sheet that contributes in the UV is the major contributor in the IR also. On the other hand, the locations with lower correlation correspond to high density regions within the Coalsack molecular cloud and regions of hot x-ray emitting plasma surrounding the molecular cloud observed by Andersson et al. (2004). For these locations, since the contribution from the molecular cloud is higher than from the HI sheet, the distance of the cloud is very crucial in determining the IR intensities. But here we have only considered an average distance of 180 pc for the entire cloud. In addition, the dust at these locations is heated by the hot plasma that results in higher dust temperatures than would be produced by the stellar radiation field alone. This has resulted in the relatively bad correlation at high intensities. In any case the presence of a correlation indicates the uniformity of the dust properties not only in the neutral sheet but also to some extent in the molecular cloud.

4.5 Conclusions

Our model predicts the intensities over the entire $28^\circ \times 28^\circ$ region towards the Coalsack. In agreement with Murthy et al. (1994) we find that the foreground sheet is responsible for scattering rather than the background molecular cloud.

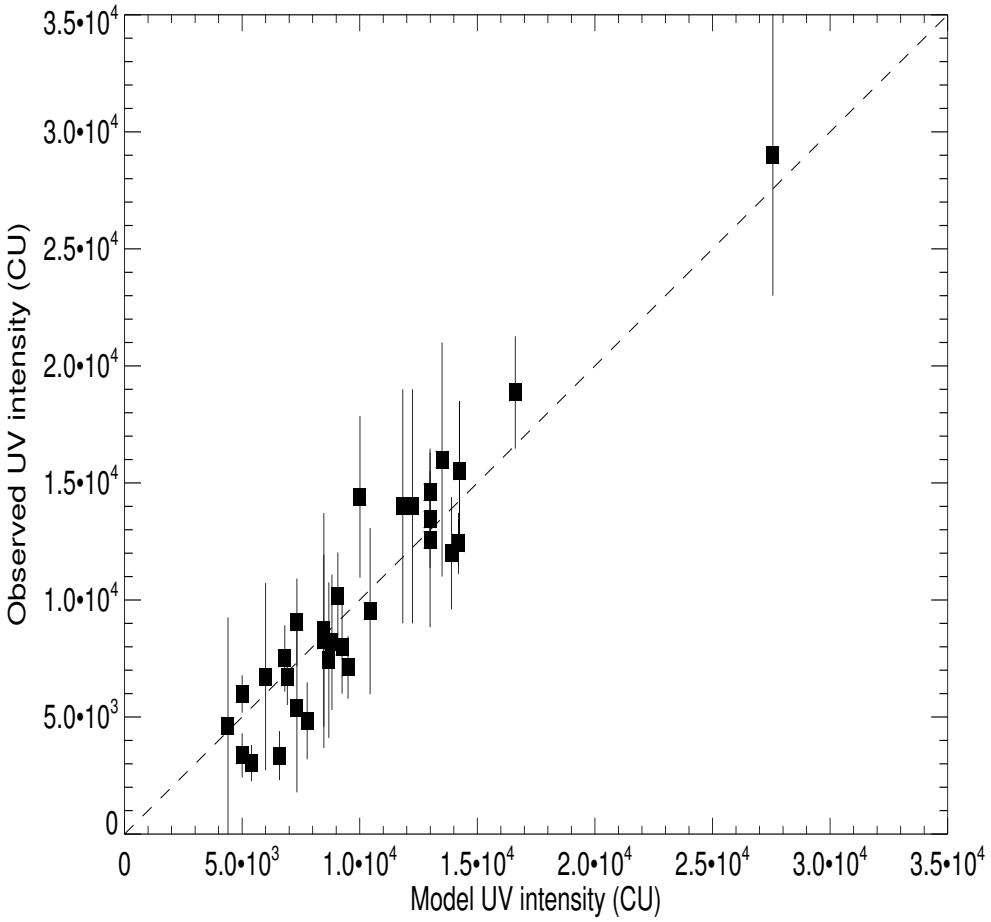

Figure 4.9: The modelled FUV (1100 Å) intensities corresponding to an albedo of 0.3 and a g value of 0.7 have been plotted against the observed values for each location. There is a very good correlation between the two, implying the uniformity of the optical properties of grains in the region.

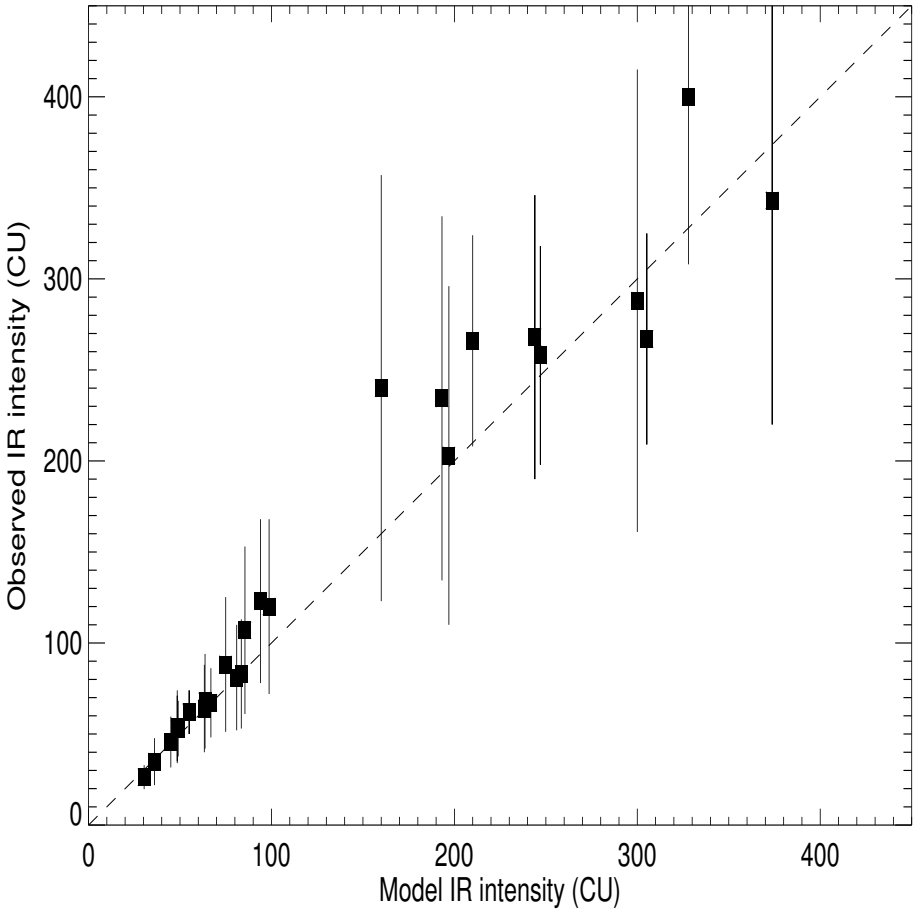

Figure 4.10: The model IR intensities corresponding to an albedo of 0.3 have been plotted against the observed IRAS (100 μm) values for each location.

We have benefitted by the increased number of observations from the FUSE spacecraft in this region as they have helped us in removing the degeneracy in g and uniquely determining its value. Using our model we have found that the albedo of the grains is 0.3 $\pm$ 0.1 at 999 Å increasing to 0.35 $\pm$ 0.1 at 1159 Å , and g is nearly constant at 0.7$\pm$0.15. These results are in good agreement with the recent predictions of Sujatha et al. (2005) in the Ophiuchus molecular cloud. Our values are also consistent with the earlier results of Witt et al. (1993), Burgh et al. (2002) and Murthy et al. (1994). The derived parameters being in good agreement with the theoretical predictions of Weingartner & Draine (2001) for R_v = 3.1 indicates that the grains have the same properties as the average Milky Way dust. This might be because the radiation field here is not as strong as in locations like M42.

Our model has been able to consistently explain both the observed FUV as well as IR 100 μm intensities using the same set of dust parameters. These results indicate that diffuse emission in the FUV in the direction of the Coalsack is mainly due to the scattering by dust grains in the foreground of the cloud, while the IR emission is due to grains within the Coalsack as well and so there wouldn't be any correlation between the observed FUV and IR intensities. This also leads to lack of correlation between the dust column density and the observed FUV intensity, unlike Schiminovich et al. (2001) who claim to obtain a strong correlation between the two using the NUVIEWS instrument. This is because the dust column density obtained from IR observations correspond to the total integrated density along the line of sight whereas the FUV intensities are from the foreground material alone for the locations studied.

Chapter 5

FUV Scattering by Dust in Orion

5.1 Introduction

The Orion Nebula (M42) is part of a molecular ridge of material extending N-S through the sword of the Orion constellation. Due to its proximity to the Sun and its association with a young stellar cluster containing many bright and massive stars, this nebula has been studied extensively at several wavelengths (reviewed by O'Dell et al., 2001). The standard model for M42 (Wen & O'Dell, 1995) is that it is a thin blister of ionized gas in front of the Orion molecular cloud (OMC-1), for which the ionization energy comes from the Trapezium stars (mainly θ^{1} Ori C). This star is a peculiar O6 star (Walborn & Panek, 1984) with a strong stellar wind and a 15.4 day periodicity in spectra (Walborn, 1981; Walborn & Nichols, 1994; Stahl et al., 1993). These stars are the youngest among the stars in the Orion Nebula Cluster (ONC), which contains around 3500 stars with a cluster mass of 1800 $M_{\odot}$. The main ionization front (MIF) of the nebula is a wall that is destroying the surface of the parent molecular cloud (OMC-1) by photoevaporation. Wen & O'Dell (1995) has modelled the MIF by using the relationship between the thickness of the emitting layer and the surface brightness of the nebula. They showed that the emitting layer is thin (0.1 pc) as compared with the lateral dimension (1 pc). In addition, there is a sheet of neutral hydrogen known as the Veil (O'Dell et al., 1992) in front of the nebula which consists of three velocity components known as A(24 km s^{-1}), B(21 km s^{-1}) and C(16 km s^{-1}).

The extinction in the nebula has been derived by comparing the Hα surface brightness with the 21 cm radio emission (O'Dell, 2000). From the correlation of neutral hydrogen column densities (obtained from HI 21 cm absorption) with extinction (O'Dell et al., 1992), dust in the foreground Veil is considered to cause the observed extinction. Stars in the ONC are known to have deviant extinction curves (Bohlin et al., 1983; Cardelli & Clayton, 1988) indicating differences in the grain sizes, abundances etc. compared to the diffuse ISM grains. The observed extinction of these stars (A_v = 1.55 mag) is in agreement with the extinction derived from surface brightness measurements of the nebula ($A_{H\beta}$ = 1.5) and shows that this anomalous extinction is produced by an excess of large grains (R_v = 5.0) in the Veil (Abel et al., 2004).

Continuum emission was observed from the nebula by O'Dell & Hubbard (1965) who found it to be much stronger than that from pure atomic processes. It was therefore attributed to scattering by dust grains in the nebula. There have been several observations of dust scattering near the Orion Nebula in the near UV (1300 − 3000Å), all with the International Ultraviolet Explorer (IUE) (Mathis et al., 1981; Perinotto & Patriarchi, 1980; Patriarchi & Perinotto, 1985). These authors assumed a spherically symmetric dust distribution and obtained an albedo of 0.44 ± 0.11 between 1300 and 3000 Å (see Fig. 5.4) with highly forward scattering grains. However these studies were limited by the need to subtract the atomic continuum present in the observed radiation. In the far-ultraviolet (FUV), on the other hand there is negligible contribution from the atomic continuum and the uncertainties are minimized to a large extent. We have used serendipitous Far Ultraviolet Spectroscopic Explorer (FUSE) observations of scattered radiation at an angular separation of $12'$ from θ^1 Ori C (Murthy et al., 2005) to derive the scattering properties of the dust grains in the far ultraviolet (FUV). We find that this emission is due to scattering of the light from the Trapezium stars by a layer of dust in front of M42 which is part of the Veil. We derive an albedo of 0.25 at 912 Å which increases to 0.4 at 1040 Å.

We have recently used FUSE and Voyager data to study the optical properties of dust grains in the directions of the Coalsack (Shalima & Murthy, 2004) and Ophiuchus (Sujatha et al., 2005). In both regions, the dust was found to actually be in foreground clouds of relatively low density in front of the dense molecular clouds and illuminated by the bright stars in the two regions, respectively. This work, represents the first determination of the optical properties of the dust grains in the FUV for Orion, where the dust is known to be much different from the general interstellar medium.

5.2 Observations

The FUSE satellite was launched in 1999 into a low earth orbit. It consists of four co-aligned optical channels out of which two are coated with lithium fluoride (LiF) and the other two with silicon carbide (SiC). Together these channels cover the spectral range between 905 Å and 1187 Å. It has three apertures, LWRS, MDRS and HIRS. The LWRS is a $30'' \times 30''$ square aperture while the MDRS is a $4'' \times 20''$ rectangular aperture. The HIRS is a $1.25'' \times 20''$ aperture. Out of these only the LWRS gives useful spectra for diffuse sources. As part of the FUSE S405/505 program, regions of nominally blank sky were observed to allow the instrument to thermalize before realignment of the spectrograph mirrors.

Murthy & Sahnow (2004) found diffuse radiation in many of these locations with intensities ranging from $1.6 \times 10^3 - 2.9 \times 10^5$ photons cm^{-2} sr^{-1} s^{-1} Å^{-1}. They used only the "NIGHT" part of the observations to exclude airglow emission and the Lyman lines of atmospheric hydrogen. They used an empirically determined background for subtraction, since standard procedures overestimated the instrumental background. The sensitivity limit of the observations is 2000 photons cm^{-2} sr^{-1} s^{-1} Å^{-1} which corresponds to an unreddened B type star of visual magnitude 16. Here we have modelled the brightest of these observations near B-type star HD36981 in Orion (S40546/01) (Table 5.1) which is described in detail

Table 5.1: FUSE observations

Data set	l (deg)	b (deg)	Time (s)	Intensity(1100Å) ($\times 10^5$ CU[c])
S4054601	208.8	-19.3	10565	2.93±0.03
S4054602	208.8	-19.3	5696	2.95±0.04

[c] 1 CU = ph cm^{-2} s^{-1} sr^{-1} Å^{-1}

in Murthy et al. (2005). They attributed the diffuse radiation to scattering from dust in front of the nebula rather than from within the nebula.

5.3 Model

Fig. 5.1 shows the DSS map of the region with the brightest stars and the FUSE location over plotted. This location (l = 208.81°, b = -19.31°) lies within the ridge of molecular material observed in C^{18}O, 13CO and CS emission by Chini et al. (1997). Although only 1.5′ from HD 36981, Murthy, Sahnow, & Henry (2005) showed that the observed emission could not be scattered radiation from that star because the broad photospheric Lyβ absorption line in the stellar spectrum is not reflected in the diffuse spectrum. We find that despite its proximity to HD 36981, 65% of the radiation at the distance of the dust is provided by θ^1 Ori C alone and 99% by the stars in Table 5.2. The spectra also shows possible blueshifted photospheric OVI absorption (France & McCandliss, 2005), characteristic of hot O type stars which is absent in relatively colder stars like HD 36981. However, the spectra doesn't show as much extinction as θ^1 Ori C, probably due to scattering through a comparitively low density region (Murthy et al., 2005).

The amount of light scattered by the dust depends on the number density of the interstellar dust grains, scattering properties of the grains and the relative geometry of the stars and dust. We have used the Henyey-Greenstein function (Henyey & Greenstein, 1941) for the scattering phase function. Although this is a

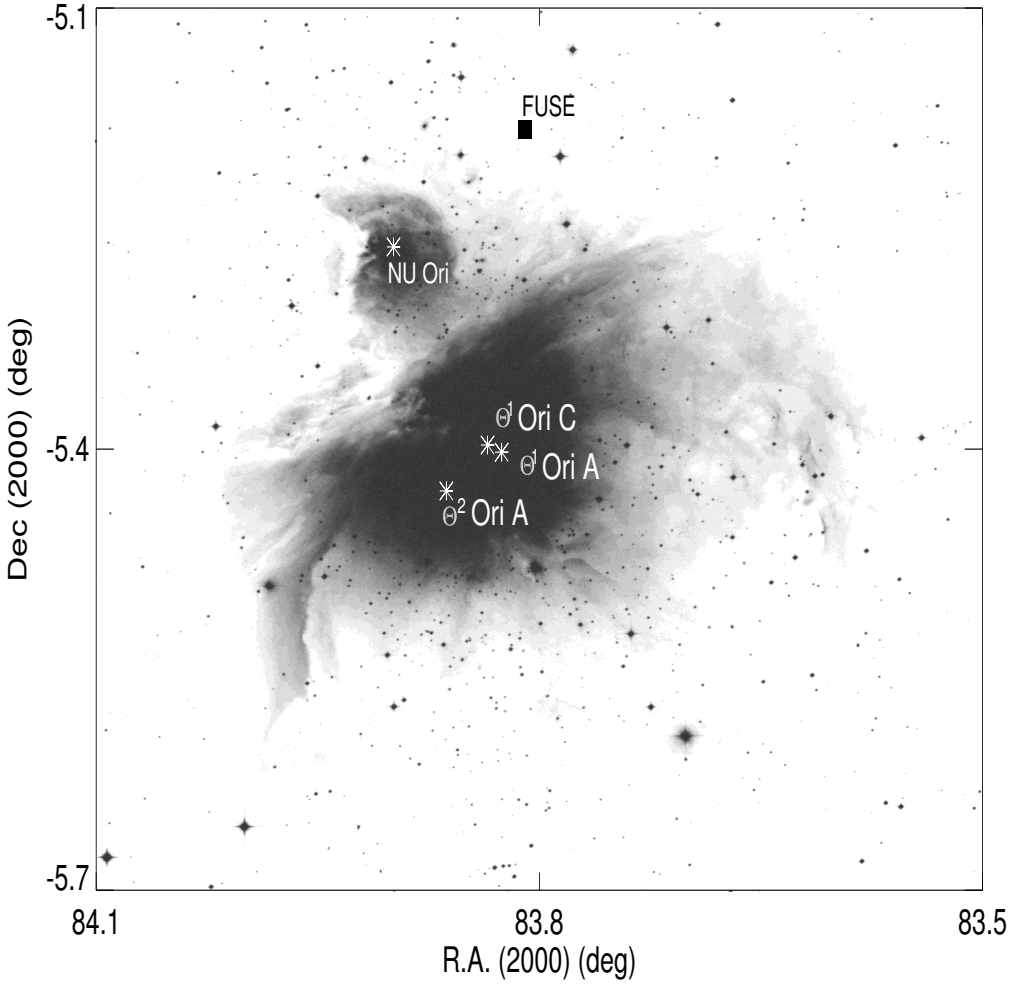

Figure 5.1: DSS map of the region with the stars (asterisks) and the FUSE location (filled square) overplotted.

Table 5.2: Properties of stars near target

Name	l (deg)	b (deg)	$R.A.^a$ (deg)	Dec^a (deg)	Sp. Type[b]	d[c] (pc)	Flux (1100 Å) at 449pc (CU[d])
θ^1 Ori C	209.01	-19.38	83.82	-5.39	O6pe	450	1500×10^5
θ^2 Ori A	209.05	-19.37	83.84	-5.41	O9.5V	450	370×10^5
θ^1 Ori A	209.01	-19.39	83.81	-5.39	B0.5V	450	150×10^5
θ^1 Ori D	209.01	-19.38	83.82	-5.39	B0.5Vp	450	250×10^5

[a] 2000 epoch
[b] SIMBAD astronomical database
[c] Hipparcos catalogue
[d] 1 CU = ph cm^{-2} s^{-1} sr^{-1} $Å^{-1}$

purely empirical function which may not represent the true scattering, particularly for strongly forward scattering grains (Weingartner & Draine, 2001), it is the most prevalent in the literature and is accurate to within 10% for g $<$ 0.8. We have used dust cross-sections from Weingartner & Draine (2001) assuming two different values for R_v (= A_v / E (B-V)): R_v = 3.1, characteristic of "standard" Milky Way dust; and R_v = 5.5, characteristic of the interstellar dust in Orion (Cardelli et al., 1989b; Fitzpatrick, 1999). These authors have used a mixture of spherical carbonaceous and silicate grains with the smallest carbonaceous grains being PAH (polycyclic aromatic hydrocarbon) molecules and the largest grains consisting of graphite. We note that Weingartner & Draine (2001) have used the ratio of visual extinction to the hydrogen column density (A_v/N(H)) of Bohlin et al. (1978) which is $\sim$ 2.5 times higher than the value observed for Orion (Shuping & Snow, 1997). Since the ratio A_v/N(H) is a measure of the extinction cross-section per hydrogen (Draine, 2003b), we have used the ratio of the measured values of A_v/N(H) for the Milky Way and the LMC and the corresponding ratios between their extinction cross-sections in order to derive extinction cross-sections for Orion. We find that the dust cross-sections in Orion (for A_v/N(H) = 3.6×10^{-22} mag cm^2) are approximately 1.6 times higher than those of Weingartner & Draine (2001) for R_v = 5.5. Therefore we have calculated the FUV intensities corresponding to these modified cross-sections apart from cross-sections for R_v = 3.1.

The observed FUSE spectrum (Fig. 5.2) shows a strong interstellar Lyβ absorption feature corresponding to a column density (N[HI]) of 6.3 $\times 10^{20}$ cm^{-2} using a χ^2 fit. When combined with the H_2 column density of 4.7 $\times$ 10^{18} cm^{-2} (France & McCandliss, 2005), we find that the total hydrogen column density is N(H) = 6.4 $\times 10^{20}$ cm^{-2}. However, HI 21 cm observations (Condon et al., 1998) show that the HI column density of the foreground cloud is only 4.5 $\times$ 10^{19} cm^{-2} indicating that the bulk of the absorbing medium must be between the contributing stars (primarily the Trapezium stars) and the point of scattering. We have derived the HI column density at the location from the NRAO VLA Sky Survey (NVSS) data of Condon et al. (1998) by using the I_{21cm}/N(HI) ratio of van der Werf & Goss (1989) where I_{21cm} is the intensity of the HI 21cm emission. It is interesting to note that the column density along the direct line of sight to the Trapezium stars is much higher with N(H) = 3.9 x 10^{21} cm^{-2} (Shuping & Snow, 1997). Thus we are actually observing light from the Trapezium stars reflected around the foreground clouds.

A schematic of our scattering geometry is shown in Fig. 5.3. The observed emission is due to scattering of the light of the Trapezium stars from dust at a distance of 1 pc (point A) from θ^1 Ori C, corresponding to the distance of Orion's Veil (Abel et al., 2004). The column density between the stars and the point of scattering is 6.4 $\times 10^{20}$ cm^{-2} with the thickness of the scattering layer being 4.5 $\times 10^{19}$ cm^{-2}. We have used a single scattering model, since the optical depth at the location, τ_{FUV} is less than 1. We have included both dust extinction as well as gas (HI and H_2) absorption. The H_2 and HI absorption cross-sections have been taken from McCandliss (2003). The continuum was derived by taking the median of 50 data points for each wavelength after eliminating the regions corresponding to the strongest spectral lines of molecular and neutral hydrogen (see Fig. 5.2). The continuum beyond 1040 Å is affected by the presence of H_2 fluorescence (France & McCandliss, 2005) and therefore we have modelled the radiation only upto 1040Å. France & McCandliss (2005) has modelled the fluorescent emission in Orion and

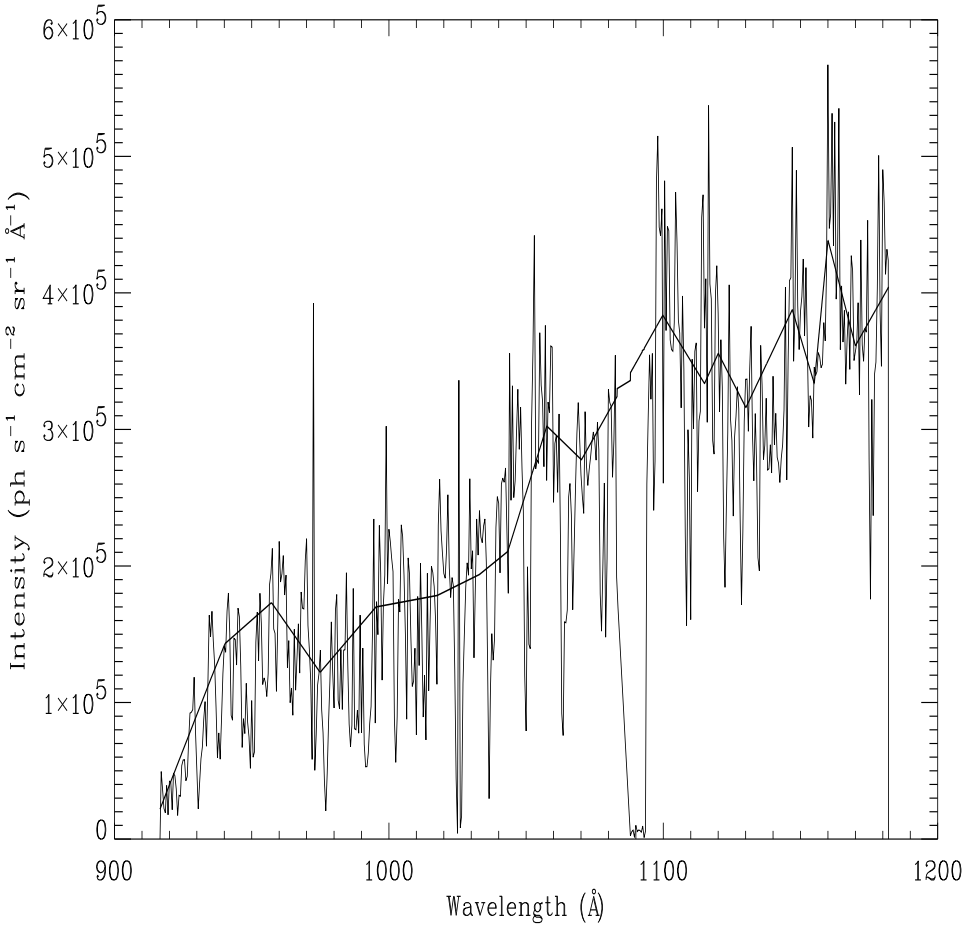

Figure 5.2: Observed diffuse spectrum from Murthy et al. (2005). The modelled continuum which is assumed to be the scattered intensity is plotted as the dark line.

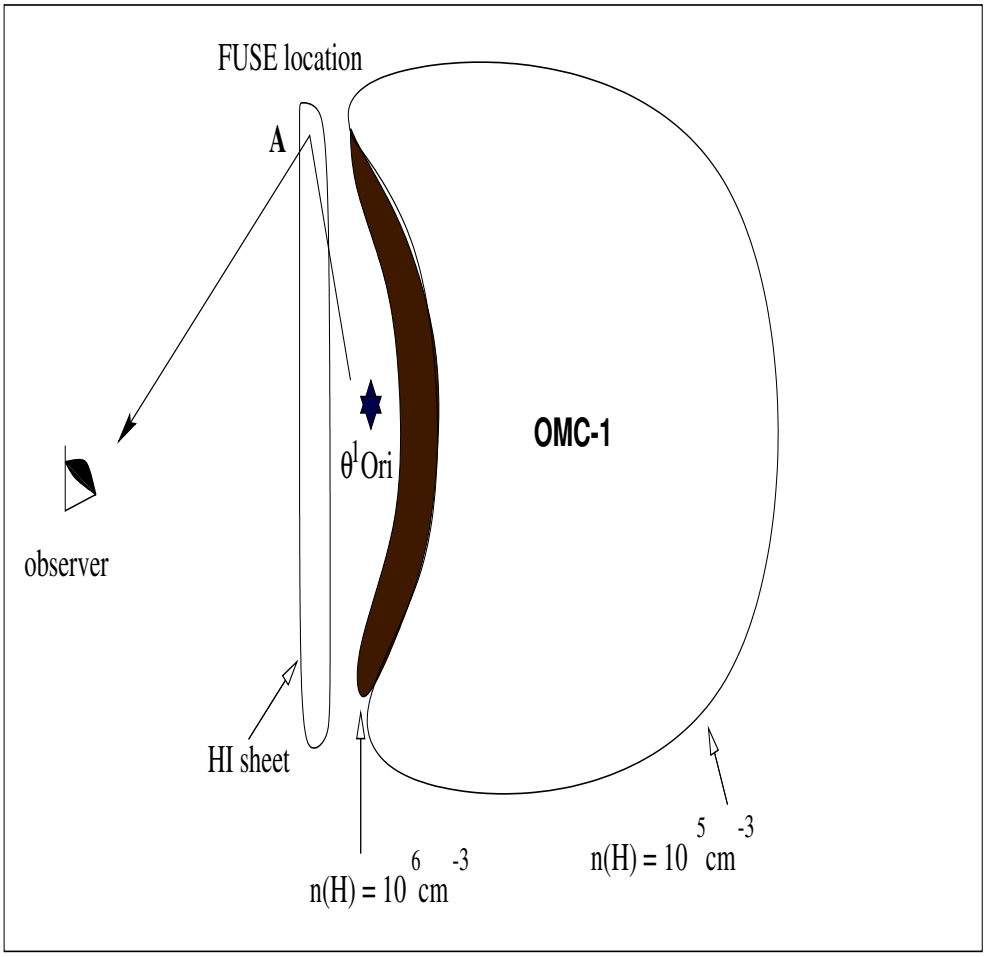

Figure 5.3: Schematic representation of the distribution of dust at the location showing the path (arrow) taken by the observed photons from the Trapezium stars towards the observer.

find that their model can account for the observed intensities at all wavelengths except between 1040 Å and 1050 Å and for the 1161 Å band of molecular hydrogen, where the model values are a factor of two less compared to the observed intensities. Finally we put all of these together to calculate the diffuse background at the FUSE location as a function of the optical parameters a and g. The optical constants were derived by comparing the model values with the observed continuum.

5.4 Results and discussion

Figs. 5.4 and 5.5 show the best fit albedo values (asterisks) as a function of wavelength corresponding to an R_v of 5.5 and 3.1 respectively. The dotted line corresponds to the theoretical predictions from Weingartner & Draine (2001) for the two corresponding grain models. Note that for the model with the modified cross-sections, we have plotted the original albedos of the $R_v = 5.5$ model since the required albedos weren't available. The main difference between the two grain models is that the abundance of small carbonaceous grains relative to hydrogen decreases from 6×10^{-5} for $R_v = 3.1$ to 3×10^{-5} for $R_v = 5.5$. From the figures it is evident that our values are in better agreement with the $R_v = 5.5$ model compared to $R_v = 3.1$. We have obtained an albedo of 0.25 at 912Å which increases to 0.4 at 1040Å. We find that increasing the cross-sections of the $R_v = 5.5$ model has led to an increase in the derived albedos (Fig. 5.4). This result is consistent with large values for R_v observed for Orion's Veil from extinction measurements of Cardelli & Clayton (1988) indicating the presence of large grains. Patriarchi & Perinotto (1985) derived large g values in the NUV for locations very close to the Trapezium cluster ($< 2.5'$) and hence concluded that the grains in Orion are larger than those in the general ISM. Cardelli & Clayton (1988) suggested that the large optical extinction was because of the formation of large grains due to coagulation and accretion and the destruction and selective acceleration of small grains by the radiation pressure of the Trapezium stars. Our results correspond to the only

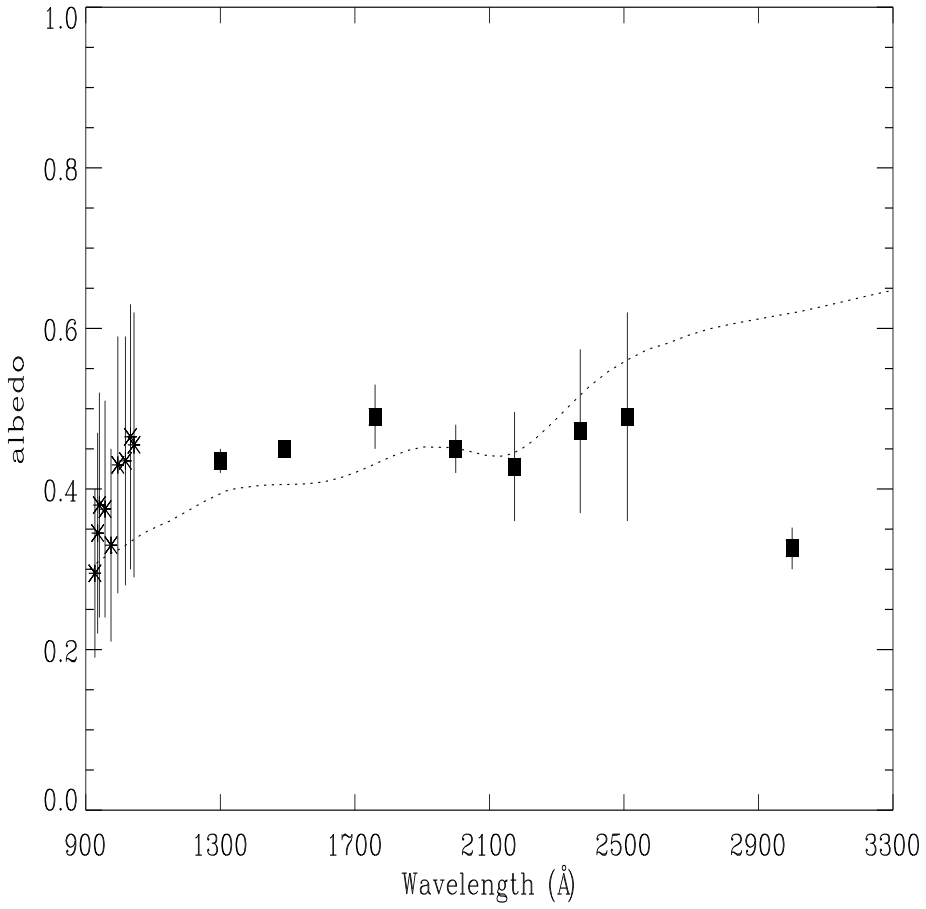

Figure 5.4: Allowed values of a as a function of wavelength for dust cross-sections enhanced 1.6 times compared to the $R_v = 5.5$ model. The dotted line represents the theoretical values of Weingartner & Draine (2001) and the filled squares represent the values obtained by Mathis et al. (1981).

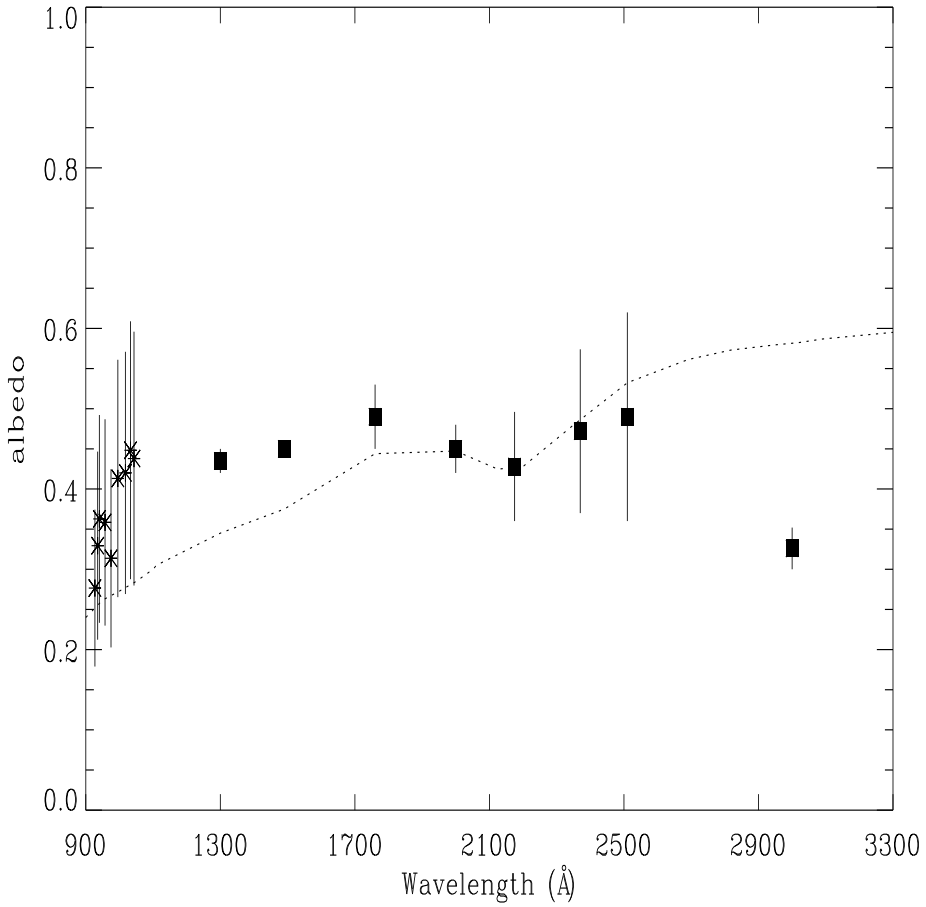

Figure 5.5: Modelled albedos for $R_v = 3.1$ with the corresponding theoretical values. Also plotted are the theoretical values of Weingartner & Draine (2001) (dotted line) and the derived values of Mathis et al. (1981) (filled squares).

derivation of the scattering parameters of dust grains in the FUV for a region with totally different dust properties.

The albedos derived here are higher than those obtained for Ophiuchus (Sujatha et al., 2005) and the Coalsack (Shalima & Murthy, 2004) where both regions correspond to scattering from foreground material since they have an average dust to gas ratio and an R_v of 3.1. Our values are also larger than those for reflection nebulae NGC 7023 (Witt et al., 1993) and NGC 2023 (Burgh et al., 2002). This may be because both reflection nebulae have small values of R_v. Apart from this, we have used larger extinction cross-sections to account for the low dust to gas ratio in the region which has resulted in the high albedo values. The dust abundance in Orion is similar to the LMC and SMC which have 24% and 13% respectively of the dust to gas ratio of the average Milky Way. However these galaxies have low extinction cross-sections (Draine, 2003b) due to low values of R_v.

There is a reduction in albedo with wavelength as in the case of NGC 2023 which indicates an increase in absorption at smaller wavelengths. This underlying similarity between the dust properties which is also seen in the theoretical models of Weingartner & Draine (2001) shows that the basic composition of the grains are the same at almost all locations. It is only the differences in the size distribution that results in variations in the absolute values of the parameters.

5.5 Summary

We have constrained the albedo of the grains near the Orion Nebula from 912 Å to 1040 Å using a dust distribution which is consistent with current models of the region. We have restricted our analysis to 1040 Å due to the presence of H_2 fluorescent emission that contaminates the spectra beyond 1040 Å and leads to high values of the observed intensities. The low HI column densities derived from the diffuse spectra makes the foreground neutral Veil the most likely location for the scattering grains. Therefore we have distributed the dust at the distance of the

Veil. This is different from previous models that assumed that grains within the nebula cause the scattering. We have used theoretical cross-sections corresponding to an R_v of 5.5 but increased it by a factor of 1.6 to include the effects of the low dust abundance in Orion.

The derived albedos are higher than those for other regions like the Ophiuchus and Coalsack, but reasonably consistent with the theoretical values of Weingartner & Draine (2001) for $R_v = 5.5$. This indicates that the scattering is produced by a grain population with an excess of large grains. Moreover, since the Veil is known to contain larger than normal grains, due to the observed anomalous extinction in stars in the region, this result indicates that the diffuse FUV radiation in the outer regions of M42 is also from the Veil.

Unfortunately there is a degeneracy in g which can be removed only by modelling more number of observations. We hope to constrain g by modelling IUE observations of the region which are available along with new FUSE observations for which we will be submitting a proposal shortly.

Chapter 6

Conclusions

The main aim of this work is to derive the properties of dust grains in the FUV for different regions in the Galaxy and find out their variation with the environment. In order to achieve this, diffuse far ultraviolet observations from three different regions of the Galaxy, each with different dust distributions and properties has been studied. They included 113 FUV observations towards the Coalsack dark cloud, 31 towards Ophiuchus and 2 towards the Orion Nebula. Both *Voyager* and FUSE data were used for the purpose. The main contributing stars for each region were obtained from the ISRF model of Sujatha et al. (2004) and Hipparcos distances were used for all of them. The stellar fluxes were derived using Kurucz models which were scaled to the observed fluxes at 1500Å. For relatively low density regions like the Ophiuchus and M42, single scattering models were used. However since the Coalsack region has a larger density with the optical depth greater than unity, we have used a complete Monte Carlo multiple scattering model.

The Ophiuchus molecular cloud is surrounded by a loop of neutral Hydrogen which has been observed in HI 21cm studies as well as at X-ray wavelengths. This material lies between the Sun and the molecular clouds in the Ophiuchus complex. This loop is probably the interface of the Local and Loop I bubbles. We have modelled 31 observations of the region obtained using the spectrometers aboard the Voyager spacecrafts with intensities ranging from $2000 - 33000$ photons cm^{-2} s^{-1} sr^{-1} Å^{-1}. We find that it is the dust in the foreground sheet of HI that is

responsible for the observed scattered radiation in the FUV and not the molecular cloud itself. We have obtained an albedo of 0.4±0.1 and a g of 0.55 ± 0.25 at 1100Å which is reasonably consistent with the theoretical predictions of Weingartner & Draine (2001) for $R_v = 3.1$ and shows that the grains in the sheet have properties similar to the diffuse ISM grains. Since the total column density at any location includes the foreground sheet as well as the background molecular clouds, we do not find any correlation between the observed FUV intensities and the total column density. However the emission is well correlated with the interstellar radiation field at the the distance of the dust for all locations. We have also modelled the observed IRAS 100μm emission for all the locations and found that the molecular cloud also contributes to the observed 100μm intensities. We do not find any correlation between the FUV intensities and the IR intensities. We therefore conclude that this is because the diffuse FUV emission is due to thin clouds in front of the stars while the infrared emission is the sum of the intensities from the background as well as foreground medium.

We have modelled the FUSE observations towards the Orion Nebula of a location that is approximately 12′ from the central Trapezium stars. The location is very bright in the FUV with intensities as high as 3×10^5 photons cm^{-2} s^{-1} sr^{-1} Å^{-1}. The current model for the nebula is that it consists of an HII region surrounding the Trapezium stars, with the molecular cloud OMC-1 behind it and a thin sheet of neutral hydrogen known as the "Veil" in front of it. The dust in the Veil has been known to be responsible for the extinction of starlight in the region. The FUSE spectra was fitted with a theoretical profile which includes both HI and H_2 lines and the total hydrogen column density that causes the extinction was found to be 6.4×10^{20} cm^{-2}. The column density of the scattering layer was obtained from HI observations to be 4.5×10^{19} cm^{-2}. We assumed the dust to be at the distance of the Veil and modelled the observed spectra from 912 − 1040 Å for two grain models corresponding to $R_v = 3.1$ and $R_v = 5.5$. The former value is

typical of dust in the general ISM while the latter value corresponds to grains in the Veil. Since dust is known to be depleted in Orion, we have also used a model with reduced extinction cross-sections compared to the $R_v = 5.5$ model. We found the derived albedo to be consistent with the $R_v = 5.5$ model which is in agreement with the value for the Veil ($R_v = 5.0$). We therefore concluded that the foreground Veil is responsible for the observed scattered emission as well. We couldn't model the intensities beyond 1040 Å due to the contamination by an unknown amount of molecular hydrogen fluorescence. We couldn't derive the other optical constant g for this region since we did not have sufficient data.

The Coalsack is a conglomerate of several molecular clouds with some neutral material in front of it. The dust distribution in the region is very similar to the Ophiuchus locations, as the neutral hydrogen sheet that surrounds the cloud is part of the sheet that surrounds the Ophiuchus complex (Corradi et al., 2004). We have therefore used a similar model for the dust distribution towards the Coalsack and constrained a and g for five wavelengths in the FUV. We find that the albedo increases from 0.2 to 0.35 when the wavelength increases from 999 Å to 1160 Å and the value of g is almost constant at 0.7 ± 0.2. In Shalima & Murthy (2004) we were unable to fix the value of g since we had only five Voyager observations. But with the availability of additional FUSE data we have been able to remove the degeneracy in g. We find that the eight brightest stars in the region contribute only 60% of the radiation field while the remaining 40% comes from $\sim$ 500 other stars in the region. Since we cannot run a detailed multiple scattering model for all the five hundred stars, we used the Monte Carlo method for only the brightest stars and single scattering for the remaining stars. We have also been able to match the IRAS 100 μm observations using the best fit parameters from the scattering model. We find that the FUV scattering comes only from the foreground sheet as in the case of the Ophiuchus region while at least half of the observed IR radiation comes from the Coalsack molecular cloud. This region is different from

the Ophiuchus in that other than the larger densities observed here, there is a very hot X-ray emitting plasma surrounding the molecular cloud. This could lead to higher dust temperatures which is probably one of the reasons for the higher IR intensities observed here. A consequence of this hot material is the presence of OVI which is characteristic of the interaction zone of hot plasma and cold molecular clouds. This has been detected in absorption for stars behind the Coalsack. OVI emission seems to be absent in our diffuse spectra and supports the result that the scattering is indeed from the foreground sheet.

Thus by modelling these three different regions in the Galaxy we find that the observed FUV intensities depend on the environment. For regions like the Ophiuchus and the Coalsack we derive similar values for the optical constants of dust grains. But in the case of Orion, we find that the observed intensities and the albedos are much higher than those derived for the other two regions indicative of different dust size distributions. This may be due to the intense radiation field in Orion which is produced by the hot O-type stars of the Trapezium while for Ophiuchus and Coalsack the radiation field intensity is much lower. However what is common in all the locations studied here is that it is the relatively thin foreground sheet that causes the observed diffuse radiation in the FUV. The greater the ISRF at the location of the dust, the larger is the observed FUV intensity. This is in agreement with Murthy & Sahnow (2004) who attributed the variations in FUV intensities to local effects rather than the total column density along the line of sight.

The significance of these results is that they represent the first determination of both a and g uniquely using DGL observations in the FUV. Previous authors (Murthy et al., 1994; Murthy & Henry, 1995; Shalima & Murthy, 2004) have modelled observations of the DGL and constrained the albedo but not g. Although for reflection nebulae (Witt et al., 1992, 1993; Burgh et al., 2002) both a and g have been uniquely determined they have uncertainties due to clumping and high

densities that can heavily influence the derived parameters. Even though the DGL is dependent on the dust geometry to some extent, for the Ophiuchus and Coalsack the dust distributions are well known and therefore the uncertainties are kept to a minimum. In addition, it is the careful selection of targets that has helped in the removal of the degeneracy in the case of Coalsack. There were several locations where the model intensities were strongly dependent on the value of g. We obtained observations of these locations using FUSE and by combining them with other FUSE and Voyager observations of the region we were able to remove the degeneracy in g. In the case of Ophiuchus it was the large number of observations that helped in constraining both a and g.

The significance of constraining the albedo in Orion is that this is the only determination of the FUV albedo for the region. Even though reflection nebulae have the drawback of having large R_v values, for the Orion nebula we have been able to constrain the albedo by using a grain model which corresponds to regions of large values of R_v. The major advantage in this case is once again the knowledge of the dust distribution in the region. The reason for not being able to derive g is that there aren't enough observations of the region.

In all the regions considered here, the spectra of the diffuse radiation is characteristic of the stars nearby. Therefore we have been able to explain the FUV intensities using dust scattering of light from nearby stars and the derived optical constants are consistent with grain models of Milky Way dust. These results indicate that at least for regions close to the galactic plane the observed diffuse FUV radiation can be interpreted as being due to scattering by dust grains as suggested by Bowyer (1991). However that may be due to the presence of a large number of bright stars and plenty of gas and dust in the galactic plane which absorbs most of the extragalactic component which Henry (1991) attributes to the diffuse FUV radiation.

6.1 Future directions

During the course of this work we have come across some major challenges and problems. It is of utmost importance to minimize the problems and simplify the methods used in order to study more complicated regions in the future. One such problem is creating the dust distribution at any location. As mentioned earlier the Monte Carlo method is a very general method which is independent of the dust geometry. However the 3 dimensional dust density distribution has to represent the actual distribution at the region being modelled. Regions studied so far were not problematic as they had fairly simple sheet-like geometries with constant densities. However most of the regions in the Galaxy have complex dust distributions with varying densities and geometries. We will be devising a new method of creating these dust distributions for spherical, cylindrical and other complex dust geometries with the help of better computer programs so that depending on the geometry required, the program will create the 3 dimensional array with the required dust densities.

Another important aspect that we wish to study further is the effect of gas heating on the equilibrium temperature of grains. We have seen in the case of the Coalsack that there is a hot X-ray emitting plasma ($\sim 10^6$ K) surrounding the molecular cloud that can heat up the grains within the cloud much more than the stellar radiation field. The presence of hot plasma is a characteristic signature of supernova induced shocks that interact with the diffuse ISM as well as regions of star formation like the Orion Nebula. We will therefore be including the gas heating of grains in our absorption model in order to minimize the uncertainties introduced by this process.

Another problem that we encountered was the degeneracy in the parameter g for the Coalsack (Shalima & Murthy, 2004) and Orion. In the case of the Coalsack we found that this could be removed by the careful selection of locations of observation. We will therefore be observing specific locations in Orion and in any region of interest in order to constrain the value of g uniquely.

A major part of the work which will be carried out in the near future will make use of recently obtained GALEX images in order to probe the origin of the diffuse FUV radiation at high latitudes. These regions are mostly devoid of dust and gas but the observations show a substantial amount of FUV intensity. Detailed modelling of these locations will be done in order to differentiate between dust scattering and the extragalactic contribution suggested by Henry (1991). This will not only help us solve the controversy of the origin of this radiation but the extragalactic component which is considered to be due to red-shifted Lyα radiation from the intergalactic medium (Henry, 1991) can provide a lot of information about the evolution of this intergalactic medium.

Appendix A

Sample calculation of scattered intensities in Orion

The coordinates of the contributing star, θ^1 Ori C are

l=209.01 and b=-19.38 and the distance is given by

ds=450.45 pc.

The luminosity, L of the star at wavelength λ is calculated from the observed flux to be

$L = 8.85 \times 10^{45} \times 10^9 \times \lambda/6.6/3$ photons s^{-1}

In order to calculate the scattered intensity due to this star at the location at 1100 Å , we use the theoretical scattering cross-section at the particular wavelength given by,

σ=6.065$\times 10^{-22}$ cm^2

Let the distance to the scattering medium (dc1) be

dc1=447pc

and the coordinates be

lc=208.81

bc=-19.31

The number density for the medium of thickness 0.1 pc (n1) is,

n1=145.631 cm^{-3}.

The column density of the remaining medium which only contributes to the extinction is,

$N = 6.8 \times 10^{20} cm^{-2}$.

Therefore, the rectangular coordinates of the star can be calculated using the following equations,

$xs = ds \times cos(l) \times cos(b) = -371.602$

$ys = ds \times sin(l) \times cos(b) = -206.073$

$zs = ds \times sin(b) = -149.504$

Similarly the coordinates of the medium can be calculated according to the equations,

$xc = dc1 \times cos(lc) \times cos(bc) = -369.637$

$yc = dc1 \times sin(lc) \times cos(bc) = -203.294$

$zc = dc1 \times sin(bc) = -147.814$

Therefore the distance between the star and the medium (rsc) is given by,

$rsc = \sqrt{((xs - xc)^2 + (ys - yc)^2 + (zs - zc)^2)} = 3.8$ pc.

The cosine of the scattering angle is given by,

$cos(\theta) = (((xs - xc) \times xc) + ((ys - yc) \times yc) + ((zs - zc) \times zc))/rsc/dc1 = 0.907202.$

The amount of extinction suffered by the starlight is given by,

$\exp(-\tau) = \exp(-N \times \sigma) = 0.662025$

Let the albedo and asymmetry factor of the grains be,

a=0.5 and g=0.7 respectively.

Therefore the scattering phase function can be written as,

$\phi = (1 - g^2)/((1 + g^2 - 2g \times cos(\theta))^{1.5})/4\pi = 0.393526 sr^{-1}$

Therefore the intensity of scattered radiation (I) is,

$I = a \times Lum \times \phi \times \sigma \times n1 \times stepsize \times \exp(-\tau)/4\pi/rsc^2 = 173547$ photons cm^{-2} s^{-1} sr^{-1} Å^{-1}.

Now including the contribution from the other stars in the region we get a total intensity of,

$I = 248104$ photons cm^{-2} s^{-1} sr^{-1} Å^{-1} which is comparable to the observed intensity by FUSE i.e. 290000 photons cm^{-2} s^{-1} sr^{-1} Å^{-1}.

Appendix B

Sample calculation of dust temperature

The energy absorbed by a dust grain is given by,

$E = (1 - a) \times E_{inc}$

In the above equation, a is the albedo of the grain and E_{inc} is the energy incident on the grain. The absorbed energy can be calulated by summing over the contributions from the different stars in the region at all wavelengths e.g. 900 - 10,000 Å. In the case of the Coalsack, for one of the locations, we get a value of $8.9\times\ 10^{-25}$ ergs s^{-1} for this quantity by adding the contribution from 107518 stars from the Hipparcos catalogue for $a = 0.3$. This value is then equated to the total energy radiated by the grain which has been calculated for various dust temperatures using the equation,

$E_{rad} = 4\pi \times ndV \times \sigma_B T_d^4$

Here σ_B is the Stefan-Boltzmann constant and n is the number density of grains corresponding to a column density of $1\times10^{21}\mathrm{cm}^{-2}$.

Equating these two quantities, we get a temperature of 12.5K for the grains. In order to calculate the infrared intensity at 100 μm, we use the same expression for the total energy radiated except that we include the wavelength dependence of the planck function. Therefore using the equation for the energy radiated in the infrared, we get,

$E_{rad}(\lambda) = 4\pi \times ndV \times B_\lambda(T_d) \times \sigma_{abs}$.

The intensity at the IRAS 100 μm detector which has a response, $R = 0.95$ at 100 μ m is calculated as

$I_{det} = \frac{ndz \times B_\lambda(T_d)\lambda^2 \times \sigma_{abs} \times R \times 10^5}{3.0} = 32.1$ MJy sr^{-1}.

This is comparable to the observed IRAS 100 μm intensity of 31.7 MJy sr^{-1}.

Appendix C

Table C.1: Table corresponding to Figures 3.3 - 3.6

Obs	Err	ISRF	UV(mod)	N(H)	N(HI)	IR(obs)	IR(mod)
1904	170	0.0000045	2080.8	3.31E+021	1.31E+021	43.6	39.3
2201	143	0.0000045	2268	3.79E+021	1.6E+021	37.8	39.3
2714	442	0.0000047	2936	2.45E+021	1.8E+021	21.3	18.5
3087	260	0.0000049	3243	2.35E+021	1.8E+021	21	17.4
3198	144	0.0000062	3312	2.43E+021	1.55E+021	36.17	33.2
3272	360	0.00000599	3240	2.83E+021	1.6E+021	30.2	29.4
3323	139	0.000006	3441.6	3.79E+021	1.3E+021	37.1	34.4
3324	183	0.00000563	3456	3.13E+021	1.4E+021	32.18	29.9
3506	53	0.00000566	3712.24	1.09E+021	1.09E+021	18.76	15.1
3514	76	0.0000062	3583.692	2.49E+021	1.57E+021	33.18	30
3738	308	0.000007	2964.05	2.12E+021	1.5E+021	25.62	28.1
4084	362	0.0000081	3387.65	2.1E+021	1.55E+021	40.4	39.9
4308	65	0.0000057	5190.84	2.88E+021	1.48E+021	31.65	33.7
4434	295	0.0000071	3396.26	4.65E+021	1.5E+021	30	27
4620	87	0.0000083	5604.56	1.11E+021	1.1E+021	15.7	13
4712	149	0.0000077	4846.63	1.85E+021	1.41E+021	27.3	28.8
4986	51	0.0000073	5262.17	4.47E+021	1.6E+021	28	25.1

Obs	Err	ISRF	UV(mod)	N(H)	N(HI)	IR(obs)	IR(mod)
5099	91	0.0000078	4812.84	3.09E+021	1.48E+021	29.77	32.3
5116	360	0.0000075	4406.124	2.63E+021	1.7E+021	27.84	25
5584	324	0.0000084	5912.47	2.38E+021	1.9E+021	41.67	40
5765	445	0.0000096	6911.64	2.08E+021	1.55E+021	40.3	42.5
5940	95	0.00001	6682.5	2.35E+021	1.5E+021	33	35
6523	125	0.00000934	5962.32	1.23E+021	1.23E+021	17.88	23
7023	258	0.000012	7669.44	1.16E+021	1.1E+021	15.3	17
7341	107	0.0000102	7550.74	1.4E+021	1.34E+021	25.69	30.3
8837	379	0.000011	8539.2	1.13E+021	1.1E+021	17.78	18.3
8917	608	0.0000123	9178.92	3.28E+021	1.35E+021	25.3	21.5
9696	680	0.0000129	9973.03	2.71E+021	1.25E+021	27.25	25.7
10255	537	0.000013	9004.39	2.56E+021	1.35E+021	25	22.3
10898	568	0.00001482	9917.64	2.58E+021	1.26E+021	49	53
33000	953	0.000035	32091.48	1.48E+021	1E+021	24.67	20.8

Bibliography

Abel, N. P., Brogan, C. L., Ferland, G. J., O'Dell, C. R., Shaw, G., & Troland, T. H. 2004, ApJ, 609, 247

Andersson, B.-G., Knauth, D. C., Snowden, S. L., Shelton, R. L., & Wannier, P. G. 2004, ApJ, 606, 341

Baker, P. L., & Burton, W. B. 1975, ApJ, 198, 281

Bloemen, J. B. G. M., Strong, A. W., Hasselwander, H. A. M., L., L. B., Cohen, R. S., Dame, T. M., Grabelsky, D. A., Thaddeus, P., Hermsen, W., & Lebrun, F. 1986, A&A, 154, 25

Bohlin, R. C., Hill, J. K., Jenkins, E. B., Savage, B. D., Snow, T. P., Jr., L. S., & York, D. G. 1983, ApJS, 51, 277

Bohlin, R. C., Savage, B. D., & Drake, J. F. 1978, ApJ, 224, 132

Bok, B. J., Sim, M. E., & Hawaeden, T. G. 1977, Nature, 266, 145

Boulanger, F., & Perault, M. 1988, ApJ, 330, 964

Bowyer, S. 1991, ARA&A, 29, 59

Burgh, E. B., McCandliss, S. R., & Feldman, P. D. 2002, ApJ, 575, 240

Cardelli, J. A., & Clayton, G. C. 1988, AJ, 95, 516

Cardelli, J. A., Clayton, G. C., & Mathis, J. S. 1989a, ApJ, 345, 245

—. 1989b, ApJ, 345, 245

Chen, H., Grenfell, T. G., Myers, P. C., & Hughes, J. D. 1997, ApJ, 478, 295

Chini, R., Reipurth, B., Ward-Thompson, D., Bally, J., Nyman, L. A., Sievers, A., & Billawala, Y. 1997, ApJ, 474, L135

Condon, J. J., Cotton, W. D., Greisen, E. W., Yin, Q. F., Perley, R. A., Taylor, G. B., & Broderick, J. J. 1998, AJ, 115, 1693

Corradi, W. J. B., Franco, G. A. P., & Knude, J. 1997, A&A, 326, 1215

—. 2004, MNRAS, 347, 1065

Dame, T. M., Hartmann, D., & Thaddeus, P. 2001, ApJ, 547, 792

Davies, R. D., & Cummings, E. R. 1975, MNRAS, 170, 95

de Geus, E. J., Bronfman, L., & Thaddeus, P. 1990, A&A, 231, 137

de Nicolau, C. E. C., & Pöppel, W. G. L. 1986, A&A, 164, 27

Désert, F. X., Boulanger, F., & Puget, J. L. 1990, A&A, 237, 215

Dickey, J. M., & Lockman, F. J. 1990, ARA&A, 28, 215

Draine, B. T. 1989, Interstellar Dust, IAU Symp., Vol. 135, ed. L. J. Allamandola and A. G. G. M. Tielens (Dordecht: Kluwer), 313

—. 2003a, ApJ, 598, 1017

—. 2003b, ARA&A, 41, 241

Draine, B. T., & Lee, H. M. 1984, ApJ, 285, 89

Egger, R. J., & Aschenbach, B. 1995, A&A, 294, L25

Evans, A. 1994, John Wiley & Sons (Chichester), Dusty Universe, 390pp

Ferlet, R., Vidal-Madjar, A., & Gry, C. 1985, ApJ, 298, 838

Fitzpatrick, E. L. 1999, PASP, 111, 63

Fitzpatrick, E. L., & Massa, D. 1988, ApJ, 328, 734

France, K., & McCandliss, S. R. 2005, ApJL, (accepted), xx

Franco, G. A. P. 1989, A&A, 215, 119

Frisch, P. C. 2002a, in The Century of Space Science, 1868, ed. J. A. M. Bleeker, J. Geiss, & M. C. E. Huber

—. 2002b, The Century of Space Science, eds. J. A. M. Bleeker, J. Geiss, & M. C. E. Huber (Kluwer, Dordecht), 1868

Gordon, K. D. 2004, in ASP Conf. Proceedings, Vol. 309, Astrophysics of Dust, ed. A. N. Witt, G. C. Clayton & B. T. Draine

Henry, R. C. 1991, ARA&A, 29, 89

—. 2002, ApJ, 570, 697

Henyey, L. C., & Greenstein, J. L. 1941, ApJ, 93, 70

Holberg, J. B. 1986, ApJ, 311, 969

Holberg, J. B., Ali, B., Carone, T. E., & Polidan, R. S. 1991, ApJ, 375, 716

Holberg, J. B., & Watkins, R. 1992, *Voyager* Ultraviolet Spectrometer Guest Observer and Data Analysis Handbook, Version 1.1, unpublished

Hulst, H. C. V. D. 1957, Light Scattering by Small Particles, John Wiley & Sons (New York)

Jura, M. 1975, ApJ, 197, 575

Kurucz, R. L. 1992, in The Stellar Populations of Galaxies, IAU Symposium, Vol. 149, ed. B. Barbuy and A. Renzini, 225

Lampton, M., Margon, B., & S.Bowyer. 1976, ApJ, 208, 177

Laor, A., & Draine, B. T. 1993, ApJ, 402, 441

Li, A., & Draine, B. T. 2001, ApJ, 554, 778

—. 2002, ApJ, 572, 232L

Magnani, L., Blitz, L., & Mundy, L. 1985, ApJ, 295, 402

Mathis, J. S. 1996, ApJ, 472, 643

Mathis, J. S., Mezger, P. G., & Panagia, N. 1983, A&A, 128, 212

Mathis, J. S., Perinotto, M., Patriarchi, P., & III, F. H. S. 1981, ApJ, 249, 99

Mathis, J. S., Rumpl, W., & Nordsieck, K. H. 1977, ApJ, 217, 425

Mathis, J. S., Whitney, B. A., & Wood, K. 2002, ApJ, 574, 812

Mattila, K. 1970, A&A, 9, 53

McCandliss, S. R. 2003, PASP, 115, 651

Murthy, J., Hall, D., Earl, M., Henry, R. C., & Holberg, J. B. 1999, ApJ, 522, 904

Murthy, J., & Henry, R. C. 1995, ApJ, 448, 848

Murthy, J., Henry, R. C., & Holberg, J. B. 1994, ApJ, 428, 233

Murthy, J., & Sahnow, D. J. 2004, ApJ, 615, 315

Murthy, J., Sahnow, D. J., & Henry, R. C. 2005, ApJ, 618, 99

Nyman, L. A., Bronfman, L., & Thaddeus, P. 1989, A&A, 216, 185

O'Dell, C. R. 2000, AJ, 119, 2311

O'Dell, C. R., & Hubbard, W. B. 1965, ApJ, 142, 591

O'Dell, C. R., Walter, D. K., & Dufour, R. J. 1992, ApJ, 399, L67

—. 2001, ARA&A, 39, 99

Osterbrock, D. E. 1989, Astrophysics of Gaseous Nebulae, University Science Books (California), 408p

Patriarchi, P., & Perinotto, M. 1985, A&A, 143, 35

Penzias, A. A., & Wilson, R. W. 1966, ApJ, 146, 666

Perinotto, M., & Patriarchi, P. 1980, ApJ, 238, 614

Perryman, M. A. C., Lindegren, L., Kovalevsky, J., Hog, E., Bastian, U., Bernacca, P. L., Creze, M., Donati, F., Grenon, M., van Leeuwen, F., van der Marel, H., Mignard, F., Murray, C. A., Poole, R. S. L., Schrijver, H., Turon, C., Arenou, F., & nd C.S. Petersen, M. F. 1997, A&A, 323, 49

Schiminovich, D., Friedman, P. G., Martin, C., & Morrissey, P. F. 2001, ApJ, 563, 161

Schlegel, D. J., Finkbeiner, D. P., & Davis, M. 1998, ApJ, 500, 525

Scoville, N. S., & Solomon, P. M. 1974, ApJL, 187, L67

Serkowski, K. 1968, ApJ, 154, 115

Shalima, P., & Murthy, J. 2004, MNRAS, 352, 1319

Shuping, R. Y., & Snow, T. P. 1997, ApJ, 480, 272

Spitzer, L. S. 1998, Physical Processes in the Interstellar Medium, John Wiley & Sons, 318p

Spitzer, L. S., & Fitzpatrick, E. L. 1993, ApJ, 409, 299

Stahl, O., Wolf, B., Gäng, T., Gummersbach, C. A., Kaufer, A., Kovacs, J., Mandel, H., & Szeifert, T. 1993, A&A, 274, L29

Sujatha, N. V., Chakraborty, P., Murthy, J., & Henry, R. C. 2004, BASI, 32, 151

Sujatha, N. V., Shalima, P., Murthy, J., & Henry, R. C. 2005, ApJ, 633, (in press)

van der Werf, P. P., & Goss, W. M. 1989, A&A, 224, 209

Walborn, N. R. 1981, ApJ, 243, L37

Walborn, N. R., & Nichols, J. S. 1994, ApJ, 425, L29

Walborn, N. R., & Panek, R. J. 1984, ApJ, 286, 718

Weingartner, J. C., & Draine, B. T. 2001, ApJ, 548, 296

Wen, Z., & O'Dell, C. R. 1995, ApJ, 438, 784

Wheelock, S., III, T. N. G., Chillemi, J., Kester, D., McCallon, H., Oken, C., White, J., Gregorich, D., Boulanger, F., Good, J., & Chester, T. 1994, *IRAS* Sky Survey Atlas Explanatory Supplement (JPL 94-11; Pasadena: JPL)

Whittet, D. C. B. 2003, IOP Series in Astronomy and Astrophysics, Dust in the Galactic Environment, 390pp

Witt, A. N., Petersohn, J. K., Bohlin, R. C., O'Connell, R. W., Roberts, M. S., Smith, A. M., & Stecher, T. P. 1992, ApJL, 395, L5

Witt, A. N., Petersohn, J. K., Holberg, J. B., Murthy, J., Dring, A., & Henry, R. C. 1993, ApJ, 410, 714